Award Number: W81XWH-13-1-0063

TITLE: A New Cell-Free System to Study BRCA1 Function

PRINCIPAL INVESTIGATOR: Dr. Johannes Walter

CONTRACTING ORGANIZATION: Harvard Medical School
Boston, MA 02115

REPORT DATE: June 2016

TYPE OF REPORT: Final

PREPARED FOR: U.S. Army Medical Research and Materiel Command
Fort Detrick, Maryland 21702-5012

REPORT DOCUMENTATION PAGE

Form Approved
OMB No. 0704-0188

1. REPORT DATE	2. REPORT TYPE	3. DATES COVERED
June 2016	Final	1 May 2013 – 30 April 2016

4. TITLE AND SUBTITLE
A New Cell-Free System to Study BRCA1 Function

5a. CONTRACT NUMBER
W81XWH-13-1-0063

5b. GRANT NUMBER
W81XWH-13-1-0063

5c. PROGRAM ELEMENT NUMBER

6. AUTHOR(S)
Johannes Walter

E-Mail: Johannes_walter@hms.harvard.edu

5d. PROJECT NUMBER

5e. TASK NUMBER

5f. WORK UNIT NUMBER

7. PERFORMING ORGANIZATION NAME(S) AND ADDRESS(ES)
Harvard Medical School
Boston, MA 02115

8. PERFORMING ORGANIZATION REPORT NUMBER

9. SPONSORING / MONITORING AGENCY NAME(S) AND ADDRESS(ES)
U.S. Army Medical Research and Materiel Command
Fort Detrick, Maryland 21702-5012

10. SPONSOR/MONITOR'S ACRONYM(S)

11. SPONSOR/MONITOR'S REPORT NUMBER(S)

12. DISTRIBUTION / AVAILABILITY STATEMENT
Approved for Public Release; Distribution Unlimited

13. SUPPLEMENTARY NOTES

14. ABSTRACT
DNA interstrand cross-links are extremely cytotoxic DNA lesions that are generated by chemotherapy agents and certain endogenous metabolites. Using this award, we showed that the tumor suppressor BRCA1-BARD1 plays a novel role in the repair of DNA interstrand cross-links (ICL). Normally, when replication forks collide with an ICL, leading strands stall 20 nucleotides from the ICL due to steric hindrance by the CMG helicase, which unwinds DNA ahead of the polymerase. Subsequently, CMG dissociates and the leading strand is extended towards the ICL, followed by excision of the cross-link by nucleases that are controlled by the Fanconi anemia pathway. In BRCA1-depleted egg extracts, the leading strands remain arrested at the -20 position because the CMG helicase fails to be unloaded. As a result, all downstream repair events are inhibited. The action of BRCA1-BARD1 at ICLs is likely direct because the complex binds to ICLs coincident with CMG removal. We further show that CMG unloading involves ubiquitin signaling and the action of the AAA+ ATPase p97. BRCA1 does not perform this novel function by acting through FANCJ, FANCM, or CTIP. Our data support a model in which stalled and converged CMG helicases undergo polyubiquitylation (possibly by BRCA1-BARD1, which has E3 ubiquitin ligase activity), followed by extraction of the ubiquitylated complex from chromatin by p97. Our results demonstrate that CMG unloading is the first active event in ICL repair, and that it is regulated by the BRCA1-BARD1 complex.

15. SUBJECT TERMS
BRCA1, BARD1, MCM2-7, CMG, DNA replication, ICL repair

16. SECURITY CLASSIFICATION OF:			17. LIMITATION OF ABSTRACT	18. NUMBER OF PAGES	19a. NAME OF RESPONSIBLE PERSON
a. REPORT	b. ABSTRACT	c. THIS PAGE			USAMRMC
U	U	U	UU	47	19b. TELEPHONE NUMBER *(include area code)*

Table of contents

Introduction
Mutations in BRCA1 account for a significant fraction of familial breast and ovarian cancers. BRCA1 is thought to suppress genome instability by promoting homologous recombination, which it does in part by helping to recruit BRCA2 and the RAD51 recombinase to sites of DNA damage. However, more recently, it has been proposed that BRCA1 performs functions in DNA interstrand cross-link (ICL) repair that are not related to HR [1]. For example, BRCA1 appears to help recruit the ICL repair factor FANCD2 to sites of damage. To further explore the role of BRCA1 in ICL repair, we employed Xenopus egg extracts, which we previously showed support ICL repair [2].

Keywords
BRCA1, BARD1, DNA interstrand cross-link, DNA repair, CMG helicase, ubiquitin, p97.

Accomplishments
Major goals of the project
See statement of work reproduced in in grey in the next section.

What was accomplished under these goals?
The original Statement of Work is reproduced below in grey. Our progress on each task is described in black. Unless stated otherwise, all experiments were performed at least twice, usually three times or more. Representative examples are shown.

Task 1: Determine whether blocking Approach inhibits FANCI-FANCD2 loading.

1a. Replicate pICL in egg extract and add aphidicolin 12 minutes after NPE addition; then perform ChIP with antibodies to FANCI, FANCD2, DNA pol e, FANCA, FANCM.
We first wanted to test whether Approach, which is inhibited in BRCA1-depleted egg extracts, is required for ICL repair. To this end, we inhibited this step by an orthogonal means. pICL was replicated for 12 minutes to allow the majority of forks to arrive at the -20 position (Figure 7A, lane 7 in [3]; see Appendix for PDF file). Reactions were then split and supplemented with buffer or the DNA polymerase inhibitor aphidicolin. Aphidicolin-treated samples exhibited little or no Approach (Figure 7A in [3], compare lanes 15-19 with 9-13), as well as a ~25% decrease in total nucleotide incorporation due to degradation of some forks that had not yet stalled at the crosslink (Figure 7B). Chromatin immunoprecipitation (ChIP) showed that BRCA1, RAD51, and FANCD2 were still recruited to the ICL in aphidicolin-treated samples (Figure 7C-E), although total recovery was also decreased by ~25%. In contrast, DNA incisions were inhibited, as measured by persistence of the converged fork structure (Figure 7F and data not shown). In addition, ICL repair was completely absent (Figure 7G). Together, these results indicate that Approach is required for incisions and downstream repair events, but not for the recruitment of BRCA1, RAD51, or FANCD2. We infer that the defect in Approach seen in BRCA1-depleted egg extracts readily explains the inhibition of ICL repair in the absence of BRCA1. However, the defect in FANCD2, BRCA2, and RAD51 loading in BRCA1-depleted extracts is not explained by defective Approach. In other words, the intermediate generated during Approach is not necessary for loading of FANCI-FANCD2, BRCA2, or RAD51.

1b. Clone, express, and purify ubiquitylated FANCI, FANCD2$^{1-561}$, and Ub-FANCD2$^{562-1443}$ in insect cells. If this approach does not work, reconstitute FANCI-FANCD2 ubiquitylation with UBE2T and FANCL.
This Task was proposed primarily as a follow up if Task 1a had shown that Approach is required for loading of FANCD2. This was not the case. Nevertheless, since we were interested in generating ubiquitylated FANCI-FANCD2 for other reasons, we proceeded with this task. We expressed and purified FANCI, FANCD2$^{1-561}$, and Ub-FANCD2$^{563-1443}$ in insect cells, but the two halves of FANCD2 did not interact efficiently, even in the presence of FANCI (data not shown). We have abandoned this approach.

1c. Perform gel shift experiments with the protein complex prepared under 1b and different DNA substrates to determine the complex's DNA binding specificity.
Given the outcome of Task 1a, this task is not applicable.

Task 2. Determine whether BRCA1 is required for MCM2-7 dissociation from ICLs.

2a. Replicate pICL in mock-depleted and BRCA1-depleted egg extracts and perform ChIP with antibodies to Mcm5, Mcm7, Cdc45, GINS, DNA pol ε, Rad51, BRCA2, and RPA.

We had previously shown that Approach correlates with the dissociation of the CMG helicase from replication forks that have stalled at an ICL [4]. We therefore postulated that the defect in Approach in BRCA1-depleted extracts is due to a defect in CMG dissociation. To test this, we performed ChIP in mock-depleted and BRCA1-depleted egg extracts. BRCA1-depletion not only inhibited Approach (Figure 5A in [3]), but also greatly slowed the dissociation of three CMG subunits, Cdc45, Mcm7, and Sld5, from the ICL (Figure 5B-D in [3]). Binding to a distal site on the plasmid was not affected (Figure S3K in [3]). This result shows that BRCA1 is required for CMG dissociation.

To determine whether BRCA1 functions directly in the unloading of the CMG complex, we examined the binding of BRCA1 to the plasmid using ChIP. Importantly, BRCA1 binding occurred shortly after leading strands arrived at the -20 position and shortly before they were extended to the -1 position (Figure S3A in [3]). Thus, BRCA1 is present at the site of the ICL during the Approach step. We also showed that BRCA1's interaction partner BARD1 binds to the ICL with exactly the same kinetics as BRCA1 (Figure S3G and H in [3]). We conclude that BRCA1-BARD1 is present at ICLs during CMG dissociation, consistent with it promoting this process directly.

In our cell-free system, two DNA replication forks converge on the ICL [5]. This raised the question of whether a single fork suffices to trigger repair. To address this question, we generated a plasmid in which the ICL is flanked on one side by an array of lac operator sites. Binding the Lac repressor (LacI) to these sites inhibits replication fork progression and allows only one fork to reach the ICL. Strikingly, in this setting, CMG unloading from the ICL was blocked and repair was inhibited, demonstrating that ICL repair requires fork convergence to allow release of CMG [6]. Given that we have implicated BRCA1-BARD1 in ICL repair, we asked whether BRCA1 fails to bind the ICL when only one fork arrives at the lesion. As shown in Figure 1, BRCA1 still bound efficiently to the ICL in the presence of LacI, demonstrating that a single fork is sufficient to recruit BRCA1. We conclude that fork convergence is required for CMG unloading, but not for BRCA1 recruitment. One interpretation is that fork convergence triggers a conformational change in CMG that makes it responsive to the action of BRCA1-BARD1, which is recruited independently of fork convergence.

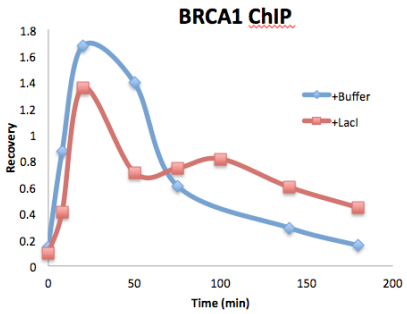

Figure 1: BRCA1 binds to ICLs independently of fork convergence. A pICL plasmid containing a lacO array was replicated in egg extract in the presence and absence of LacI, as indicated, and at different times, samples were withdrawn for BRAC1 ChIP analysis.

Task 3. Determine the functional interplay between BRCA1 and FANCJ /FANCM

3a. Replicate pICL in mock-depleted and BRCA1-depleted egg extracts and perform ChIP with antibodies to FANCJ and FANCM.

BRCA1-BARD1 might itself promote CMG unloading or act through an effector. We considered four possible effectors of BRCA1-BARD1. Two of these, FANCM and FANCJ, are DNA helicases. We speculated that their helicase activities might be required to displace CMG. FANCJ was particularly attractive since it binds to BRCA1. We considered two other potential effectors, ABRAXAS and CTIP, both of which also bind to BRCA1. We have now raised antibodies to FANCM, FANCJ, CTIP, and ABRAXAS and depleted the corresponding proteins. In no case was there evidence of a defect in CMG unloading (data not shown). Consistent with the above results, ChIP showed that FANCJ recruitment to ICLs is not reduced by BRCA1 depletion (data not shown).

3b. Perform co-immunoprecipitations between FANCJ and BRCA1.

Given that FANCJ is not involved in CMG unloading, we did not perform this task.

Task 4. Identification and characterization of new BRCA1 effectors using mass spectrometry

4a. Prepare chromatin from mock-depleted and BRCA1-depleted egg extracts in preparation for mass spectrometry analysis.

We have not initiated this task.

4b. Send chromatin samples to our collaborators in Germany for mass spectrometry analysis.

We have not initiated this task.

4c. For novel proteins whose binding to chromatin depends on BRCA1: clone the gene, express the protein, raise antibodies, immunodeplete the protein from egg extracts, and measure the effect on ICL repair, Approach, MCM2-7 dissociation, and FANCJ/FANCM loading.
We have not initiated this task.

Task 5. Identification of BRCA1 domains that are required for ICL repair

5a. Clone and express BRCA1-BARD1, BRCA1^{S1379F}-BARD1, BRCA1^{I26A}-BARD1, BRCA1$^{\Delta CC}$-BARD1, or other mutants in insect cells.
We expressed wild type BRCA1-BARD1 in insect cells and purified the protein. We have not expressed the mutant proteins.

5b. Supplement BRCA1-depleted egg extracts with recombinant BRCA1-BARD1, BRCA1^{S1379F}-BARD1, BRCA1^{I26A}-BARD1, or BRCA1$^{\Delta CC}$-BARD1 and measure the effects on ICL repair.
Re-addition of recombinant wild type BRCA1-BARD1 to BRCA1-depleted egg extract did not restore ICL repair (data not shown). To rule out that our BRCA1 antibody non-specifically depleted a protein required for CMG dissociation, we depleted BRCA1 with other antibodies. We found that depletion of egg extract with these antibodies also led to the stabilization of CMG on DNA (data not shown). We believe that most likely, BRCA1 removal co-depletes an essential BRCA1 co-factor, but our data argue that such a co-factor does not correspond to CTIP, FANCJ, FANCM, or ABRAXAS.

To gain further evidence that the BRCA1-BARD1 complex participates in CMG unloading, we sought to disrupt the BRCA1-BARD1 complex, which forms through interactions between the RING domains of BRCA1 and BARD1. Cell-based experiments had shown that expression of a BARD1 fragment corresponding to the BARD1 RING domain disrupts the BRCA1-BARD1 complex and phenocopies BRCA1 deficiency [7]. We purified this RING peptide and added it at high concentrations to Xenopus egg extracts. Importantly, this disrupted the endogenous BRCA1-BARD1 complex, and it caused a similar defect in Approach and CMG unloading as BRCA1 depletion (Figure 6A-D [3]). In contrast, a mutant RING peptide that binds poorly to BRCA1 had no effect (Figure 6B-D in [3]). These data support our model that the BRCA1-BARD1 complex is involved in CMG unloading.

To further investigate the role of BRCA1 in ICL repair and CMG unloading, we sought to inhibit BRCA1-BARD1 binding to ICLs. The BRCA1-BARD1 complex is recruited to sites of DNA damage by ubiquitin signaling [8]. To disrupt ubiquitin signaling, we employed ubiquitin vinyl-sulfone (UbVS), a specific, irreversible inhibitor of deubiquitylating enzymes. Incubation of *Xenopus* egg extract with UbVS blocks ubiquitin turnover, leading to the depletion of free ubiquitin [9]. Extracts were incubated with buffer, UbVS, or UbVS and excess free ubiquitin prior to addition of pICL. Although DNA synthesis was not significantly inhibited by the addition of UbVS (Figure 2A in [3]), ICL repair was abolished (Figure 2B in [3]). Repair was only partially rescued by the addition of free ubiquitin, suggesting that ubiquitin turnover is essential for efficient repair.

To examine the effect of UbVS on BRCA1 loading at ICLs, we used chromatin immunoprecipitation (ChIP). As shown in Figures 2C-E [3], Rap80, BRCA1, and FANCD2 were not recruited to ICLs when UbVS was present. Recruitment was rescued by the addition of free ubiquitin, indicating that recruitment defects were due to ubiquitin depletion.
To investigate how UbVS affects ICL repair, nascent strand products (Figure 2F in [3]) were analyzed by denaturing polyacrylamide gel electrophoresis. UbVS treatment had no effect on the arrival of leading strands at the ICL (Figure 2G in [3], compare lanes 7, 13, and 19), consistent with replication proceeding normally (Figure 2A in [3]). In contrast, UbVS completely blocked the Approach of leading strands to the -1 position, as well as formation of all downstream nascent strand products (Figure 2G in [3], compare lanes 7-11 with 13-17). Addition of free ubiquitin with UbVS restored Approach, Insertion, and Extension, albeit with delayed kinetics (Figure 2G in [3], lanes 19-23). Importantly, unloading of Cdc45, MCM7, and Sld5 was severely delayed in UbVS-treated reactions (Figure 2H-J in [3]). As for Approach, CMG unloading was partially restored by the addition of free ubiquitin. Together, these results demonstrate that ubiquitin signaling is required to both recruit BRCA1 and remove the CMG helicase from stalled replication forks, further supporting the idea that BRCA1 promotes CMG dissociation. Notably, addition of free ubiquitin did not efficiently restore ICL repair (Fig. 2B in [3]). This suggests that ubiquitin turnover is required for efficient ICL repair.

Two recent papers showed that at the end of S phase, the MCM7 subunit of CMG is ubiquitylated [10, 11]. Furthermore, they showed that CMG removal from chromatin requires the p97 ATPse (or "segregase"), which extracts ubiquitylated proteins from membranes or multi-protein complexes. These results suggest that during replication termination, the MCM7 subunit of CMG is ubiquitylated and that CMG is subsequently removed from the chromatin.

We asked whether p97 is required for CMG unloading during ICL repair. To this end, we replicated plasmids containing cisplatin or psoralen ICLs in egg extracts containing DMSO or the specific p97 inhibitor NMS-873 [12]. At different times, we performed ChIP of CDC45, a component of CMG. In the presence of NMS-873, there was a large delay in the dissociation of CDC45 from chromatin on both DNA templates (Figure 2). We repeated this experiment but pulled down the plasmid and then blotted for MCM6 and Cdc45. As shown in Figure 3, this approach confirmed that p97 inhibition blocked CMG unloading. Therefore, as seen during replication termination, the removal of CMG complexes from chromatin during ICL repair requires p97.

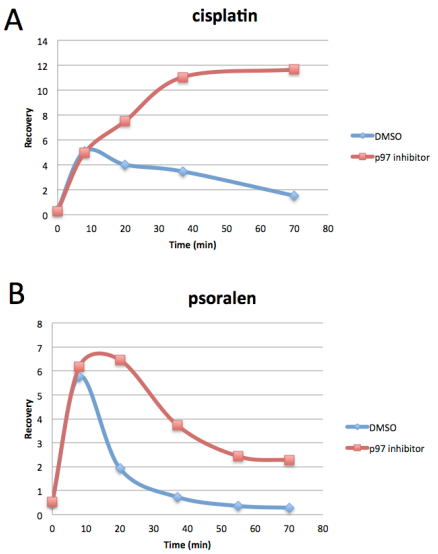

Figure 2: p97 is required for CMG unloading – ChIP assay. A plasmid containing a cisplatin (A) or psoralen (B) ICL was replicated in egg extract in the presence DMSO (blue traces) or NMS-873, a specific inhibitor of p97 (red traces). At different times, chromatin samples were subjected to Cdc45 ChIP.

We are also examining whether MCM7 is ubiquitylated during ICL repair. We first addressed whether we could detect the ubiquitylation of MCM7 during replication of undamaged DNA, as reported [10, 11]. To this end, we replicated a plasmid in egg extract. At the peak of replication, plasmid was recovered and the isolated chromatin was blotted for MCM7. As shown in Figure 4, lane 1, a ladder of MCM7 species was readily detected, which resembled the ubiquitylated species previously reported [10]. When the extract was supplemented with ubiquitin vinyl sulfone, an inhibitor of de-ubiquitylating enzymes that reduces free ubiquitin levels in the extract [13], the extent of MCM7 modification was diminished (Figure 4, lane 2), consistent with the slow-migrating bands representing ubiquitylated forms of MCM7.

Figure 3: p97 is required for CMG unloading – plasmid pull-down assay. Plasmids containing a cisplatin or psoralen ICL were replicated in the presence DMSO or NMS-873, as indicated. At different times, plasmids were pulled down and the chromatin samples blotted for the indicated antibodies.

To confirm that the modified MCM7 species detected are ubiquitylated, we replicated plasmid in egg extracts supplemented with 6xhis-tagged ubiquitin. At the peak of replication, we stopped the reaction and passed the extract over nickel beads to recover the 6xhis ubiquitin, and we blotted for MCM7. As shown in Figure 5, the MCM7 blot contained a similar series of species as shown in Figure 4. In the absence of DNA, most of the slow migrating forms of MCM7 in the precipitate disappeared (except for one band, that represents a replication-independent ubiquitylation form of MCM7). The data show that the slow mobility forms of MCM7 are ubiquitylated and that the modification is DNA-dependent.

We will now test whether MCM7 ubiquitylation occurs during ICL repair and whether this event depends on BRCA1-BARD1. If so, it will support our model that when two replication forks converge on an ICL, BRCA1-BARD1 promotes the ubiquitylation of MCM7, which in turn leads to the removal of the CMG complex from chromatin via the p97 ATPase.

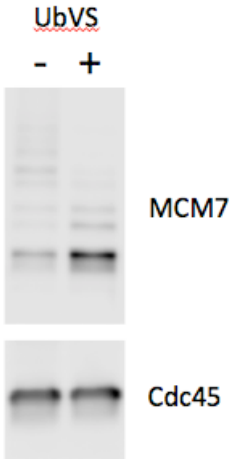

Figure 4: MCM7 is modified during DNA replication. Plasmid was replicated in Xenopus egg extract, recovered, and the chromatin fraction blotted with antibodies against MCM7 and PCNA.

The overarching goal of this proposal is to develop new cell-free approaches to study BRCA1, including its various functional motifs. A major cellular role of BRCA1 is to regulate whether a double-strand break is repaired via homologous recombination or non-homologous end-joining (NHEJ) [14]. BRCA1 is thought to favor the homologous recombination pathway by promoting resection, the first event in HR that is also inhibitory for NHEJ [14]. As a first step towards reconstituting this function of BRCA1 in vitro, we addressed whether NHEJ could be faithfully recapitulated in frog egg extracts. To this end, we incubated blunt-ended, radiolabeled, linear DNA molecules in egg extracts and monitored ligation of the

DNA ends via the appearance of circular DNA molecules. We found that frog egg extracts efficiently ligate DNA ends in a manner that depends on KU70/80 (Figure 1A in [15]; see appendix), DNA-PK (Figure 1C in [15]), XLF (Figure 1D in [15]), and DNA LIGASE 4-XRCC4 (Figure 1D in [15]). In addition, ligation depends on the catalytic activity of DNA-PKcs (Figure 1B in [15]). Therefore, NHEJ in frog egg extracts requires the four core NHEJ factors that are essential for NHEJ in cells. Importantly, in nucleoplasmic extracts derived from frog eggs, NHEJ is suppressed due to active resection (data not shown). Since these extracts also contain the NHEJ machinery, something must be tipping the balance in favor of resection. We hypothesize that BRCA1 is integral to this activity, and in the future, we will test this idea by immunodepleting BRCA1 from the nucleoplasmic extract. If NHEJ is favored in the absence of BRCA1, it will allow us to determine how BRCA1 promotes HR and suppresses NHEJ. In this event, we will seek to rescue the defect with WT BRCA1, as well as the various mutants of BRCA1 described at the beginning of this section.

Another important function of BRCA1 is to promote homology-directed repair of one-ended double stranded DNA breaks such as occur during replication fork collapse. To reconstitute this event in egg extracts, we replicated a plasmid containing a single, site-specific nick. When a replication fork reaches the nick in the template strand, the fork breaks, yielding a one-ended dsDNA break (data not shown). We are now using immunodepletion of BRCA1 from egg extracts to determine whether BRCA1 promotes the repair of such breaks in egg extracts. Rescue will then be carried out with WT and mutant BRCA1 complexes.

5c. Deplete CTIP or FANCJ to determine whether this mimics any defects in ICL repair observed for the BRCA1^{S1379F}-BARD1 mutant.

Depletion of neither CTIP nor FANCJ mimicked the CMG unloading defect seen in BRCA1-depleted extracts (see task 3a).

Task 6. Identification of BRCA1 ubiquitylation targets via mass spectrometry analysis

6a. Prepare chromatin from BRCA1-depleted egg extracts supplemented with rBRCA1-BARD1 or rBRCA1^{I26A}-BARD1 in preparation for mass spectrometry analysis.

We have not performed this task because we have been unable to rescue BRCA1-depletion with recombinant BRCA1 protein.

6b. Send chromatin samples to our collaborators in Germany for mass spectrometry analysis.

We have not performed this task because we have been unable to rescue BRCA1-depletion with recombinant BRCA1 protein.

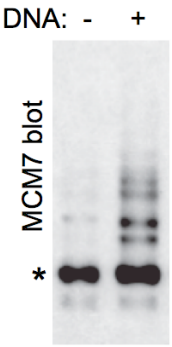

Figure 5: Modified forms of MCM7 are ubiquitylated. Plasmid was replicated in Xenopus egg extract in the presence of 6his-Ub. 6xhis was recovered and the isolated material blotted for MCM7.

6c. Ubiquitylation events that are BRCA1-dependent will be functionally characterized. For example, MCM2-7 with the ubiquitylation site(s) mutated to arginine will be expressed in insect cells and then added to MCM2-7-depleted egg extracts to determine the effects on ICL repair.

In preparation for mutational analysis of MCM2-7, we cloned and made viruses for all six subunits of the MCM2-7 complex. The MCM7 cDNA encodes a flag tag on its C-terminus. We then co-infected insect cells with all six viruses. After 48 hours, cells were lysed and the MCM2-7 complex was purified on Flag affinity resin. This yielded a substantial amount of pure MCM2-7 complex (Figure 6). However, we have found that this complex does not restore DNA replication in egg extracts immunodepleted of MCM2-7 (data not shown). To improve the expression and purification of MCM2-7, we invested a lot of time and effort to move to a multi-bac system in which all six MCM subunits are encoded by the same baculovirus. We have also prepared many multi-bac viruses in which the MCM2-7 complex is tagged on different subunits and either at the N-terminus or C-terminus. We are currently purifying these proteins and will test which (if any) are functional for DNA replication. Once a functional MCM2-7 complex is obtained, we will mutate key lysine residues to identify those whose ubiquitylation is required for CMG unloading during ICL repair.

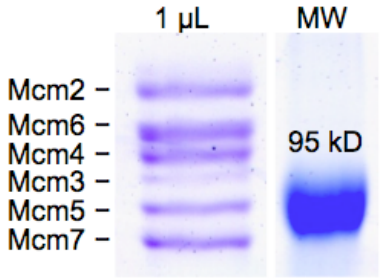

Figure 6: Purified MCM2-7 complex. One µl of MCM2-7 complex purified from insect cells was analysed via SDS page alongside a MW ladder and stained with Coomassie blue.

Training opportunities
The trainees listed below profited greatly from their association with this project. In all cases, they learned a powerful approach (cell-free egg extracts) to interrogate genome maintenance processes and underwent rigorous training in the design and interpretation of molecular biology experiments, including weekly meetings with the PI. All trainees were heavily involved in the preparation of scientific manuscripts and therefore learned a lot about effective scientific writing. On the strength of his work on this project, David Long obtained an Assistant Professor position at the Medical University of South Carolina. Julien Duxin will start a Group Leader position at the Novo Nordisk Foundation Center for Protein Research in Copenhagen, Denmark. Thomas Graham will start a post-doctoral position in the laboratory of Vanessa Ruta at Rockefeller University.

Dissemination of results
The results were disseminated primarily via talks given by the PI at conferences and universities (see below), and through publications (see below).

Plans for next reporting period
Not applicable (Final report)

4. Impact
Impact on discipline
To date, it has been assumed that BRCA1's primary role in ICL repair is to support homologous recombination. However, our data strongly support the novel concept that BRCA1 also promotes the first step in ICL repair, the removal of the replicative DNA helicase from forks that have stalled at the lesion. This insight sheds new light on the mechanism by which BRCA1 might suppress genome instability and cancer. We are now trying to understand how BRCA1 performs this function. An obstacle has been our inability so far to rescue the BRCA1 depletion with purified BRCA1-BARD1 complex. Co-depletion of FANCM, FANCJ, ABRAXAS, and CTIP does not appear to be the underlying cause of this failure. In an important new insight, we have found that the p97 ATPase is required for CMG unloading. We favor a model in which BRCA1-BARD1 ubiquitylates CMG on the MCM7 subunit, followed by CMG extraction from chromatin by the p97 ATPase. As outlined above, we have also developed other cell-free systems to interrogate BRCA1 function. Together, our data will significantly impact our understanding of BRCA1's role in tumor suppression.

Impact on other disciplines
Nothing to report

Impact on technology transfer
Nothing to report

Impact on society beyond science and technology
Nothing to report

5. Changes/Problems
Nothing to report

6. Products
Publications, conference papers, and presentations

Journal Publications:
1. Long, D.T., Joukov, V., Budzowska, M., and Walter, J.C. (2014). BRCA1 promotes unloading of the CMG helicase from a stalled DNA replication fork. ***Molecular Cell*** 56, 174-185.

2. Graham, T.G., Walter, J.C.*, and Loparo, J.J.* (2016). Two-stage synapsis of DNA ends during non-homologous end-joining. ***Molecular Cell*** 61, 850-8.
* co-corresponding authors

Presentations:

2013	Invited Speaker	University of Toronto, Canada
2013	Invited Seminar	Memorial Sloan Kettering Molecular Biology Program, New York

2013	Invited Seminar	Harvard University, Cambridge
2013	Invited Seminar	UMASS, Worcester
2014	Invited Speaker	National Cancer Institute, Amsterdam, Netherlands
2014	Invited Seminar	CNIO, Madrid, Spain
2014	Invited Speaker	Cell Proliferation and Genome Integrity Conference, Santander, Spain
2014	Invited Speaker	ABCAM Maintenance of Genome Stability Meeting, St. Kitts
2014	Invited Speaker	Department of Biochemistry and Molecular Biology, Mayo Clinic, Rochester
2014	Invited Speaker	DNA repair conference, Beijing
2014	Invited Seminar	Blaffer Lecture at the MD Anderson Cancer Center, Houston, TX
2014	Invited Seminar	University of Montreal, Canada
2015	Invited Seminar	Department of Biochemistry, Stanford University
2015	Invited Speaker	Gordon Research Conference, Mammalian DNA Repair, Ventura, CA
2015	Invited Seminar	Salk Institute, La Jolla, CA
2015	Invited Speaker	Keystone Genome Integrity Meeting, Canada
2015	Keynote Speaker	Salk Institute Cell Cycle Meeting ("Newport Lecture")
2015	Invited Speaker	FASEB DNA helicases meeting, Steamboat Springs, Colorado
2015	Invited Speaker	Gordon Research Conference, Nucleic Acids, University of New England
2015	Invited Seminar	University of Zurich, Switzerland
2015	Invited Seminar	Department of Biology, MIT, Boston
2015	Invited Seminar	Gene Regulation and Genomics Seminar Series, UT Southwestern
2016	Keynote Speaker	Gordon Research Seminar on Mutagenesis, Ventura, CA
2016	Invited Speaker	ABCAM Maintenance of Genome Stability Meeting, Panama
2016	Invited Speaker	DNA repair conference, Egmond an Zee, Netherlands
2016	Keynote Speaker	Buffalo Area DNA Replication and Repair Meeting, Buffalo, NY

Websites
Nothing to report

Technologies or techniques
We developed a novel single molecule assay for non-homologous end joining [15].

Inventions, patents, licenses
Nothing to report

Other products
We generated antibodies to Xenopus laevis BRCA2 [3], RAP80 [3], XLF [15], XRCC4 [15], and KU80 [15], which we will distribute freely to other researchers.

7. Participants and other collaborating organizations

Individuals who worked on the project

Name:	Johannes Walter
Project Role:	PI
Person months:	8
Contribution:	Supervised project.
Funding support:	From 12/1/2013-present, salary was paid by the Howard Hughes Medical Institute

Name:	David Long
Project Role:	Post-doctoral fellow
Person months:	12
Contribution:	Dr. Long investigated the role of BRCA1 in promoting CMG unloading and sought to perform a structure function analysis of the BRCA1 protein.
Funding support:	NIH K99 award

Name:	Vladimir Joukov
Project Role:	Post-doctoral fellow

Person months: 18
Contribution: Dr. Joukov investigated whether the BRCA1-controlled CMG unloading step is affected in the absence of FANCJ, CTIP, or ABRAXAS.

Name: Kyle Vrtis
Project Role: Post-doctoral fellow
Person months: 13
Contribution: Dr. Vrtis developed the cell-free system that will be used to examine the role of BRCA1 in replication fork breakage.

Name: Ravi Amunugama
Project Role: Post-doctoral fellow
Person months: 13
Contribution: Dr. Amunugama investigated the role of BRCA1-dependent fork remodeling during ICL repair.

Name: Julien Duxin
Project Role: Post-doctoral fellow
Person months: 14
Contribution: Dr. Duxin investigated the role of CMG unloading in DNA repair.

Name: Thomas Graham
Project Role: Graduate Student
Person months: 10
Contribution: Mr. Graham developed the cell-free system that will be used to examine the role of BRCA1 in DSB repair.

Change in active support since last reporting period
Nothing to report

Other organizations involved as partners
Nothing to report

8. Special reporting requirements
Nothing to report

References

1. Bunting, S.F., Callen, E., Kozak, M.L., Kim, J.M., Wong, N., Lopez-Contreras, A.J., Ludwig, T., Baer, R., Faryabi, R.B., Malhowski, A., et al. (2012). BRCA1 Functions Independently of Homologous Recombination in DNA Interstrand Crosslink Repair. Molecular cell.
2. Raschle, M., Knipscheer, P., Enoiu, M., Angelov, T., Sun, J., Griffith, J.D., Ellenberger, T.E., Scharer, O.D., and Walter, J.C. (2008). Mechanism of replication-coupled DNA interstrand crosslink repair. Cell *134*, 969-980.
3. Long, D.T., Joukov, V., Budzowska, M., and Walter, J.C. (2014). BRCA1 promotes unloading of the CMG helicase from a stalled DNA replication fork. Mol Cell *56*, 174-185.
4. Fu, Y.V., Yardimci, H., Long, D.T., Guainazzi, A., Bermudez, V.P., Hurwitz, J., van Oijen, A., Scharer, O.D., and Walter, J.C. (2011). Selective Bypass of a Lagging Strand Roadblock by the Eukaryotic Replicative DNA Helicase. Cell *146*, 931-941.
5. Raschle, M., Knipsheer, P., Enoiu, M., Angelov, T., Sun, J., Griffith, J.D., Ellenberger, T.E., Scharer, O.D., and Walter, J.C. (2008). Mechanism of replication-coupled DNA interstrand crosslink repair. Cell *134*, 969-980.
6. Zhang, J., Dewar, J.M., Budzowska, M., Motnenko, A., Cohn, M.A., and Walter, J.C. (2015). DNA interstrand cross-link repair requires replication-fork convergence. Nat Struct Mol Biol.
7. Westermark, U.K., Reyngold, M., Olshen, A.B., Baer, R., Jasin, M., and Moynahan, M.E. (2003). BARD1 participates with BRCA1 in homology-directed repair of chromosome breaks. Molecular and cellular biology *23*, 7926-7936.
8. Yan, J., and Jetten, A.M. (2008). RAP80 and RNF8, key players in the recruitment of repair proteins to DNA damage sites. Cancer Lett *271*, 179-190.
9. Dimova, N.V., Hathaway, N.A., Lee, B.H., Kirkpatrick, D.S., Berkowitz, M.L., Gygi, S.P., Finley, D., and King, R.W. (2012). APC/C-mediated multiple monoubiquitylation provides an alternative degradation signal for cyclin B1. Nature cell biology *14*, 168-176.
10. Moreno, S.P., Bailey, R., Campion, N., Herron, S., and Gambus, A. (2014). Polyubiquitylation drives replisome disassembly at the termination of DNA replication. Science *346*, 477-481.

11. Maric, M., Maculins, T., De Piccoli, G., and Labib, K. (2014). Cdc48 and a ubiquitin ligase drive disassembly of the CMG helicase at the end of DNA replication. Science *346*, 1253596.
12. Magnaghi, P., D'Alessio, R., Valsasina, B., Avanzi, N., Rizzi, S., Asa, D., Gasparri, F., Cozzi, L., Cucchi, U., Orrenius, C., et al. (2013). Covalent and allosteric inhibitors of the ATPase VCP/p97 induce cancer cell death. Nature chemical biology *9*, 548-556.
13. Dimova, N.V., Hathaway, N.A., Lee, B.H., Kirkpatrick, D.S., Berkowitz, M.L., Gygi, S.P., Finley, D., and King, R.W. (2012). APC/C-mediated multiple monoubiquitylation provides an alternative degradation signal for cyclin B1. Nat Cell Biol *14*, 168-176.
14. Ceccaldi, R., Rondinelli, B., and D'Andrea, A.D. (2016). Repair Pathway Choices and Consequences at the Double-Strand Break. Trends Cell Biol *26*, 52-64.
15. Graham, T.G., Walter, J.C., and Loparo, J.J. (2016). Two-Stage Synapsis of DNA Ends during Non-homologous End Joining. Mol Cell *61*, 850-858.

9. Appendices

1. Long, D.T., Joukov, V., Budzowska, M., and Walter, J.C. (2014). BRCA1 promotes unloading of the CMG helicase from a stalled DNA replication fork. ***Molecular Cell*** 56, 174-185.

2. Graham, T.G., Walter, J.C.*, and Loparo, J.J.* (2016). Two-stage synapsis of DNA ends during non-homologous end-joining. ***Molecular Cell*** 61, 850-8.

CellPress

Molecular Cell
Article

BRCA1 Promotes Unloading of the CMG Helicase from a Stalled DNA Replication Fork

David T. Long,[1,3] Vladimir Joukov,[1] Magda Budzowska,[1] and Johannes C. Walter[1,2,*]
[1]Department of Biological Chemistry and Molecular Pharmacology
[2]Howard Hughes Medical Institute
Harvard Medical School, Boston, MA 02115, USA
[3]Present address: Department of Biochemistry and Molecular Biology, Medical University of South Carolina, Charleston, SC 29425, USA
*Correspondence: johannes_walter@hms.harvard.edu
http://dx.doi.org/10.1016/j.molcel.2014.08.012

SUMMARY

The tumor suppressor protein BRCA1 promotes homologous recombination (HR), a high-fidelity mechanism to repair DNA double-strand breaks (DSBs) that arise during normal replication and in response to DNA-damaging agents. Recent genetic experiments indicate that BRCA1 also performs an HR-independent function during the repair of DNA interstrand crosslinks (ICLs). Here we show that BRCA1 is required to unload the CMG helicase complex from chromatin after replication forks collide with an ICL. Eviction of the stalled helicase allows leading strands to be extended toward the ICL, followed by endonucleolytic processing of the crosslink, lesion bypass, and DSB repair. Our results identify BRCA1-dependent helicase unloading as a critical, early event in ICL repair.

INTRODUCTION

Mutations in *BRCA1* predispose individuals to hereditary breast and ovarian cancers (Narod and Foulkes, 2004). Growing evidence also indicates that BRCA1 loss plays an important role in the development of sporadic cancers (Chalasani and Livingston, 2013; De Leeneer et al., 2012). In the absence of BRCA1, cells develop multiple chromosomal abnormalities, implicating genome maintenance in tumor suppression (Zhang, 2013). Consistent with this, BRCA1 has been linked to various aspects of the DNA damage response (Wu et al., 2010) including error-free repair of DNA double-strand breaks (DSBs) (Bekker-Jensen and Mailand, 2010).

BRCA1 forms a heterodimeric complex with BARD1 (BRCA1-associated RING domain protein 1), which is required for BRCA1 stability and function (Choudhury et al., 2004; Westermark et al., 2003). BRCA1 activity is also modulated by numerous protein interactions that form distinct BRCA1-containing complexes (Silver and Livingston, 2012; Wang, 2012). In response to DSBs, BRCA1 regulates repair pathway choice, promoting template-directed repair by homologous recombination (HR) over nonhomologous end joining (NHEJ), an error-prone pathway (Kass and Jasin, 2010). BRCA1 is thought to support resection of DSB ends, leading to the generation of a 3′ single-stranded DNA (ssDNA) tail that is bound by the RAD51 recombinase. BRCA1 also associates with BRCA2 (via PALB2/FANCN) (Zhang et al., 2009), which stimulates RAD51 loading onto ssDNA (Jensen et al., 2010; Liu et al., 2010).

BRCA1-deficient cells are sensitive to various DNA-damaging agents, including DNA interstrand crosslinks (ICLs) (Bhattacharyya et al., 2000). ICLs covalently link the two strands of the double helix, thereby blocking cellular processes that require strand separation, such as DNA replication and transcription. Cellular resistance to ICLs is dependent on both the BRCA and Fanconi anemia (FANC) proteins, which act together in a common DNA repair pathway (Kim and D'Andrea, 2012). ICL repair involves a DSB intermediate, which is formed after replication forks collide with an ICL (Räschle et al., 2008; McHugh et al., 2001). As such, ICL sensitivity in BRCA1-deficient cells has been attributed primarily to BRCA1's HR functions.

Recent genetic data indicate that BRCA1 has an additional function during ICL repair that is distinct from its established role in HR. In 2010, Nussenzweig's group showed that the HR defect in *BRCA1*-deficient cells is almost completely reversed by mutation of 53BP1 (Bunting et al., 2010), an NHEJ protein that modulates chromatin structure at DNA breaks. These results argued that the primary function of BRCA1 in DSB repair is to promote resection by antagonizing 53BP1. More recently, they discovered that loss of 53BP1 does not rescue the ICL sensitivity observed in *BRCA1*-deficient cells, even though RAD51 foci formation was largely restored (Bunting et al., 2012). These results argue that BRCA1 performs an additional function in ICL repair that is independent of DSB resection, RAD51 loading, and 53BP1. Notably, FANCD2 foci formation was impaired in *BRCA1*-deficient cells after exposure to DNA crosslinking agents (Bunting et al., 2012), suggesting that BRCA1's HR-independent function might involve recruitment of FANCD2 to ICLs.

Using *Xenopus* egg extracts, we previously established a cell-free system that recapitulates replication-coupled repair of a single, site-specific cisplatin ICL on a plasmid (pICL; Figure 1A) (Räschle et al., 2008). Error-free removal of the crosslink regenerates a SapI restriction site, which is used to assay repair. Upon addition of pICL to egg extracts, replication initiates at a random location, and two replication forks rapidly converge on the ICL and stall (Figure 1Bi). The 3′ ends of the two stalled leading strands are initially located ~20–40 nucleotides from the

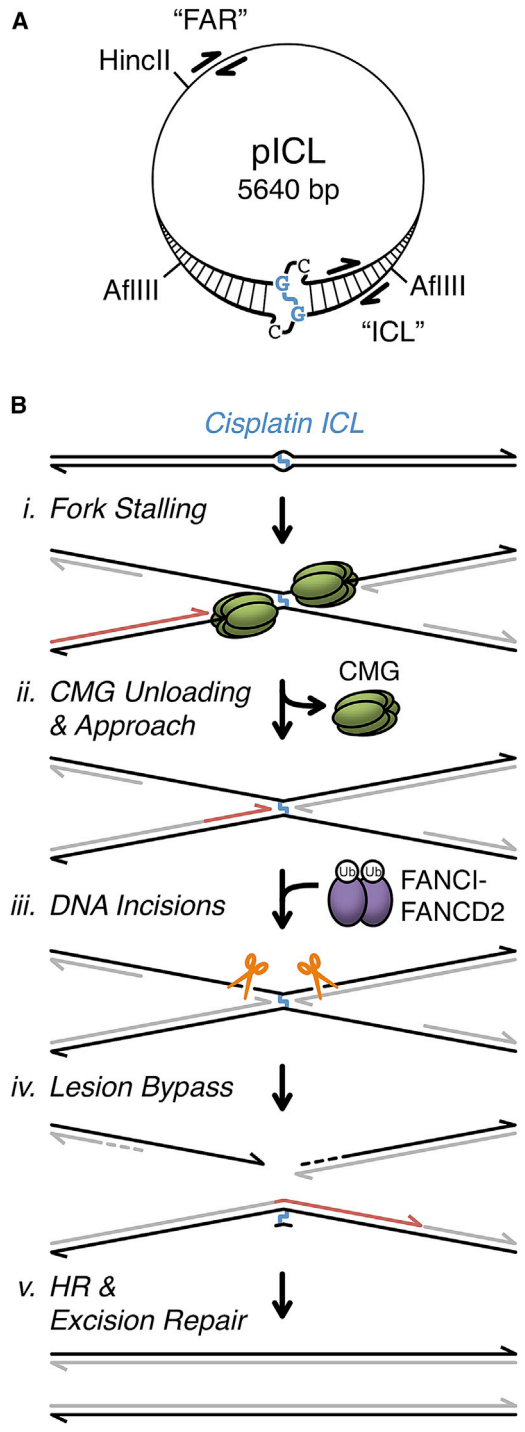

Figure 1. ICL Repair in *Xenopus* Egg Extract

(A) pICL schematic. ICL and crosslinked nucleotides are shown in blue. ChIP primer pairs are shown for "ICL" (25–132 bp from ICL) and "FAR" (2,523–2,622 bp from ICL) loci.

(B) Model of ICL repair (Fu et al., 2011; Knipscheer et al., 2009; Long et al., 2011; Räschle et al., 2008). Parental DNA strands are black, and nascent strands are gray, or red for emphasis. CMG, replicative helicase complex comprised of Cdc45, MCM7, and Sld5; Ub, ubiquitin. See Figure S7 for revised model.

crosslink ("-20 position"). After an ~15 min delay, the leading strands are extended to within one nucleotide of the crosslink ("-1 position"). Extension of leading strands from -20 to -1 ("Approach;" Figure 1Bii) occurs concurrently with unloading of the CMG replicative DNA helicase (Fu et al., 2011), which is comprised of Cdc45, *M*CM2-7, and *G*INS (Ilves et al., 2010). Based on this correlation, we proposed that leading strand stalling at -20 is due to steric hindrance by CMG, and that Approach requires CMG unloading (Fu et al., 2011). Concurrent with Approach, the FANC pathway is activated, leading to monoubiquitylation of the FANCI-FANCD2 complex. Ubiquitylated FANCI-FANCD2 promotes incisions by XPF-ERCC1 and possibly other endonucleases, creating a DSB in one sister chromatid (Figure 1Biii) (Klein Douwel et al., 2014; Knipscheer et al., 2009). The leading strand is then extended past the unhooked ICL by translesion DNA polymerases (Figure 1Biv), creating an intact template for recombination-mediated repair of the DSB (Figure 1Bv) (Long et al., 2011). Finally, the unhooked adduct is probably removed by excision repair (Muniandy et al., 2010), although this event does not occur in egg extracts.

Here we show that ubiquitin signaling targets BRCA1 to ICL-stalled forks where BRCA1 promotes unloading of the CMG helicase, allowing Approach and subsequent ICL repair. Our results identify CMG unloading as a critical, early event in ICL repair and identify a new function for BRCA1 in the DNA damage response.

RESULTS

Ubiquitin Signaling Is Required for Chromatin Unloading of the Replicative Helicase

Ubiquitin signaling plays an integral role in targeting repair factors to sites of damaged chromatin (Pinder et al., 2013). To investigate the role of ubiquitin signaling in ICL repair, we employed ubiquitin vinyl sulfone (UbVS), a highly specific, irreversible inhibitor of deubiquitylating enzymes (Borodovsky et al., 2001). Incubation of *Xenopus* egg extract with UbVS blocks ubiquitin turnover, leading to the depletion of free ubiquitin (Dimova et al., 2012). Extracts were incubated with buffer, UbVS, or UbVS and excess free ubiquitin prior to addition of pICL. Although DNA synthesis was not significantly inhibited by the addition of UbVS (Figure 2A), ICL repair was abolished (Figure 2B). Only a limited amount of repair was rescued by the addition of free ubiquitin, suggesting that turnover of ubiquitylated substrates is important for repair, even in the presence of excess ubiquitin (Nijman et al., 2005; Oestergaard et al., 2007). Consistent with this idea, addition of free ubiquitin reversed the FANCD2 ubiquitylation defect caused by UbVS, but did not restore the FANCD2 deubiquitylation that is normally observed late in the reaction (Figures S1A and S1B available online).

DSBs trigger a histone modification cascade that includes histone ubiquitylation and subsequent recruitment of various repair factors to the site of damage, including Rap80, BRCA1, and FANCD2 (Wang et al., 2004; Yan and Jetten, 2008). To determine whether a similar response is activated during ICL repair in egg extracts, we used chromatin immunoprecipitation (ChIP) to analyze protein recruitment to pICL. As shown in Figures 2C–2E,

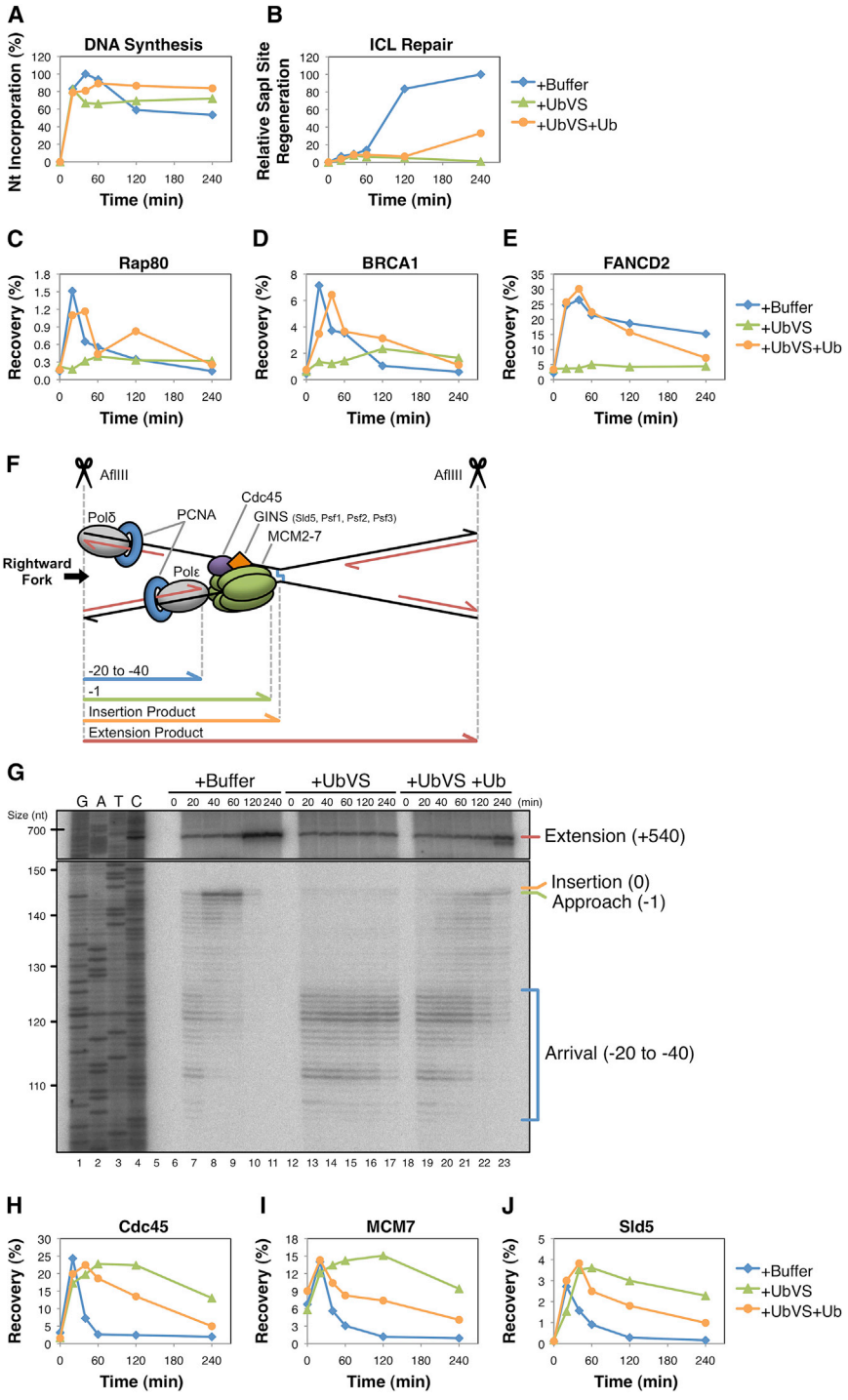

Figure 2. Ubiquitin Signaling Is Required for Replicative Helicase Unloading

(A and B) pICL was replicated in egg extract supplemented with buffer (+Buffer), 14 μM UbVS (+UbVS), or 14 μM UbVS and 50 μM ubiquitin (+UbVS+Ub). Samples were analyzed by agarose gel electrophoresis to determine the efficiency of (A) replication and (B) ICL repair (described in Experimental Procedures).

(C–E) Protein recruitment to the ICL was analyzed by ChIP with the indicated antibodies.

(F) Schematic of leading strand intermediates from the rightward moving fork as it bypasses the ICL.

(G) Nascent strand products were analyzed by denaturing PAGE.

(H–J) ICL recruitment was analyzed by ChIP with the indicated antibodies. Note that the MCM7 ChIP signal starts high because MCM2-7 has already been loaded onto DNA at the 0 min time point as a result of licensing in HSS extract (see Experimental Procedures). All data shown was analyzed from a single experiment. See Figure S1 for primary gel data, ChIP recovery at the FAR locus, quantification of nascent strand products, and experimental replicates.

Rap80, BRCA1, and FANCD2 were each recruited to ICLs, but not when UbVS was present. Recruitment was rescued by the addition of free ubiquitin, indicating that recruitment defects were due to ubiquitin depletion.

To investigate how UbVS affects ICL repair, nascent strand products (Figure 2F) were analyzed by denaturing PAGE. UbVS treatment had no effect on the arrival of leading strands at the ICL (Figure 2G; compare lanes 7, 13, and 19; Figures S1K–S1Q for experimental replicates), consistent with replication proceeding normally (Figure 2A). In contrast, UbVS completely blocked the Approach of leading strands to the -1 position, as well as formation of all downstream nascent strand products (Figure 2G; compare lanes 7–11 with lanes 13–17). Addition of free ubiquitin with UbVS restored Approach, Insertion, and Extension, albeit with delayed kinetics (Figure 2G; lanes 19–23).

We showed previously that Approach correlates with dissociation of the CMG helicase (Fu et al., 2011). These results suggested that failure of the Approach step after ubiquitin depletion might be caused by persistence of CMG at the ICL. To test this idea, several helicase components were analyzed by ChIP. Strikingly, unloading of Cdc45, MCM7, and Sld5 was severely delayed in UbVS-treated reactions (Figures 2H–2J). As for Approach, CMG unloading was partially restored by the addition of free ubiquitin. Together, these results demonstrate that ubiquitin signaling is required to remove the CMG helicase from replication forks after collision with an ICL, and they support our previous hypothesis (Fu et al., 2011) that helicase removal is an essential, early, and active process associated with ICL repair.

BRCA1 Functions at Stalled Forks Prior to DSB Formation

We wanted to know which ubiquitin-dependent pathway promotes CMG unloading. We showed previously that failure to ubiquitylate FANCD2 blocks incisions, which occur downstream of Approach and CMG unloading (Fu et al., 2011; Knipscheer et al., 2009). Defective FANCD2 ubiquitylation therefore cannot account for the effect of UbVS. Notably, recent evidence indicates that BRCA1 has an HR-independent role in ICL repair (Bunting et al., 2012), and that it contributes to fork stability (Silver and Livingston, 2012). Given that ubiquitin signaling is required for BRCA1 recruitment (Figure 2D), we postulated that BRCA1 might function as an effector of ubiquitin signaling in ICL repair.

To investigate how BRCA1 contributes to ICL repair, we first used ChIP to address when BRCA1 is recruited to ICLs relative to other events of repair. Fifteen minutes after replication of pICL was initiated, MCM7 and Cdc45 accumulated at the crosslink, coincident with fork convergence (Figure 3A) (Fu et al., 2011). The ssDNA-binding protein RPA initially accumulated at the ICL with converging forks, but after a short delay, its abundance increased further (Figure 3A; red trace), likely due to lagging strand resection (Räschle et al., 2008). BRCA1 and its binding partner BARD1 were recruited to the crosslink ~7–10 min after fork convergence and well before the disappearance of converged fork structures, which are lost as a result of dual incisions (Figure 3B). Notably, BRCA2, RAD51, FANCI, and FANCD2 were all recruited ~5 min after BRCA1 (Figure 3C), consistent with BRCA1's established role in the recruitment of these proteins to sites of DNA damage (Bhattacharyya et al., 2000; Garcia-Higuera et al., 2001; Greenberg et al., 2006; Smogorzewska et al., 2007). Collectively, the data are consistent with BRCA1 having an early role at stalled forks prior to DSB formation (Bunting et al., 2012).

To determine whether BRCA1 is required for cell-free ICL repair, pICL was replicated in mock-depleted or BRCA1-depleted egg extract (Figure 3D). Although replication of pICL occurred with similar kinetics in both reactions (Figure 3E), ICL repair was delayed by at least 1 hr in BRCA1-depleted extracts (Figure 3F). A small amount of BRCA1 was still recruited to the crosslink at late times in BRCA1-depleted reactions (Figure 3G; green trace). As such, the delayed appearance of repair products (Figure 3F; green trace) may be due to residual BRCA1 not removed by depletion.

Consistent with immunofluorescence localization studies in mammalian cells (Bhattacharyya et al., 2000; Garcia-Higuera et al., 2001; Greenberg et al., 2006), recruitment of BRCA2, RAD51, and FANCD2 to ICLs was reduced in the absence of BRCA1 (Figures 3H–3J). These defects were not due to codepletion of BRCA2, RAD51, or FANCD2 from egg extract (Figure S2A). Although FANCD2 recruitment was impaired by BRCA1 depletion, FANCD2 ubiquitylation occurred normally (Figure 3D), consistent with previous reports (Bunting et al., 2012; Vandenberg et al., 2003). Loss of BRCA1 led to a severe incision defect (Figures 3K and 3L), indicating that FANCD2 ubiquitylation is not sufficient for DNA incisions without its localization to ICLs. High-level Chk1 phosphorylation was also delayed (Figure 3D; compare 60 min time points), consistent with a defect in DSB formation. Together, these results indicate that BRCA1 functions at ICL-stalled replication forks, where it recruits BRCA2, RAD51, and FANCD2.

BRCA1 Is Not Required for Resection at ICL-Stalled Forks

Given that BRCA1 has been implicated in resection of DSBs (Bouwman et al., 2010; Bunting et al., 2010; Schlegel et al., 2006; Yun and Hiom, 2009), we examined the BRCA1 dependence of this process in our cell-free system. Depletion of BRCA1 from extract led to a slight increase in the recruitment of RPA to ICLs (Figure 4A). However, when the amount of ssDNA on pICL was analyzed directly by quantitative PCR, similar levels of ssDNA were detected in mock-depleted and BRCA1-depleted reactions (Figures 4B–4D). These results argue that loss of BRCA1 does not compromise resection of ICL-stalled forks. Instead, defective RAD51 binding in the absence of BRCA1 (see Figure 3G) may elevate the amount of RPA present on chromatin.

BRCA1 Promotes CMG Unloading

We then analyzed the formation of nascent strand products in mock- and BRCA1-depleted reactions. As seen for UbVS-treated reactions, depletion of BRCA1 severely compromised the Approach of leading strands to the -1 position (Figure 5A; Figures S3G–S3J for experimental replicates). BRCA1 depletion also inhibited CMG unloading (Figures 5B–5D; Figures S3N–S3P for experimental replicates), as seen in UbVS-treated reactions. Notably, CMG unloading and Approach are not dependent on RAD51 (Long et al., 2011) or FANCD2 (Knipscheer et al., 2009), indicating that defective helicase removal in the absence of BRCA1 is not an indirect consequence of defective RAD51 or FANCD2 recruitment. Moreover, recruitment of BRCA1 to the ICL occurred shortly after the arrival of forks at -20 and just before the Approach to -1 (Figure S3A), consistent with BRCA1 playing a direct role in promoting Approach. Importantly, BRCA1 depletion had no significant effect on helicase unloading during replication of undamaged plasmids (Figures S3B–S3D). Together, these results indicate that BRCA1 is required to unload the replicative helicase from ICL-stalled forks, but not from forks undergoing termination.

When BRCA1-depleted extracts were supplemented with recombinant BRCA1-BARD1 heterodimer (Joukov et al., 2006), helicase eviction was not restored (data not shown), suggesting that the activity of the complex is dependent on additional binding factors or specific modifications (Silver and Livingston, 2012; Wang, 2012). Therefore, to further investigate whether BRCA1 is required for CMG unloading, BRCA1 activity was inhibited with a fragment of BARD1 (Westermark et al., 2003). BRCA1 and BARD1 interact through their respective RING domains, with two α helices from each domain combining to form a four-helix bundle (Brzovic et al., 2001). In cells, expression of a RING peptide was shown to inhibit BRCA1 function, leading to defects in HR and hypersensitivity to DNA crosslinking agents (Westermark et al., 2003). As reported previously (Joukov et al., 2001), BRCA1 antibodies quantitatively immunodepleted BARD1 from egg extract and vice versa (Figure S3E; lanes 4 and 6), demonstrating that BRCA1 and BARD1 are present as a stable 1:1 complex.

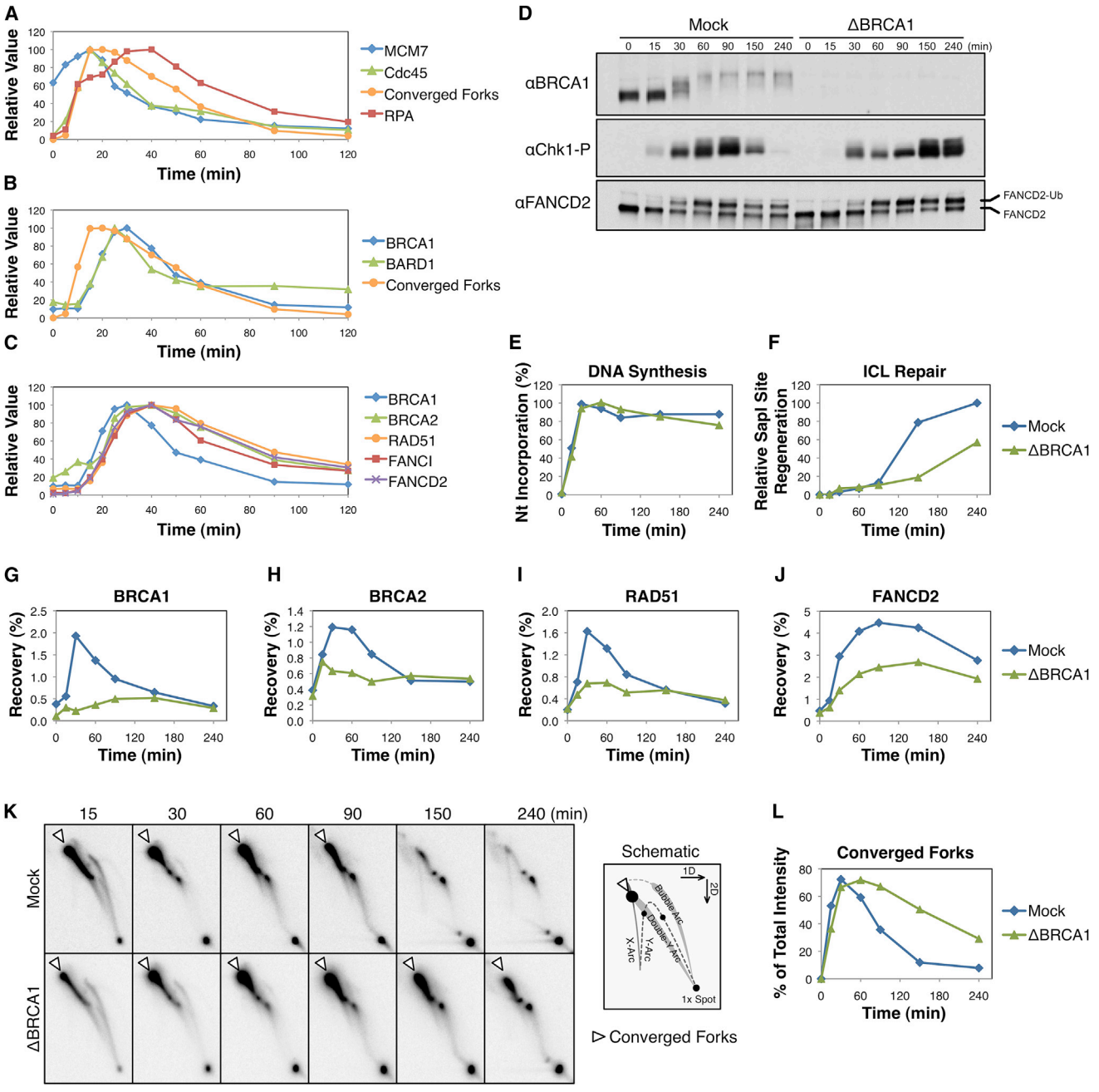

Figure 3. BRCA1 Has an Early Role at ICL-Stalled Forks

(A–C) pICL was replicated in egg extract, and ICL recruitment of various proteins was analyzed by ChIP. Samples were also analyzed for accumulation of ICL-stalled forks (Converged Forks) by agarose gel electrophoresis. Relative recovery shown with data normalized to peak accumulation. All data shown were analyzed from a single experiment with Converged Forks duplicated in (A) and (B), and BRCA1-ChIP duplicated in (B) and (C). pICL was replicated in mock-depleted (Mock) or BRCA1-depleted (ΔBRCA1) extract. Samples from the same reaction were analyzed by the following: western blot with the indicated antibodies (D), agarose gel electrophoresis to determine the efficiency of replication (E) and ICL repair (F), ChIP with the indicated antibodies (G–J), and 2D agarose gel electrophoresis (2DGE) (K) to analyze accumulation of converged forks (open arrowhead, see schematic and Figure 1Bi), which is quantified in (L). See Figure S2 for primary gel data, replicates of ICL repair data, and ChIP recovery at the FAR locus.

Importantly, BARD1 RING peptide ($RING^{WT}$) recovered BRCA1, but not BARD1 (Figure S3F; lane 5), arguing that the peptide disrupted the BRCA1-BARD1 complex. Insertion of a single-alanine residue into each α helix of the RING domain disrupted its binding to BRCA1 (Figure S3F; lane 7), and this mutant peptide ($RING^{AA}$) served as a negative control for BRCA1 inhibition.

When the $RING^{WT}$ peptide was added to egg extracts, it only slightly delayed Approach and CMG unloading (data not shown).

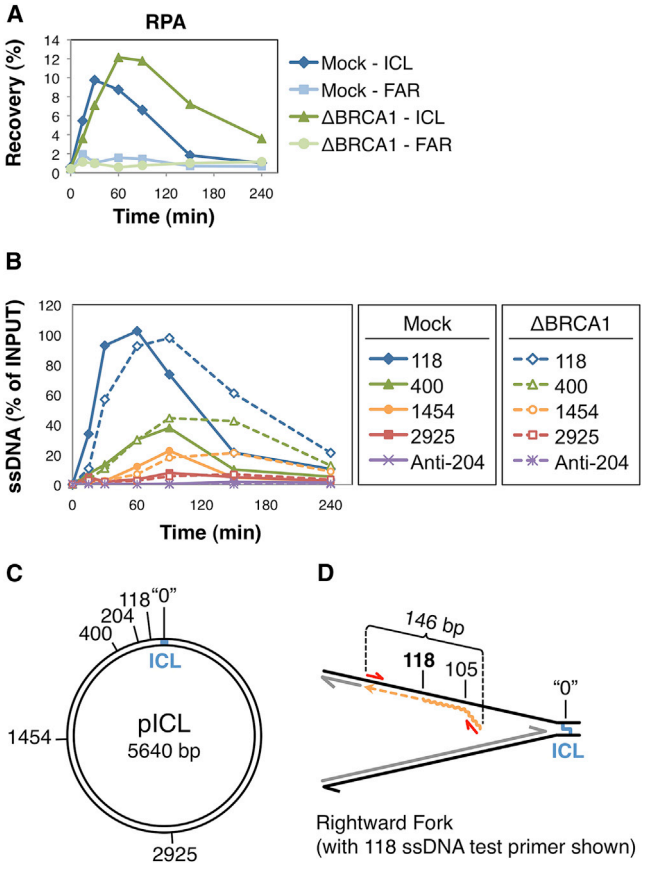

Figure 4. Analysis of Strand Resection during ICL Repair

(A–C) Mock-depleted and BRCA1-depleted samples from Figures 3D–3L were used to analyze the following: (A) RPA recruitment by ChIP, and (B) the presence of ssDNA by quantitative PCR (described in Experimental Procedures). The table indicates the distance in base pairs from the 3′ end of the Test primer to the ICL ("0"). The same information is also graphically indicated in (C).

(D) Stalled fork schematic showing the 118 ssDNA Test primer (wavy orange line), which is extended (dashed orange line) after annealing to ssDNA. Amplification of the extended Test primer with Left and Right primers (red arrows) produces a 146 bp product that is analyzed by quantitative PCR.

To improve the efficacy of peptide inhibition, we partially depleted BRCA1 prior to peptide addition. Depletion of BRCA1 to ~25% of endogenous levels (Figure S4A) by itself had little or no effect on any aspect of ICL repair measured (Figures 6A–6D and S4B–S4K; data not shown). However, when the partially depleted extract was supplemented with $RING^{WT}$ peptide, Approach and helicase unloading were both impaired (Figures 6A–6D; Figures S4B–S4K for experimental replicates). Importantly, the $RING^{AA}$ peptide caused no inhibition. Together, the data indicate that the integrity of the BRCA1-BARD1 complex is required to promote unloading of the CMG helicase complex and subsequent leading strand Approach.

During DSB repair, BRCA1 is recruited to DNA through a phosphospecific interaction with Abraxas (Wang et al., 2007). This interaction is mediated through BRCA1's tandem BRCT domains, which bind to a phospho-SXXF motif at the C terminus of Abraxas. To investigate the role that this interaction plays during ICL repair, egg extracts were supplemented with peptides containing the phospho-SXXF motif from Abraxas (pSPTF), or a nonphosphorylated control (SPTF). In the presence of pSPTF, recruitment of BRCA1 to the ICL was inhibited (Figure S4Q). BRCA1 recruitment was only partially inhibited by the SPTF peptide, consistent with the nonphosphorylated peptide having reduced affinity for BRCA1 (Wang et al., 2007). Notably, compared to SPTF, pSPTF had a greater inhibitory effect on Approach (Figure S4L; compare lanes 14 and 19) and CMG unloading (Figures S4R and S4S; compare 80 min time points). Together, these results argue that BRCA1's helicase-unloading activity is dependent on BRCT-mediated recruitment to chromatin.

CMG Unloading and Leading Strand Approach Support DNA Incisions

To determine the role that Approach plays in ICL repair, we sought to block this event by a direct and independent means that does not involve perturbation of BRCA1 or the ubiquitin system. To this end, pICL was replicated for 12 min to allow the majority of forks to arrive at the -20 position. Reactions were then split and supplemented with buffer or the DNA polymerase inhibitor aphidicolin (Errico et al., 2007). Aphidicolin-treated samples exhibited little or no Approach (Figure 7A), as well as an ~25% decrease in total nucleotide incorporation due to degradation of some forks that had not yet stalled at the crosslink (Figure 7B). ChIP showed that BRCA1, RAD51, and FANCD2 were still recruited to the ICL in aphidicolin-treated samples (Figures 7C–7E), although total recovery was also decreased by ~25%. In contrast, DNA incisions were inhibited, as measured by persistence of the converged fork structure (Figures 7F and S5I), and this mirrored what we observed in BRCA1-depleted reactions (Figure 3L). Together, these results indicate that Approach, and by extension, CMG unloading, are required for incisions and downstream repair events (Figure 7G). In addition, they show that BRCA1 helps recruit RAD51 and FANCD2 independently of Approach.

Both BRCA1 and Polymerase Extension Contribute to Helicase Unloading

Interestingly, blocking the Approach step with aphidicolin delayed CMG unloading (Figures S5J–S5L). These results suggested that the DNA polymerase also contributes to helicase removal. To investigate the relationship between BRCA1-dependent and polymerase-dependent helicase unloading, pICL was replicated in mock- or BRCA1-depleted extract until forks had stalled at the ICL. Each reaction was then split and supplemented with buffer or aphidicolin, as in Figure 7A. Analysis of the helicase complex by ChIP showed that BRCA1 depletion and aphidicolin treatment caused additive inhibition of CMG unloading (Figures 7H–7J). These results indicate that BRCA1 and DNA polymerase can promote CMG unloading through independent mechanisms.

DISCUSSION

The CMG helicase is a highly processive molecular motor that binds tightly to DNA. Little is known about how CMG is

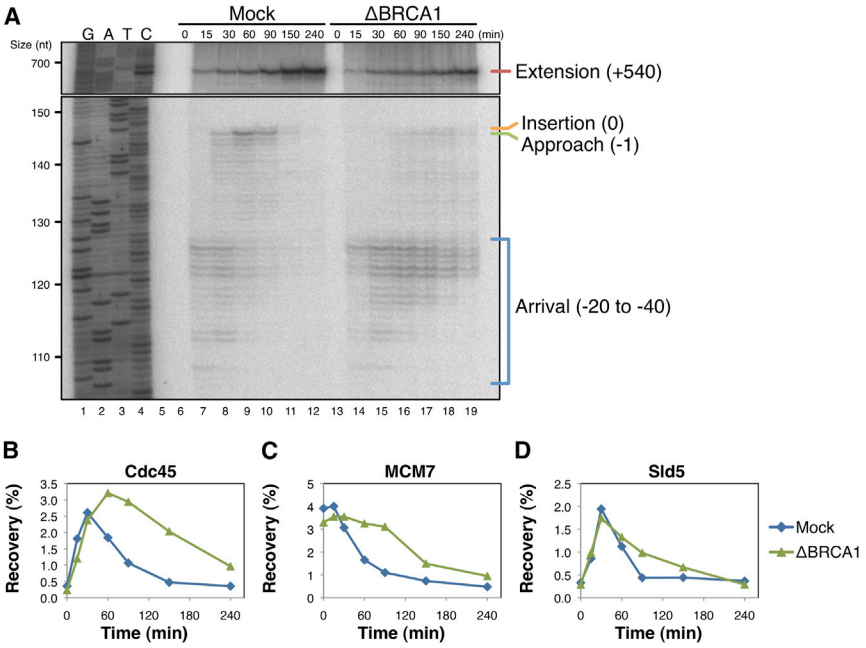

Figure 5. BRCA1 Depletion Inhibits Leading Strand Approach and Helicase Unloading

Mock-depleted or BRCA1-depleted samples from Figure 3 were analyzed by denaturing PAGE (A) and by ChIP with the indicated antibodies (B)–(D). See Figure S3 for quantification of nascent strand products, ChIP recovery at the FAR locus, and experimental replicates.

dismantled from chromatin, both when replication forks meet during termination and in response to certain forms of replication stress. We previously found that when forks encounter an ICL, the Approach of leading strands from the -20 to the -1 position correlates with dissociation of CMG from the site of damage (Fu et al., 2011). Here we show that inhibiting CMG dissociation in various ways also blocks Approach and ICL repair. These data establish CMG unloading as a critical, early step in ICL repair.

We further present multiple lines of evidence that CMG unloading requires the BRCA1-BARD1 complex. BRCA1 immunodepletion and disruption of the BRCA1-BARD1 complex with a dominant-negative peptide both inhibit CMG unloading. In addition, preventing BRCA1 localization to ICLs by disrupting ubiquitin signaling or BRCT-phosphopeptide interactions inhibits CMG unloading. Finally, the timing of BRCA1 binding to ICLs and CMG unloading are highly correlated. Together, our results show that the BRCA pathway functions to evict the helicase from stalled replication forks. Importantly, BRCA1 is not required for helicase unloading during replication termination (Figures S3B–S3D). Perhaps there is a difference in the arrangement of CMG helicases during ICL repair and termination that allows BRCA1-BARD1 to discriminate between the two situations.

Our data uncover other interesting mechanistic features of ICL repair. When we added aphidicolin immediately after replication forks stalled at the ICL, Approach failed, and ICL repair was inhibited (Figure 7A). Interestingly, aphidicolin also caused a delay in CMG unloading in both mock-depleted and BRCA1-depleted reactions (Figures 7H–7J). One interpretation of this observation is that the polymerase contributes to helicase eviction by exerting mechanical force on the stalled CMG complex (positioned immediately in front of the polymerase). Alternatively, aphidicolin treatment may stabilize the interaction between DNA polymerase and DNA (Cheng and Kuchta, 1993), thereby indirectly preventing another BRCA1-independent mechanism of helicase unloading. In either case, both BRCA1- and DNA polymerase-linked mechanisms likely cooperate to achieve efficient helicase eviction. One attractive model is that the E3 ligase activity of BRCA1-BARD1 (Hashizume et al., 2001) ubiquitylates one or more CMG components, destabilizing the complex and/or helping facilitate its displacement by DNA polymerase.

We recently showed that FANCI-FANCD2 promotes ICL incisions by recruiting the XPF-ERCC1 nuclease to sites of damage (Klein Douwel et al., 2014; Knipscheer et al., 2009). Interestingly, in the presence of aphidicolin, FANCD2 was still localized to ICLs, but incisions were severely inhibited. Therefore, the recruitment of FANCD2 to ICLs is not sufficient for incision when Approach is blocked (Figure 7A). We speculate that extension of the leading strand to the -1 position after CMG unloading creates a DNA structure that is recognized by FANCI-FANCD2-dependent nucleases. Alternatively, the delay in CMG unloading seen in the presence of aphidicolin might account for the incision defect. Thus, the presence of CMG at ICLs might shield the structure from endonucleolytic processing.

A future challenge is to determine how the various genome maintenance functions of BRCA1 contribute to tumor suppression. Interestingly, the crosslink sensitivity of BRCA1-deficient cells is less severe than for those carrying mutations in other ICL repair factors (Bridge et al., 2005; Niedzwiedz et al., 2004; Ohashi et al., 2005; Qing et al., 2011). This could be explained by the fact that a polymerase-linked mechanism can promote helicase unloading in the absence of BRCA1. Moreover, the FANC pathway is still activated in the absence of BRCA1, as evidenced by normal FANCD2 ubiquitylation in response to ICLs (Bunting et al., 2012). As such, repair might still proceed, albeit with reduced efficiency and higher propensity for error.

In conclusion, our results show that the BRCA and FANC pathways execute an ordered series of fork-processing events (helicase eviction, DNA incisions, and HR) that promote error-free removal of ICLs from DNA (Figure S7).

EXPERIMENTAL PROCEDURES

Xenopus Egg Extracts and DNA Replication

Preparation of *Xenopus* egg extracts was performed as described previously (Lebofsky et al., 2009). For DNA replication, plasmids were first incubated in a high-speed supernatant (HSS) of egg cytoplasm (final concentration 7.5 ng

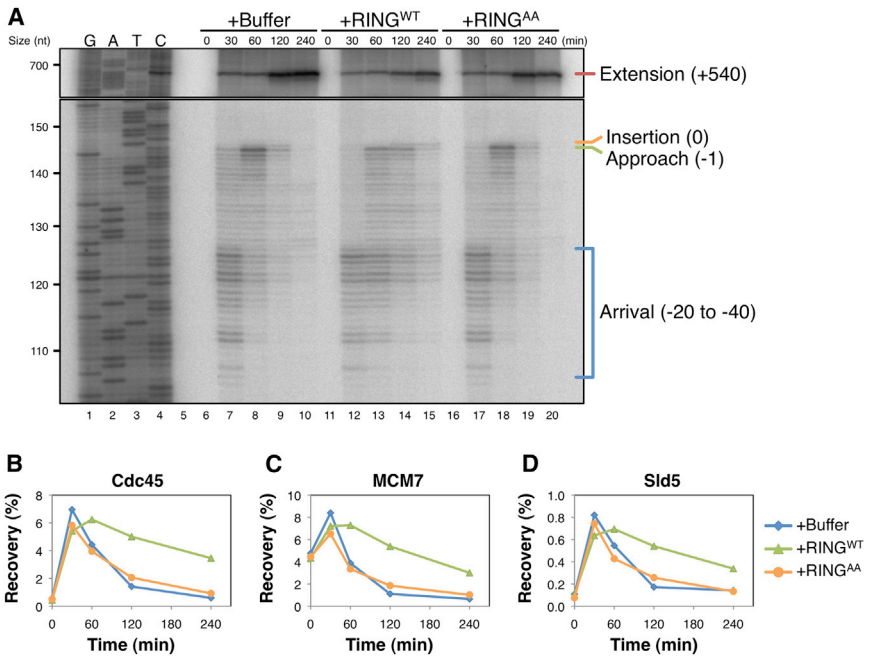

Figure 6. The BRCA1-BARD1 Complex Is Required to Promote Leading Strand Approach and Helicase Unloading

pICL was replicated in extracts that were partially depleted of BRCA1 (Figure S4A), then supplemented with buffer (+Buffer), wild-type RING peptide (+RING^{WT}), or RING peptide containing two alanine insertions (+RING^{AA}). Samples from the same reaction were analyzed by denaturing PAGE (A) and by ChIP with the indicated antibodies (B) and (C). See Figure S4 for quantification of nascent strand products, ChIP recovery at the FAR locus, and experimental replicates.

DNA/μL extract) for 20 min at 21°C, leading to the formation of prereplication complexes (pre-RCs). Next, two volumes of nucleoplasmic egg extract (NPE) were added to one volume of HSS, initiating Cdk2-dependent replication at pre-RCs. For all figures, the 0 min time point corresponds to NPE addition. For DNA labeling, reactions were supplemented with [α-^{32}P]dATP, which is incorporated into nascent strands during replication. For UbVS reactions, NPE was supplemented with 14 μM UbVS alone, or with 50 μM ubiquitin (both from Boston Biochem, Cambridge) prior to mixing with HSS. Reactions were stopped with ten volumes stop solution A (0.5% SDS, 25 mM EDTA, 50 mM Tris-HCl [pH 7.5]), and replication intermediates were purified as described (Räschle et al., 2008). Replication and repair intermediates were separated by 0.8% native agarose gels and visualized using a phosphorimager to determine replication efficiency (Lebofsky et al., 2009). All experiments were performed at least twice, and a representative result is shown. Veterinary care is provided by the Center for Animal Resources and Comparative Medicine at Harvard Medical School (AAALAC accredited).

ICL Repair Assay

Repair efficiency was calculated essentially as described (Räschle et al., 2008). pICL contains a single, site-specific cisplatin ICL that interrupts a SapI recognition site (see Enoiu et al., 2012 for description and preparation). ICL repair is assayed by SapI cleavage, which requires error-free removal of the crosslink. To quantify the formation of SapI-cleavable products, DNA samples were digested with either HincII alone, or HincII and SapI, then separated by a native agarose gel and visualized using a phosphorimager. SapI cleavage of HincII-linearized molecules produces two fragments that are 2.3 and 3.3 kb in size. Fragments of similar size are also generated when ICL-stalled fork arms are broken or cleaved. Since these intermediates do not represent ICL repair products, they were quantified in the HincII-digested samples and subtracted from the HincII/SapI-generated fragments. This yields the amount of fragments produced exclusively by SapI cleavage. To determine the efficiency of repair as a percentage of the total DNA replicated, radioactivity in each sample is normalized to correct for variation introduced during sample preparation. To this end, a small amount of an unrelated, undamaged plasmid (pQuant) was included in the reaction (0.375 ng DNA/μL final concentration in HSS) to serve as an internal standard for quantification. The percentage of SapI-cleavable products is then calculated by comparing the normalized value of SapI fragments to the radioactivity present in the known amount of pQuant (which is 1/20 the amount of pICL added to the reaction). ICL repair data are shown with peak values set to 100% and background SapI fragments from contaminating uncrosslinked plasmid subtracted out.

ChIP and Quantitative Real-Time PCR

ChIP was performed essentially as described (Long et al., 2011). Reaction samples were crosslinked in egg lysis buffer (ELB; 10 mM HEPES-KOH [pH 7.7], 2.5 mM $MgCl_2$, 50 mM KCl, 250 mM sucrose, and 1 mM DTT) containing 1% formaldehyde for 10 min at 21°C. Crosslinking was stopped by adding glycine to a final concentration of 125 mM followed by passage through a Micro Bio-Spin 6 Chromatography column (Bio-Rad, Hercules) to remove excess formaldehyde. The flowthrough was diluted to 500 μl with sonication buffer (20 mM Tris-HCl [pH 7.5], 150 mM NaCl, 2 mM EDTA, 0.5% NP-40, 5 μg/mL aprotinin plus leupeptin, and 2 mM PMSF) and subjected to sonication, yielding DNA fragments ~300–500 bp in size. Following immunoprecipitation with the indicated antibodies, formaldehyde crosslinks were reversed, and DNA was purified for analysis by quantitative real-time PCR with the following primer pairs: "ICL" (5′-AGCCAGATTTTTCCTCCT CTC-3′ and 5′-CATGCATTGGTTCTGCACTT-3′) and "FAR" (5′-AACGCCAA TAGGGACTTTCC-3′ and 5′-GGGCGTACTTGGCATATGAT-3′). Antibodies for ChIP were purified using protein A Sepharose beads (GE Healthcare, Piscataway).

2D Gel Electrophoresis

Purified pICL intermediates were digested with HincII and then analyzed by native/native 2DGE. The first-dimension gel consisted of 0.4% agarose run in 1xTBE buffer at 0.75 V/cm for 26 hr at 21°C. The desired lane was then cast across the top of the second-dimension gel, which consisted of 1% agarose with 0.3 μg/mL ethidium bromide, and run in 1xTBE containing 0.3 μg/mL ethidium bromide at 4.5 V/cm for 14 hr at 4°C. DNA from the resulting gel was transferred to a 0.45 μm positively charged nylon transfer membrane (GE Healthcare, Piscataway), crosslinked with a 120 mJ/cm^2 UV exposure, and visualized using a phosphorimager.

ssDNA Analysis

ssDNA was detected by quantitative PCR as described (Holstein and Lydall, 2012). Native DNA samples were first incubated at low temperature, allowing ssDNA to anneal with a "Test" primer that contains a unique sequence at its 5′ end. A single round of primer extension then creates a novel DNA product whose amount is proportional to the original amount of ssDNA. The novel product is then amplified using "Left" and "Right" primers at high temperatures to prevent annealing of the Test primer. ssDNA quantity is calculated using a ssDNA standard curve. Primer locations denote the distance from the 3′ end of the Test primer to the ICL. The "118," "400," "1454," and "2925" Test primers anneal to the lagging strand template, while the "Anti-204" Test primer anneals to the leading strand template, serving as a control for dsDNA. See Figure 4D for schematic.

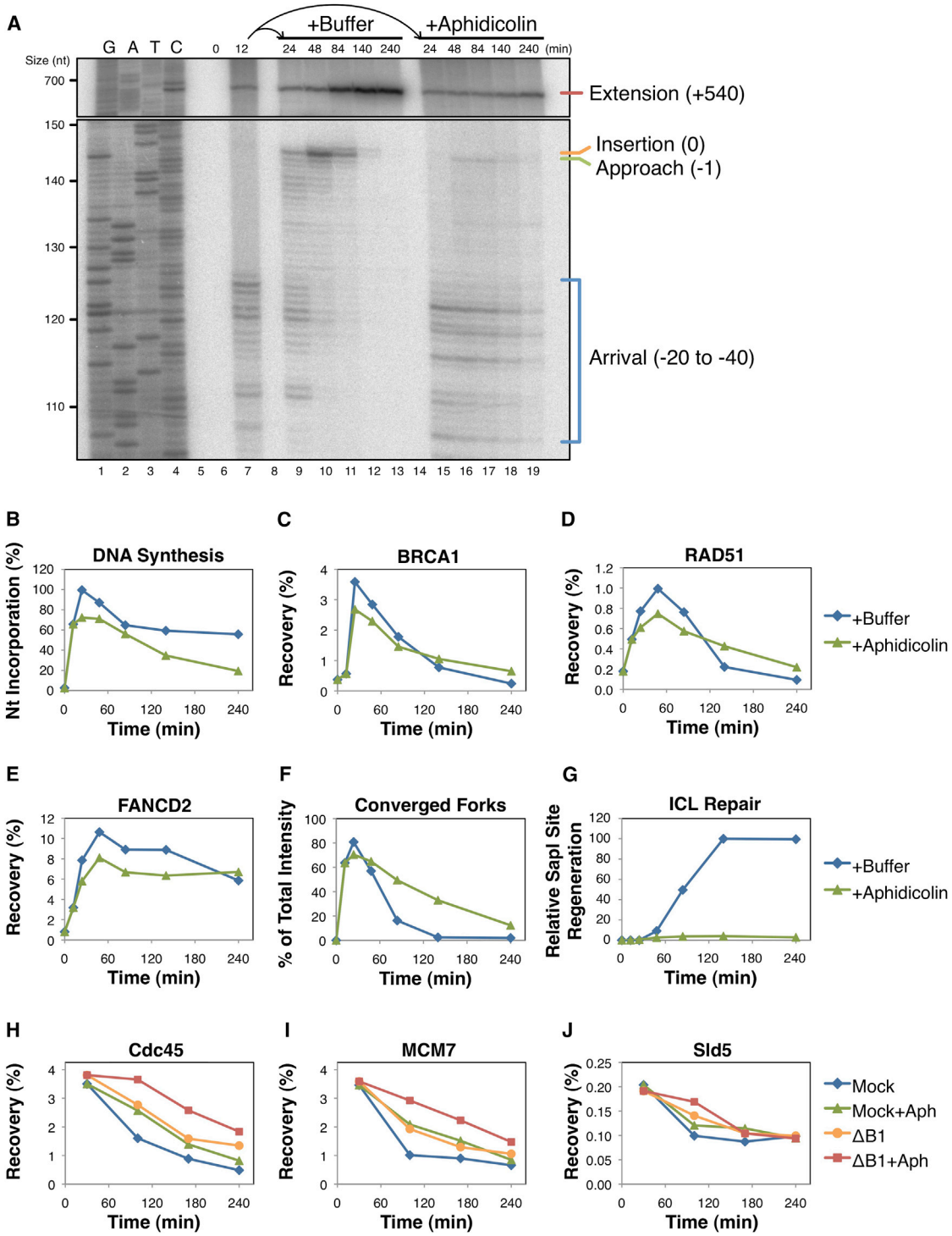

Figure 7. BRCA1 and DNA Polymerase Independently Promote Helicase Unloading

(A–G) pICL was replicated in egg extract for 12 min. The reaction was then split and supplemented with buffer (+Buffer) or 50 μM aphidicolin (+Aphidicolin) to block polymerase activity. Samples from the same reaction were analyzed by the following: (A) denaturing PAGE, (B) agarose gel electrophoresis to determine the efficiency of replication, (C)–(E) ChIP with the indicated antibodies, (F) 2DGE to visualize the accumulation of converged forks, and (G) agarose gel electrophoresis to determine the efficiency of ICL repair. See Figure S5 for primary gel data, quantification of nascent strand products, and ChIP recovery at the FAR locus. (H–J) pICL was replicated in mock-depleted (Mock) or BRCA1-depleted (ΔB1) extract for 30 min. Each reaction was then split and supplemented with buffer or aphidicolin (+Aph) to block polymerase extension. Protein recruitment to the ICL was analyzed by ChIP with the indicated antibodies. See Figure S6 for primary experimental data.

The following primer sequences were used: (118) test 5′-TGACTGCGCAC CAGGCATAGTCAGGAGAGGA-3′, left 5′-TTCCATAGAAAAGCCTTGACTTG AGGT-3′, right 5′-TGACTGCGCACCAGGCATAG-3′; (400) test 5′-TGACTG CGCACAGCGTACGAGTGAGAGACAC-3′, left 5′-CCCTGGCTCACAAATACC ACTGAG-3′, right 5′-TGACTGCGCACAGCGTACGA-3′; (1,454) test 5′-TGA CTGCGCACCAGGCATAGTTGATGAAGGA-3′, left 5′-GCTCCATGGCTTCCA AGGTGT-3′, right 5′-TGACTGCGCACCAGGCATAG-3′; (2,925) test 5′-TGA CTGCGCACCAGGCATAGCGATGACTAAT-3′, left 5′-TGCCAAGTACGCCC CCTATTG-3′, right 5′-TGACTGCGCACCAGGCATAG-3′; and (anti-204) test 5′-TGACTGCGCACCAGGCATGACTTGAGGTTAG-3′, left 5′-TGACTGCGCA CCAGGCATGA-3′, right 5′-TCAGGAGAGGAGGAAAAATCTGG-3′.

Nascent Strand Analysis

Nascent strand analysis was performed as described (Räschle et al., 2008). Briefly, pICL was replicated in the presence of [α-^{32}P]dATP, and purified pICL intermediates were digested with AflIII, followed by addition of 0.5 volumes stop solution B (95% formamide, 20 mM EDTA, 0.05% bromophenol blue, and 0.05% xylene cyanol). Radiolabeled nascent strands were then separated by a 7% denaturing polyacrylamide gel, transferred to filter paper, dried, and visualized using a phosphorimager. Sequencing ladders were generated with primer S (5′-CATGTTTTACTAGCCAGATTTTTCCTCCTCT CCTG-3′) using the Cycle Sequencing Kit (USB, Cleveland).

Antibodies and Immunodepletion

The following rabbit polyclonal antibodies were described previously: BRCA1 (raised against *X.l.*BRCA1 residues 1,001–1,192) (Joukov et al., 2001), BARD1 (Joukov et al., 2001), RAD51 (Long et al., 2011), FANCI (Knipscheer et al., 2009), FANCD2 (Räschle et al., 2008), RPA (Walter and Newport, 2000), PCNA (Kochaniak et al., 2009), Cdc45 (Walter and Newport, 2000), MCM7 (Fang and Newport, 1993), Sld5 (Kubota et al., 2003) (provided by H. Takisawa, Osaka University), and Polε (Waga et al., 2001) and Polδ (Fukui et al., 2004) (both provided by S. Waga, Osaka University). Chk1-P (S345) was purchased from Cell Signaling Technology, Danvers. BRCA2 antibodies were raised in rabbits against *X.l.*BRCA2 residues 1,842–2,080. Rap80 antibodies were raised in rabbits against a 223 residue *X.l.*Rap80 protein fragment (see GenBank Accession CX130807). The cDNA encoding this fragment was generated from a *Xenopus laevis* mRNA library by PCR with the following primers: left, 5′-CCGGAATTCGTACAGGAAATAGATGATCAAT GCTCA-3′; and right, 5′-CATAGTTTAGCGGCCGCTGGCTCCAGATCCGTT CCTGCACC-3′. The PCR fragment was digested with EcoRI and NotI, then cloned into the corresponding sites of a pET29a vector. To deplete BRCA1, *Xenopus* egg extracts were incubated with antibodies prebound to protein A Sepharose beads (50 μg total IgGs from serum per μL of beads) at a 4:1 ratio of extract to beads for 40 min at 4°C for three rounds.

BRCA1 Inhibitory Peptides

*X.l.*BARD1 residues 2–195 corresponding to *H.s.*BARD1 residues 2–202 containing the RING domain were cloned into pGEX-6P-1 to create an N-terminal GST fusion construct. The RING^{AA} alanine insertions (after amino acids 35 and 100) were introduced by Site-Directed Mutagenesis (Agilent Technologies, Santa Clara). Recombinant RING-GST fusions were expressed using BL21 cells induced by 0.5 mM IPTG and purified using glutathione Sepharose 4B (GE Healthcare, Piscataway). Where indicated, extract was supplemented with 38 μM RING^{WT} or RING^{AA} peptide. The following peptides (*X.l.*Abraxas residues 398–408) were synthesized by Tufts University Core Facility: VEVSRSKpSPTF (pSPTF) and VEVSRSKSPTF (SPTF). Where indicated, extract was supplemented with 3 mM pSPTF or SPTF peptide. Due to nonspecific inhibitory effects, SPTF peptides were added to extract after replication forks had converged on the ICL.

BRCA1-BARD1 Purification

The *X.l.*BRCA1-BARD1 heterodimeric complex was purified from insect cells as in Joukov et al. (2006). Full-length FLAG-BRCA1 and HA-BARD1 were each cloned into pFastBac and used to generate the corresponding recombinant baculoviruses (Bac-to-Bac Baculovirus Expression System, Life Technologies, Carlsbad). Sf9 cells were coinfected with both viruses, and the heterodimer was purified from cell lysates by sequential affinity chromatography using anti-FLAG M2 agarose and anti-HA agarose (both from Sigma-Aldrich, St. Louis). The eluted heterodimer was then dialyzed (20 mM HEPES [pH 7.6], 100 mM KCl, 2.5 mM $MgCl_2$, 250 mM sucrose, 1 mM DTT) and frozen at −80°C.

SUPPLEMENTAL INFORMATION

Supplemental Information includes seven figures and can be found with this article online at http://dx.doi.org/10.1016/j.molcel.2014.08.012.

ACKNOWLEDGMENTS

We thank A. D'Andrea, D. Livingston, and R. Scully for critical reading of the manuscript. We also thank D. Livingston for the generous gift of BRCA1 and BRCA2 antibodies. V.J. generated the *X.l.*BARD1 peptide construct and antibodies for *X.l.*BRCA1, BRCA2, and Rap80, and M.B. made the initial observation of aphidicolin's effect on MCM7 unloading. D.T.L. and J.C.W. designed and analyzed experiments, D.T.L. performed experiments, and D.T.L. and J.C.W. prepared the manuscript. This work was supported by the American Cancer Society Postdoctoral Fellowship PF-10-146-01-DMC and NIH award K99GM102325 to D.T.L., the Department of Defense Breast Cancer Research Program Award W81XWH-04-1-0524 to V.J., the Human Frontiers Science Program Long-Term Fellowship LT000773/2010-L to M.B., and a Department of Defense grant (BC120436) and NIH grants to J.C.W. (HL098316 and GM80676). J.C.W. is an investigator at the Howard Hughes Medical Institute.

Received: March 4, 2014
Revised: June 30, 2014
Accepted: August 7, 2014
Published: September 11, 2014

REFERENCES

Bekker-Jensen, S., and Mailand, N. (2010). Assembly and function of DNA double-strand break repair foci in mammalian cells. DNA Repair (Amst.) *9*, 1219–1228.

Bhattacharyya, A., Ear, U.S., Koller, B.H., Weichselbaum, R.R., and Bishop, D.K. (2000). The breast cancer susceptibility gene BRCA1 is required for subnuclear assembly of Rad51 and survival following treatment with the DNA cross-linking agent cisplatin. J. Biol. Chem. *275*, 23899–23903.

Borodovsky, A., Kessler, B.M., Casagrande, R., Overkleeft, H.S., Wilkinson, K.D., and Ploegh, H.L. (2001). A novel active site-directed probe specific for deubiquitylating enzymes reveals proteasome association of USP14. EMBO J. *20*, 5187–5196.

Bouwman, P., Aly, A., Escandell, J.M., Pieterse, M., Bartkova, J., van der Gulden, H., Hiddingh, S., Thanasoula, M., Kulkarni, A., Yang, Q., et al. (2010). 53BP1 loss rescues BRCA1 deficiency and is associated with triple-negative and BRCA-mutated breast cancers. Nat. Struct. Mol. Biol. *17*, 688–695.

Bridge, W.L., Vandenberg, C.J., Franklin, R.J., and Hiom, K. (2005). The BRIP1 helicase functions independently of BRCA1 in the Fanconi anemia pathway for DNA crosslink repair. Nat. Genet. *37*, 953–957.

Brzovic, P.S., Rajagopal, P., Hoyt, D.W., King, M.C., and Klevit, R.E. (2001). Structure of a BRCA1-BARD1 heterodimeric RING-RING complex. Nat. Struct. Biol. *8*, 833–837.

Bunting, S.F., Callén, E., Wong, N., Chen, H.T., Polato, F., Gunn, A., Bothmer, A., Feldhahn, N., Fernandez-Capetillo, O., Cao, L., et al. (2010). 53BP1 inhibits homologous recombination in Brca1-deficient cells by blocking resection of DNA breaks. Cell *141*, 243–254.

Bunting, S.F., Callén, E., Kozak, M.L., Kim, J.M., Wong, N., López-Contreras, A.J., Ludwig, T., Baer, R., Faryabi, R.B., Malhowski, A., et al. (2012). BRCA1 functions independently of homologous recombination in DNA interstrand crosslink repair. Mol. Cell *46*, 125–135.

Chalasani, P., and Livingston, R. (2013). Differential chemotherapeutic sensitivity for breast tumors with "BRCAness": a review. Oncologist *18*, 909–916.

Cheng, C.H., and Kuchta, R.D. (1993). DNA polymerase epsilon: aphidicolin inhibition and the relationship between polymerase and exonuclease activity. Biochemistry *32*, 8568–8574.

Choudhury, A.D., Xu, H., and Baer, R. (2004). Ubiquitination and proteasomal degradation of the BRCA1 tumor suppressor is regulated during cell cycle progression. J. Biol. Chem. *279*, 33909–33918.

De Leeneer, K., Coene, I., Crombez, B., Simkens, J., Van den Broecke, R., Bols, A., Stragier, B., Vanhoutte, I., De Paepe, A., Poppe, B., and Claes, K. (2012). Prevalence of BRCA1/2 mutations in sporadic breast/ovarian cancer patients and identification of a novel de novo BRCA1 mutation in a patient diagnosed with late onset breast and ovarian cancer: implications for genetic testing. Breast Cancer Res. Treat. *132*, 87–95.

Dimova, N.V., Hathaway, N.A., Lee, B.-H., Kirkpatrick, D.S., Berkowitz, M.L., Gygi, S.P., Finley, D., and King, R.W. (2012). APC/C-mediated multiple monoubiquitylation provides an alternative degradation signal for cyclin B1. Nat. Cell Biol. *14*, 168–176.

Enoiu, M., Ho, T.V., Long, D.T., Walter, J.C., and Schärer, O.D. (2012). Construction of plasmids containing site-specific DNA interstrand cross-links for biochemical and cell biological studies. Methods Mol. Biol. *920*, 203–219.

Errico, A., Costanzo, V., and Hunt, T. (2007). Tipin is required for stalled replication forks to resume DNA replication after removal of aphidicolin in *Xenopus* egg extracts. Proc. Natl. Acad. Sci. USA *104*, 14929–14934.

Fang, F., and Newport, J.W. (1993). Distinct roles of cdk2 and cdc2 in RP-A phosphorylation during the cell cycle. J. Cell Sci. *106*, 983–994.

Fu, Y.V., Yardimci, H., Long, D.T., Ho, T.V., Guainazzi, A., Bermudez, V.P., Hurwitz, J., van Oijen, A., Schärer, O.D., and Walter, J.C. (2011). Selective bypass of a lagging strand roadblock by the eukaryotic replicative DNA helicase. Cell *146*, 931–941.

Fukui, T., Yamauchi, K., Muroya, T., Akiyama, M., Maki, H., Sugino, A., and Waga, S. (2004). Distinct roles of DNA polymerases delta and epsilon at the replication fork in *Xenopus* egg extracts. Genes Cells *9*, 179–191.

Garcia-Higuera, I., Taniguchi, T., Ganesan, S., Meyn, M.S., Timmers, C., Hejna, J., Grompe, M., and D'Andrea, A.D. (2001). Interaction of the Fanconi anemia proteins and BRCA1 in a common pathway. Mol. Cell *7*, 249–262.

Greenberg, R.A., Sobhian, B., Pathania, S., Cantor, S.B., Nakatani, Y., and Livingston, D.M. (2006). Multifactorial contributions to an acute DNA damage response by BRCA1/BARD1-containing complexes. Genes Dev. *20*, 34–46.

Hashizume, R., Fukuda, M., Maeda, I., Nishikawa, H., Oyake, D., Yabuki, Y., Ogata, H., and Ohta, T. (2001). The RING heterodimer BRCA1-BARD1 is a ubiquitin ligase inactivated by a breast cancer-derived mutation. J. Biol. Chem. *276*, 14537–14540.

Holstein, E.-M., and Lydall, D. (2012). Quantitative amplification of single-stranded DNA. Methods Mol. Biol. *920*, 323–339.

Ilves, I., Petojevic, T., Pesavento, J.J., and Botchan, M.R. (2010). Activation of the MCM2-7 helicase by association with Cdc45 and GINS proteins. Mol. Cell *37*, 247–258.

Jensen, R.B., Carreira, A., and Kowalczykowski, S.C. (2010). Purified human BRCA2 stimulates RAD51-mediated recombination. Nature *467*, 678–683.

Joukov, V., Chen, J., Fox, E.A., Green, J.B.A., and Livingston, D.M. (2001). Functional communication between endogenous BRCA1 and its partner, BARD1, during *Xenopus laevis* development. Proc. Natl. Acad. Sci. USA *98*, 12078–12083.

Joukov, V., Groen, A.C., Prokhorova, T., Gerson, R., White, E., Rodriguez, A., Walter, J.C., and Livingston, D.M. (2006). The BRCA1/BARD1 heterodimer modulates ran-dependent mitotic spindle assembly. Cell *127*, 539–552.

Kass, E.M., and Jasin, M. (2010). Collaboration and competition between DNA double-strand break repair pathways. FEBS Lett. *584*, 3703–3708.

Kim, H., and D'Andrea, A.D. (2012). Regulation of DNA cross-link repair by the Fanconi anemia/BRCA pathway. Genes Dev. *26*, 1393–1408.

Klein Douwel, D., Boonen, R.A., Long, D.T., Szypowska, A.A., Raschle, M., Walter, J.C., and Knipscheer, P. (2014). XPF-ERCC1 acts in unhooking DNA interstrand crosslinks in cooperation with FANCD2 and FANCP/SLX4. Mol. Cell *54*, 460–471.

Knipscheer, P., Räschle, M., Smogorzewska, A., Enoiu, M., Ho, T.V., Schärer, O.D., Elledge, S.J., and Walter, J.C. (2009). The Fanconi anemia pathway promotes replication-dependent DNA interstrand cross-link repair. Science *326*, 1698–1701.

Kochaniak, A.B., Habuchi, S., Loparo, J.J., Chang, D.J., Cimprich, K.A., Walter, J.C., and van Oijen, A.M. (2009). Proliferating cell nuclear antigen uses two distinct modes to move along DNA. J. Biol. Chem. *284*, 17700–17710.

Kubota, Y., Takase, Y., Komori, Y., Hashimoto, Y., Arata, T., Kamimura, Y., Araki, H., and Takisawa, H. (2003). A novel ring-like complex of *Xenopus* proteins essential for the initiation of DNA replication. Genes Dev. *17*, 1141–1152.

Lebofsky, R., Takahashi, T., and Walter, J.C. (2009). DNA replication in nucleus-free *Xenopus* egg extracts. Methods Mol. Biol. *521*, 229–252.

Liu, J., Doty, T., Gibson, B., and Heyer, W.-D. (2010). Human BRCA2 protein promotes RAD51 filament formation on RPA-covered single-stranded DNA. Nat. Struct. Mol. Biol. *17*, 1260–1262.

Long, D.T., Räschle, M., Joukov, V., and Walter, J.C. (2011). Mechanism of RAD51-dependent DNA interstrand cross-link repair. Science *333*, 84–87.

McHugh, P.J., Spanswick, V.J., and Hartley, J.A. (2001). Repair of DNA interstrand crosslinks: molecular mechanisms and clinical relevance. Lancet Oncol. *2*, 483–490.

Muniandy, P.A., Liu, J., Majumdar, A., Liu, S.T., and Seidman, M.M. (2010). DNA interstrand crosslink repair in mammalian cells: step by step. Crit. Rev. Biochem. Mol. Biol. *45*, 23–49.

Narod, S.A., and Foulkes, W.D. (2004). BRCA1 and BRCA2: 1994 and beyond. Nat. Rev. Cancer *4*, 665–676.

Niedzwiedz, W., Mosedale, G., Johnson, M., Ong, C.Y., Pace, P., and Patel, K.J. (2004). The Fanconi anaemia gene FANCC promotes homologous recombination and error-prone DNA repair. Mol. Cell *15*, 607–620.

Nijman, S.M.B., Huang, T.T., Dirac, A.M.G., Brummelkamp, T.R., Kerkhoven, R.M., D'Andrea, A.D., and Bernards, R. (2005). The deubiquitinating enzyme USP1 regulates the Fanconi anemia pathway. Mol. Cell *17*, 331–339.

Oestergaard, V.H., Langevin, F., Kuiken, H.J., Pace, P., Niedzwiedz, W., Simpson, L.J., Ohzeki, M., Takata, M., Sale, J.E., and Patel, K.J. (2007). Deubiquitination of FANCD2 is required for DNA crosslink repair. Mol. Cell *28*, 798–809.

Ohashi, A., Zdzienicka, M.Z., Chen, J., and Couch, F.J. (2005). Fanconi anemia complementation group D2 (FANCD2) functions independently of BRCA2- and RAD51-associated homologous recombination in response to DNA damage. J. Biol. Chem. *280*, 14877–14883.

Pinder, J.B., Attwood, K.M., and Dellaire, G. (2013). Reading, writing, and repair: the role of ubiquitin and the ubiquitin-like proteins in DNA damage signaling and repair. Front. Genet. *4*, 45.

Qing, Y., Yamazoe, M., Hirota, K., Dejsuphong, D., Sakai, W., Yamamoto, K.N., Bishop, D.K., Wu, X., and Takeda, S. (2011). The epistatic relationship between BRCA2 and the other RAD51 mediators in homologous recombination. PLoS Genet. *7*, e1002148.

Räschle, M., Knipscheer, P., Enoiu, M., Angelov, T., Sun, J., Griffith, J.D., Ellenberger, T.E., Schärer, O.D., and Walter, J.C. (2008). Mechanism of replication-coupled DNA interstrand crosslink repair. Cell *134*, 969–980.

Schlegel, B.P., Jodelka, F.M., and Nunez, R. (2006). BRCA1 promotes induction of ssDNA by ionizing radiation. Cancer Res. *66*, 5181–5189.

Silver, D.P., and Livingston, D.M. (2012). Mechanisms of BRCA1 tumor suppression. Cancer Discov. *2*, 679–684.

Smogorzewska, A., Matsuoka, S., Vinciguerra, P., McDonald, E.R., Hurov, K.E., Luo, J., Ballif, B.A., Gygi, S.P., Hofmann, K., D'Andrea, A.D., et al. (2007). Identification of the FANCI protein, a monoubiquitinated FANCD2 paralog required for DNA repair. Cell *129*, 289–301.

Vandenberg, C.J., Gergely, F., Ong, C.Y., Pace, P., Mallery, D.L., Hiom, K., and Patel, K.J. (2003). BRCA1-independent ubiquitination of FANCD2. Mol. Cell *12*, 247–254.

Waga, S., Masuda, T., Takisawa, H., and Sugino, A. (2001). DNA polymerase epsilon is required for coordinated and efficient chromosomal DNA replication in *Xenopus* egg extracts. Proc. Natl. Acad. Sci. USA *98*, 4978–4983.

Walter, J., and Newport, J. (2000). Initiation of eukaryotic DNA replication: origin unwinding and sequential chromatin association of Cdc45, RPA, and DNA polymerase alpha. Mol. Cell *5*, 617–627.

Wang, B. (2012). BRCA1 tumor suppressor network: focusing on its tail. Cell Biosci. *2*, 6.

Wang, X., Andreassen, P.R., and D'Andrea, A.D. (2004). Functional interaction of monoubiquitinated FANCD2 and BRCA2/FANCD1 in chromatin. Mol. Cell. Biol. *24*, 5850–5862.

Wang, B., Matsuoka, S., Ballif, B.A., Zhang, D., Smogorzewska, A., Gygi, S.P., and Elledge, S.J. (2007). Abraxas and RAP80 form a BRCA1 protein complex required for the DNA damage response. Science *316*, 1194–1198.

Westermark, U.K., Reyngold, M., Olshen, A.B., Baer, R., Jasin, M., and Moynahan, M.E. (2003). BARD1 participates with BRCA1 in homology-directed repair of chromosome breaks. Mol. Cell. Biol. *23*, 7926–7936.

Wu, J., Lu, L.-Y., and Yu, X. (2010). The role of BRCA1 in DNA damage response. Protein Cell *1*, 117–123.

Yan, J., and Jetten, A.M. (2008). RAP80 and RNF8, key players in the recruitment of repair proteins to DNA damage sites. Cancer Lett. *271*, 179–190.

Yun, M.H., and Hiom, K. (2009). CtIP-BRCA1 modulates the choice of DNA double-strand-break repair pathway throughout the cell cycle. Nature *459*, 460–463.

Zhang, J. (2013). The role of BRCA1 in homologous recombination repair in response to replication stress: significance in tumorigenesis and cancer therapy. Cell Biosci. *3*, 11.

Zhang, F., Fan, Q., Ren, K., and Andreassen, P.R. (2009). PALB2 functionally connects the breast cancer susceptibility proteins BRCA1 and BRCA2. Mol. Cancer Res. *7*, 1110–1118.

Molecular Cell, Volume *56*

Supplemental Information

BRCA1 Promotes Unloading of the CMG Helicase from a Stalled DNA Replication Fork

David T. Long, Vladimir Joukov, Magda Budzowska, and Johannes C. Walter

Figure S1

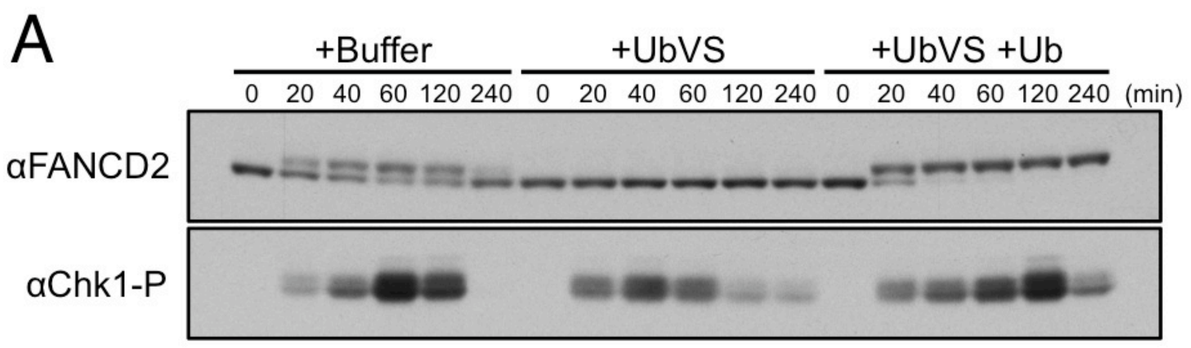
A
+Buffer
+UbVS
+UbVS +Ub
0 20 40 60 120 240 0 20 40 60 120 240 0 20 40 60 120 240 (min)
αFANCD2
αChk1-P

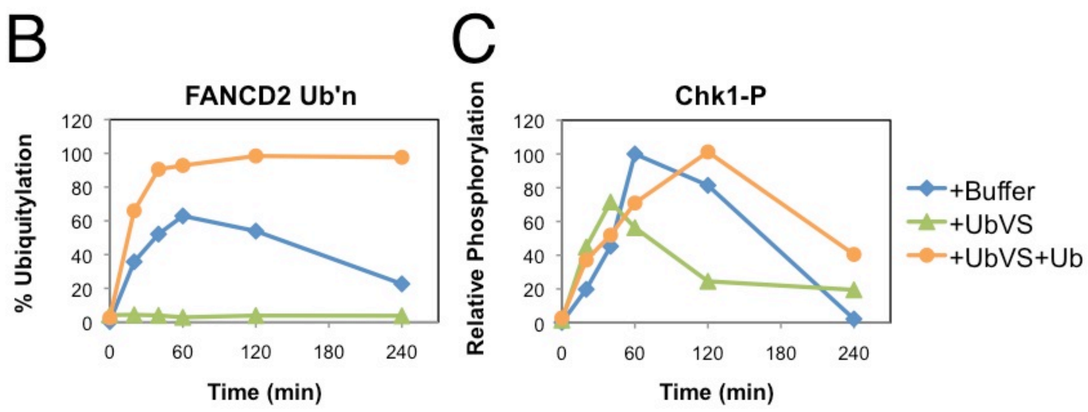
B
FANCD2 Ub'n
% Ubiquitylation
Time (min)
C
Chk1-P
Relative Phosphorylation
Time (min)
+Buffer
+UbVS
+UbVS+Ub

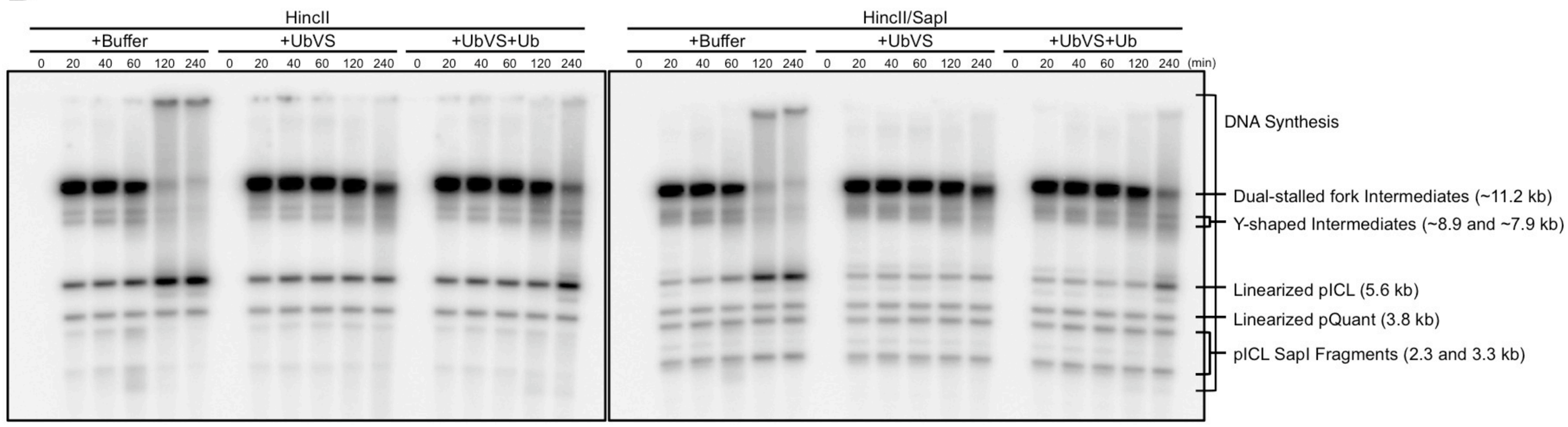
D
HincII
HincII/SapI
+Buffer
+UbVS
+UbVS+Ub
0 20 40 60 120 240 (min)
DNA Synthesis
Dual-stalled fork Intermediates (~11.2 kb)
Y-shaped Intermediates (~8.9 and ~7.9 kb)
Linearized pICL (5.6 kb)
Linearized pQuant (3.8 kb)
pICL SapI Fragments (2.3 and 3.3 kb)

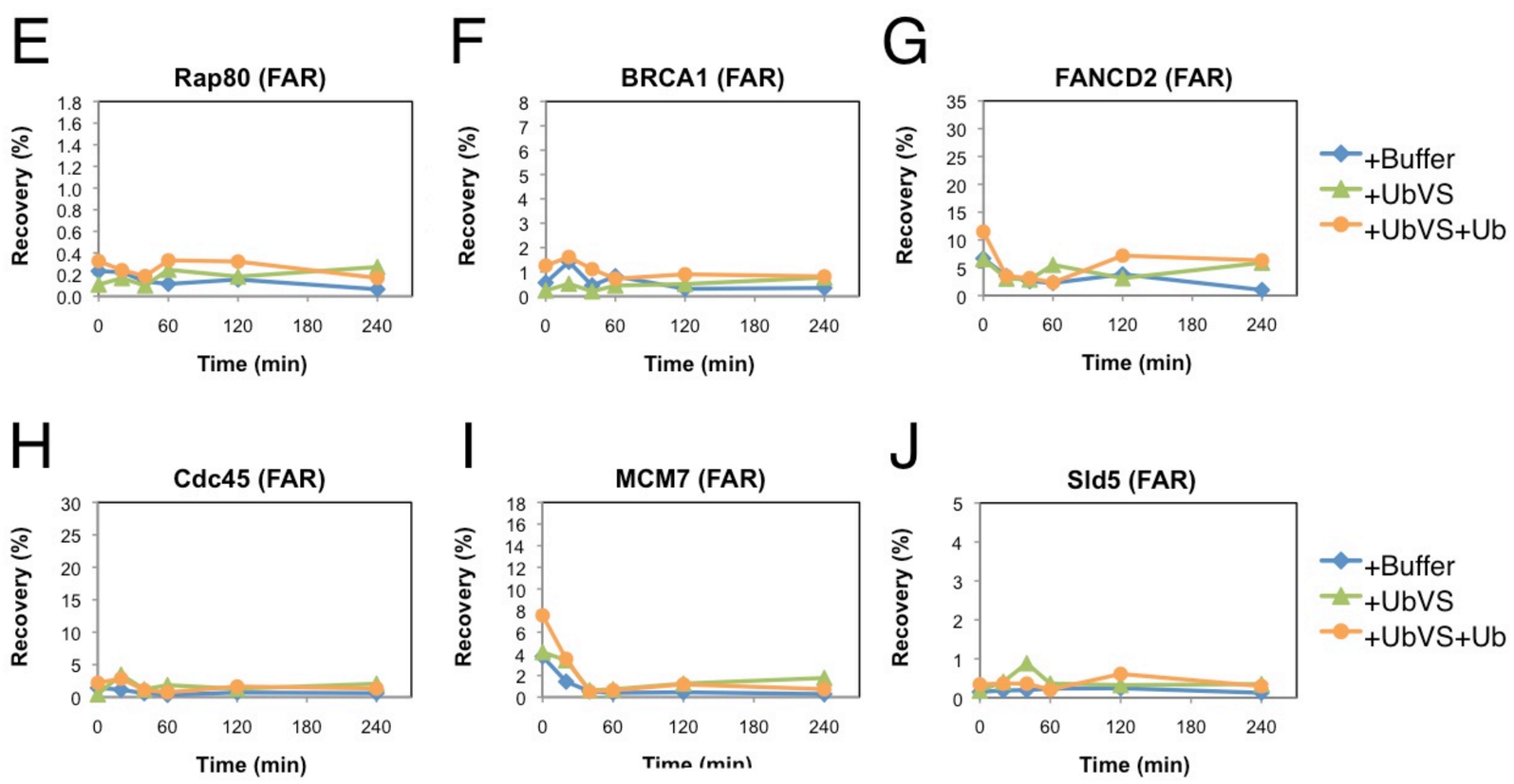
E
Rap80 (FAR)
F
BRCA1 (FAR)
G
FANCD2 (FAR)
Recovery (%)
Time (min)
+Buffer
+UbVS
+UbVS+Ub
H
Cdc45 (FAR)
I
MCM7 (FAR)
J
Sld5 (FAR)

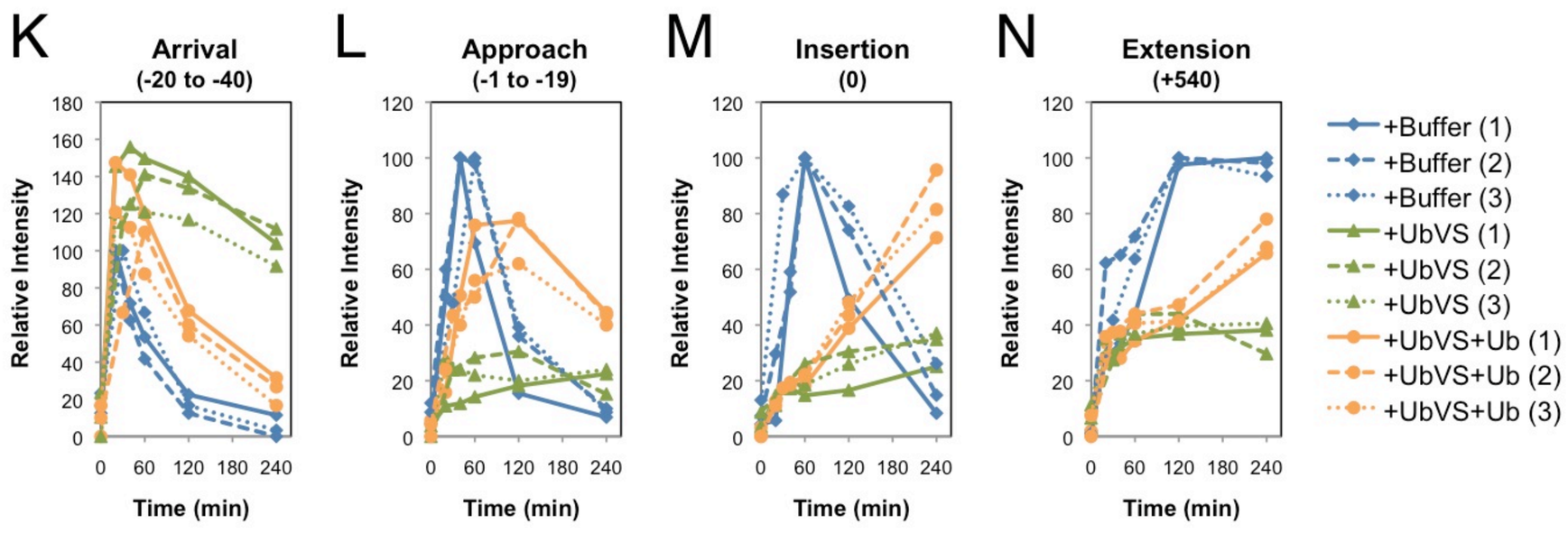
K
Arrival
(-20 to -40)
L
Approach
(-1 to -19)
M
Insertion
(0)
N
Extension
(+540)
Relative Intensity
Time (min)
+Buffer (1)
+Buffer (2)
+Buffer (3)
+UbVS (1)
+UbVS (2)
+UbVS (3)
+UbVS+Ub (1)
+UbVS+Ub (2)
+UbVS+Ub (3)

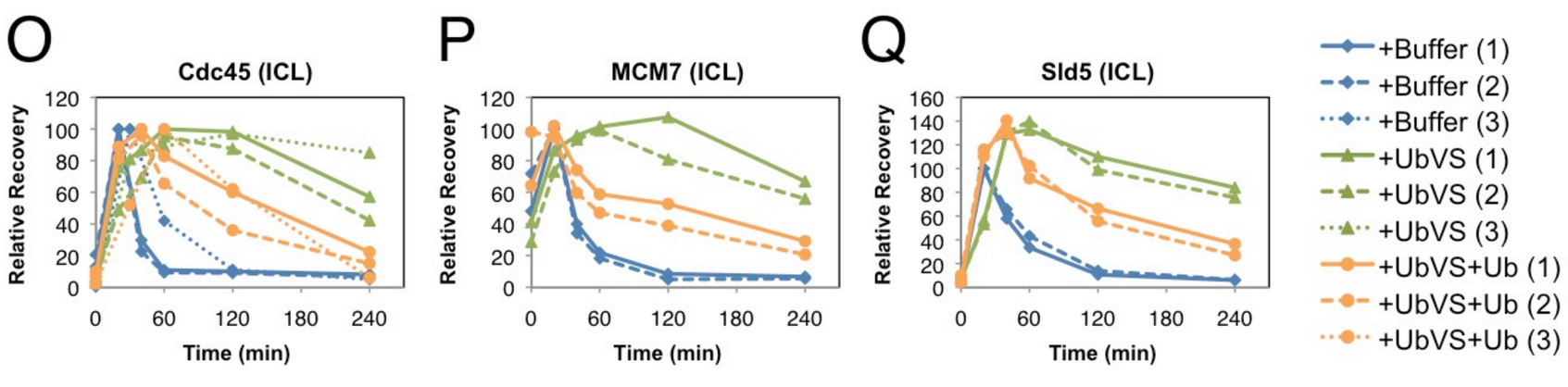
O
Cdc45 (ICL)
P
MCM7 (ICL)
Q
Sld5 (ICL)
Relative Recovery
Time (min)
+Buffer (1)
+Buffer (2)
+Buffer (3)
+UbVS (1)
+UbVS (2)
+UbVS (3)
+UbVS+Ub (1)
+UbVS+Ub (2)
+UbVS+Ub (3)

Figure S2

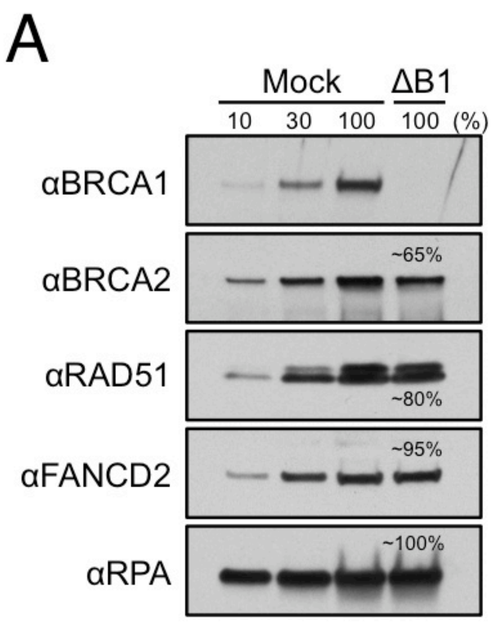
A
Mock
ΔB1
10 30 100 100 (%)
αBRCA1
αBRCA2
~65%
αRAD51
~80%
αFANCD2
~95%
~100%
αRPA

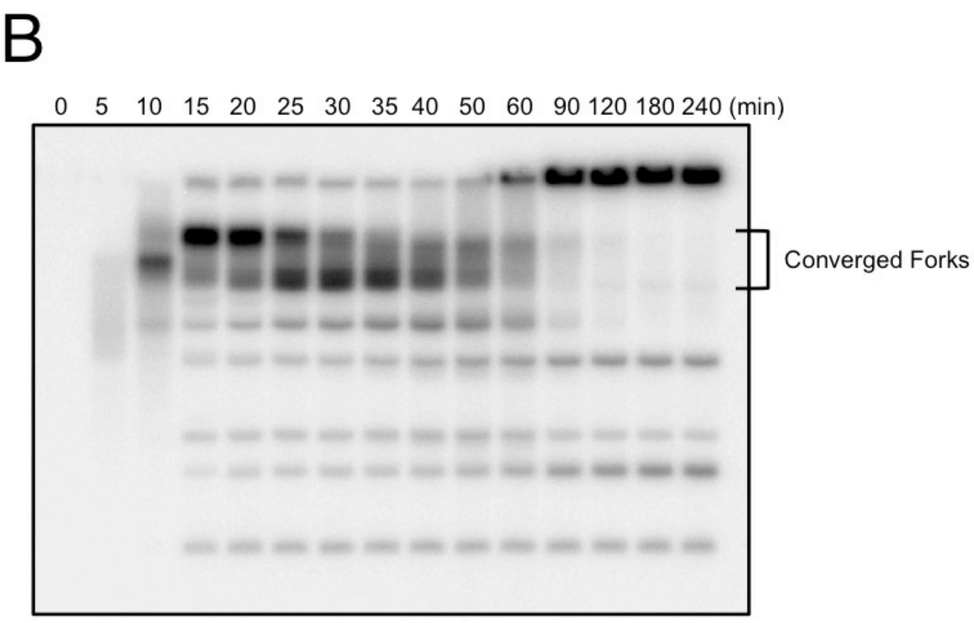
B
0 5 10 15 20 25 30 35 40 50 60 90 120 180 240 (min)
Converged Forks

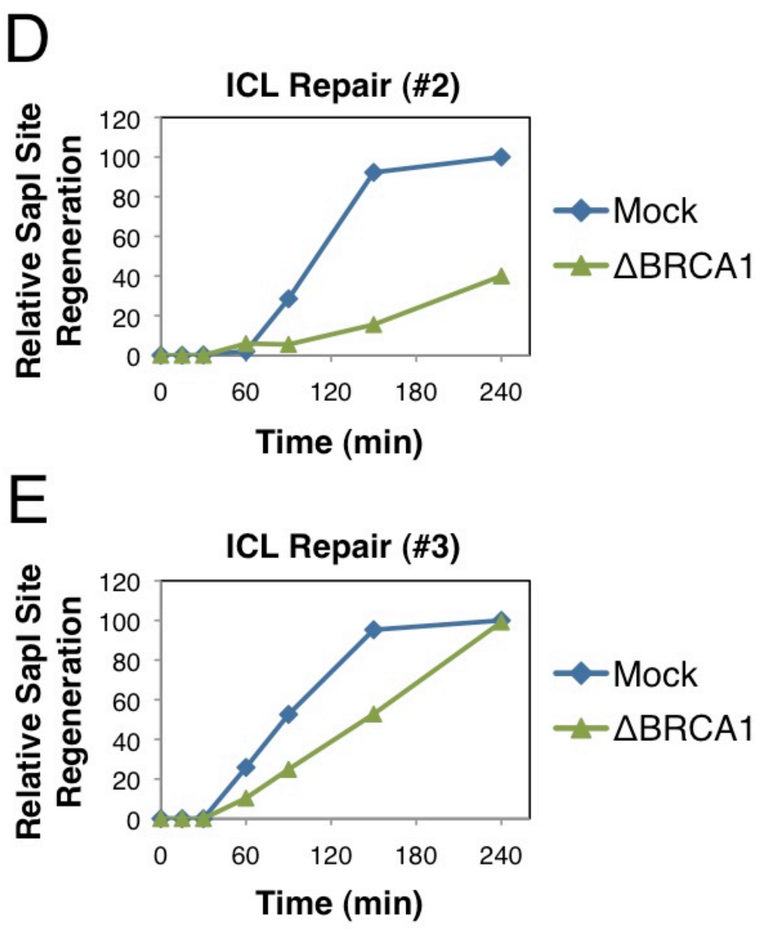
D
ICL Repair (#2)
Relative SapI Site Regeneration
Time (min)
Mock
ΔBRCA1
E
ICL Repair (#3)
Relative SapI Site Regeneration
Time (min)
Mock
ΔBRCA1

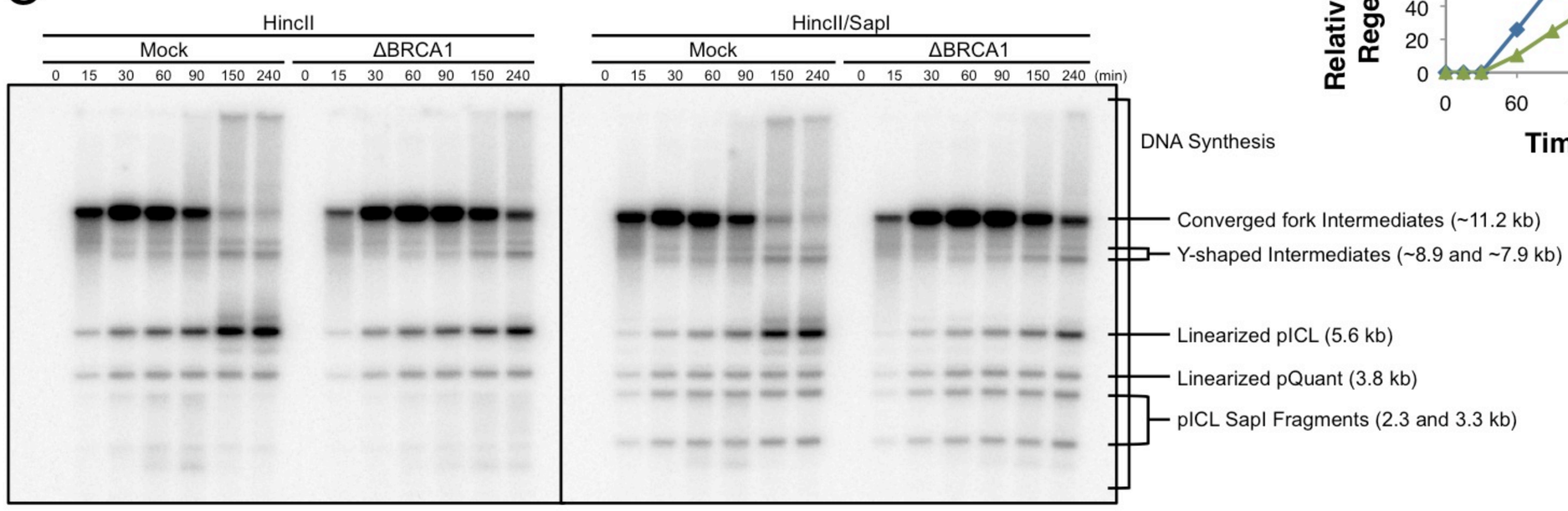
C
HincII
HincII/SapI
Mock
ΔBRCA1
0 15 30 60 90 150 240 (min)
DNA Synthesis
Converged fork Intermediates (~11.2 kb)
Y-shaped Intermediates (~8.9 and ~7.9 kb)
Linearized pICL (5.6 kb)
Linearized pQuant (3.8 kb)
pICL SapI Fragments (2.3 and 3.3 kb)

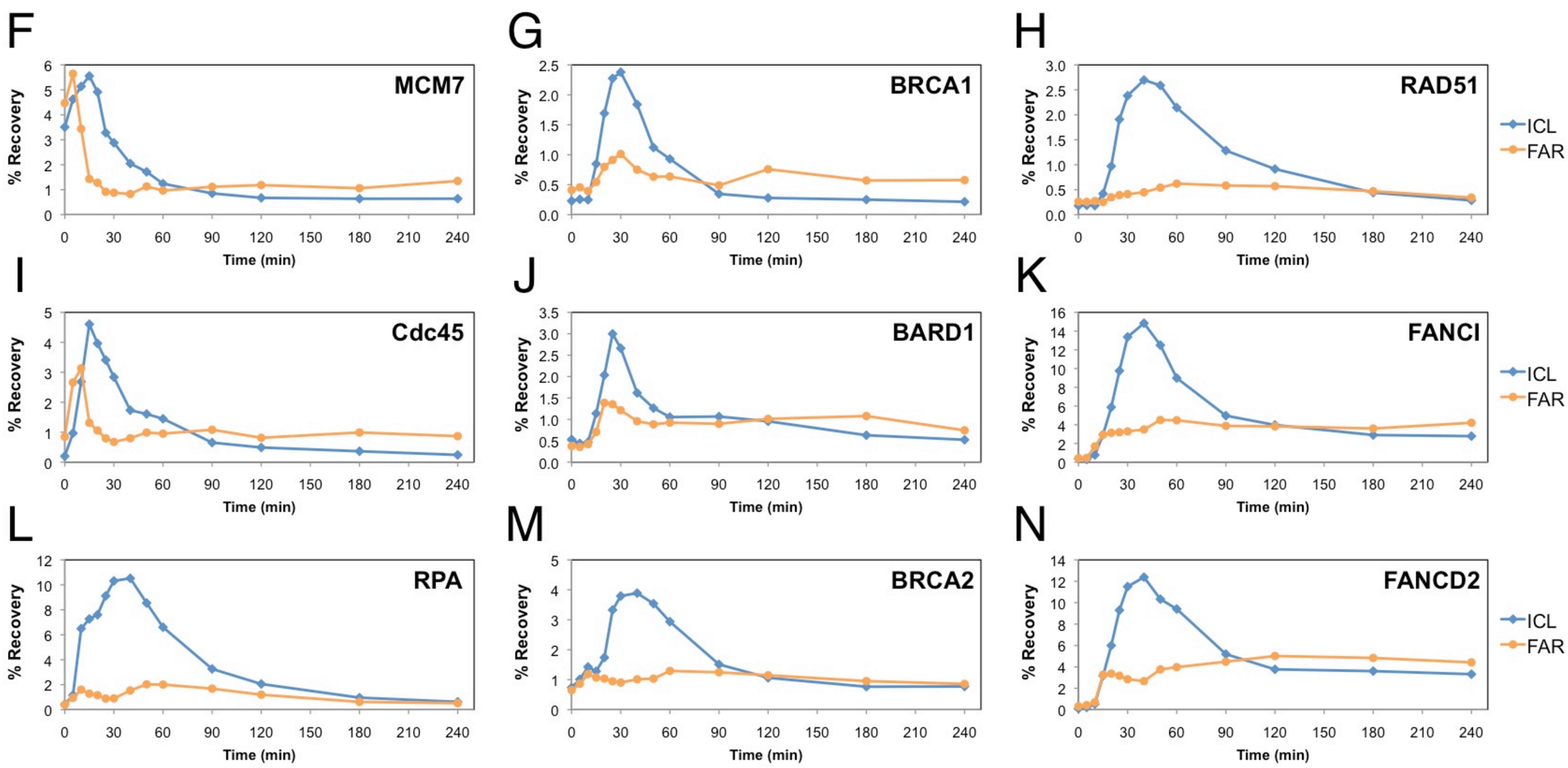
F
MCM7
G
BRCA1
H
RAD51
% Recovery
Time (min)
ICL
FAR
I
Cdc45
J
BARD1
K
FANCI
L
RPA
M
BRCA2
N
FANCD2

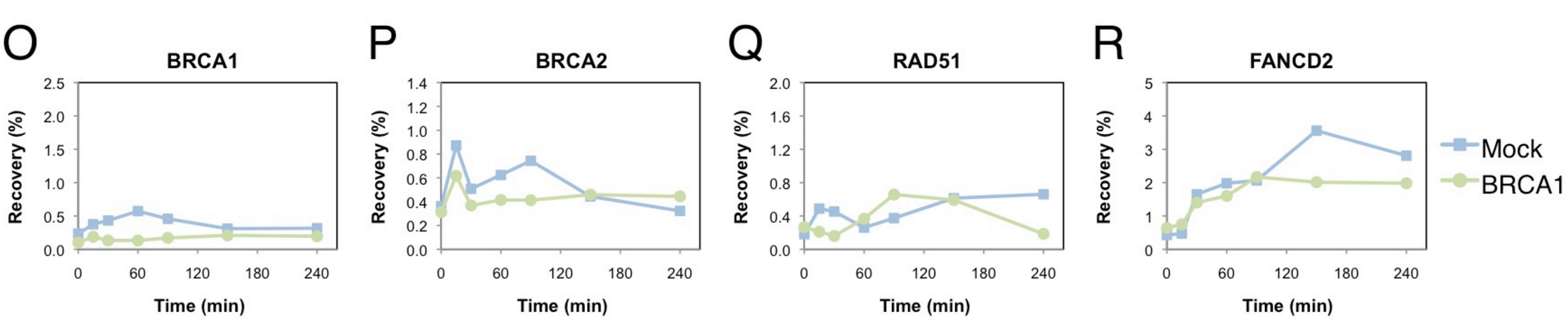
O
BRCA1
P
BRCA2
Q
RAD51
R
FANCD2
Recovery (%)
Time (min)
Mock
BRCA1

Figure S3

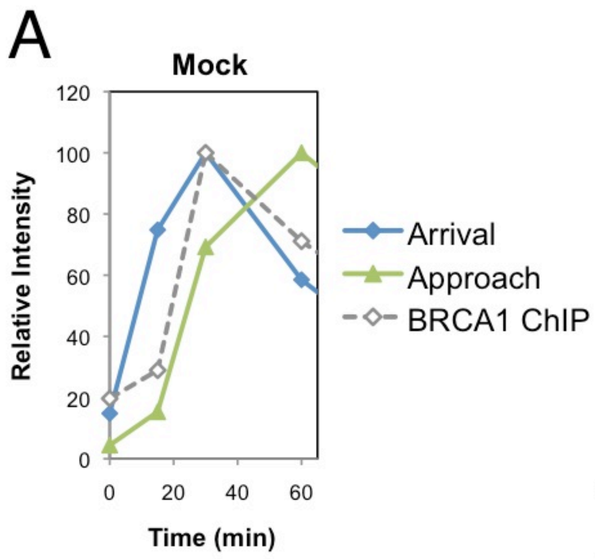
A
Mock
Relative Intensity
Time (min)
Arrival
Approach
BRCA1 ChIP

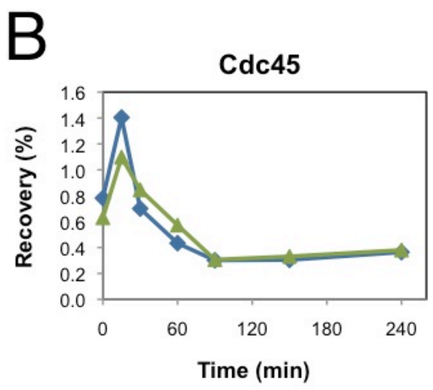
B
Cdc45
Recovery (%)
Time (min)

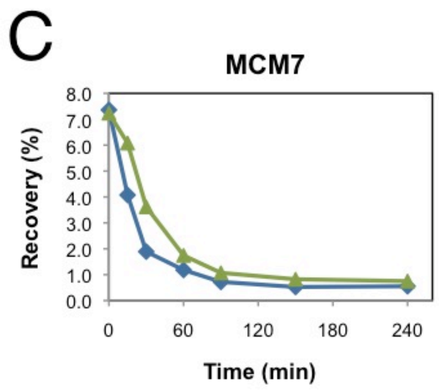
C
MCM7
Recovery (%)
Time (min)

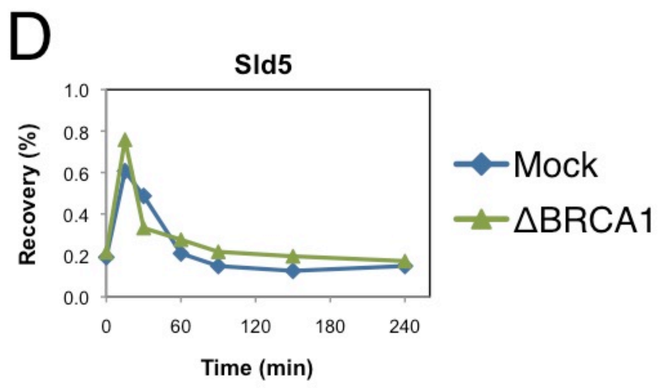
D
Sld5
Recovery (%)
Time (min)
Mock
ΔBRCA1

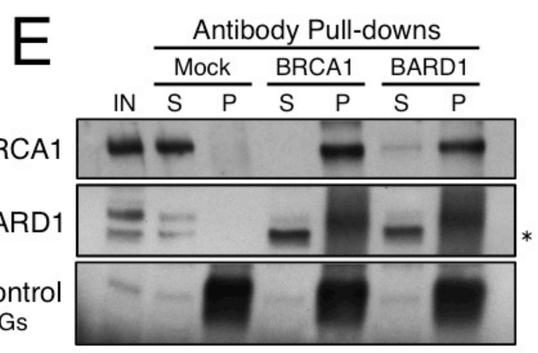
E
Antibody Pull-downs
Mock
BRCA1
BARD1
IN
S
P
αBRCA1
αBARD1
Loading Control
αRabbit IgGs
*
1 2 3 4 5 6 7

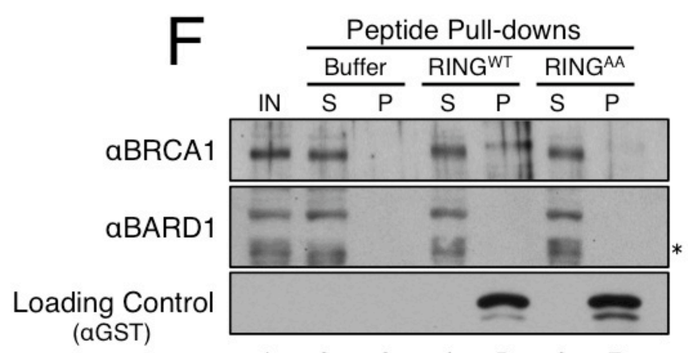
F
Peptide Pull-downs
Buffer
RING^WT
RING^AA
IN
S
P
αBRCA1
αBARD1
Loading Control
(αGST)
*
1 2 3 4 5 6 7

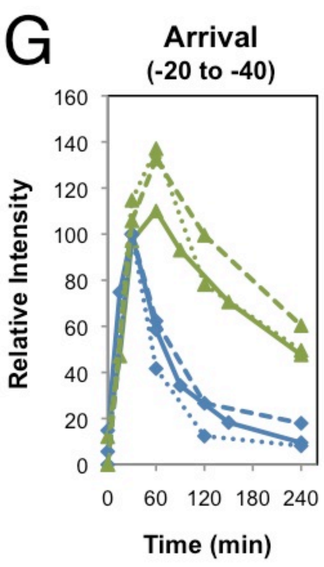
G
Arrival
(-20 to -40)
Relative Intensity
Time (min)

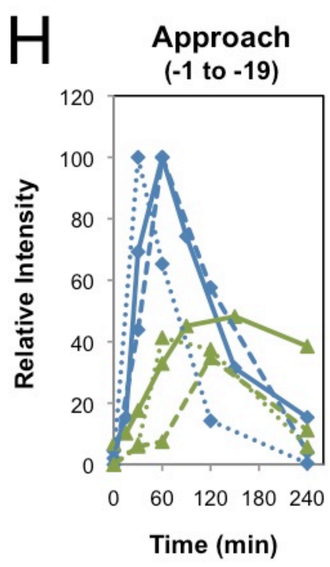
H
Approach
(-1 to -19)
Relative Intensity
Time (min)

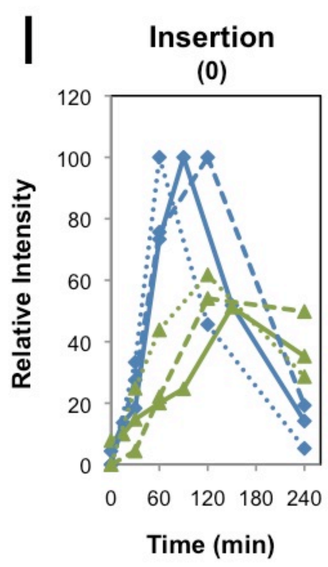
I
Insertion
(0)
Relative Intensity
Time (min)

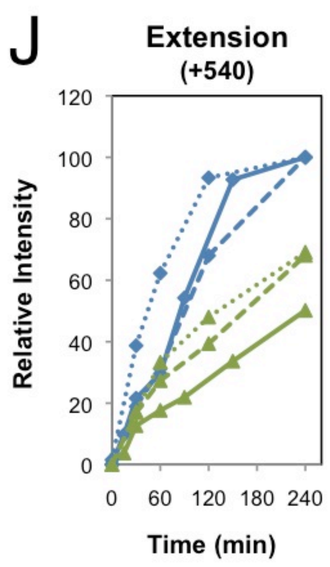
J
Extension
(+540)
Relative Intensity
Time (min)

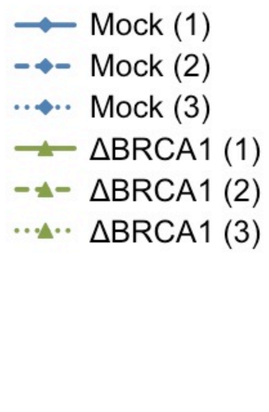
Mock (1)
Mock (2)
Mock (3)
ΔBRCA1 (1)
ΔBRCA1 (2)
ΔBRCA1 (3)

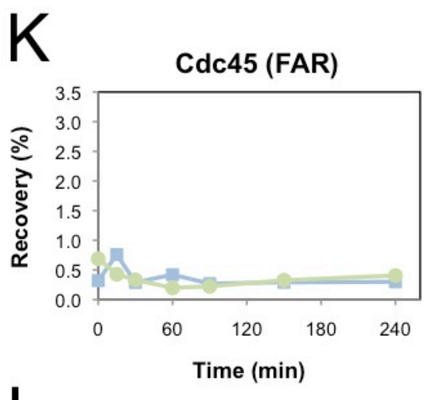
K
Cdc45 (FAR)
Recovery (%)
Time (min)
Mock
ΔBRCA1

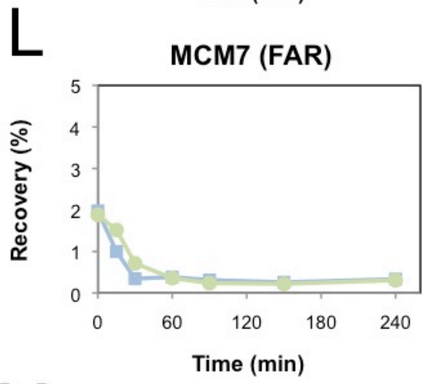
L
MCM7 (FAR)
Recovery (%)
Time (min)
Mock
ΔBRCA1

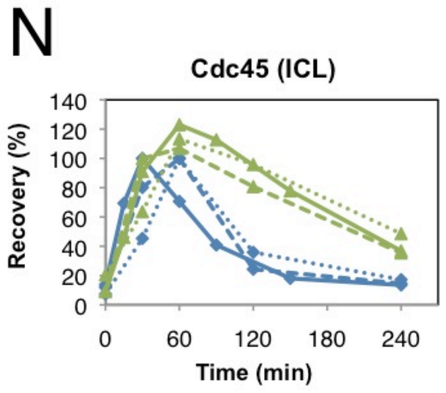
N
Cdc45 (ICL)
Recovery (%)
Time (min)

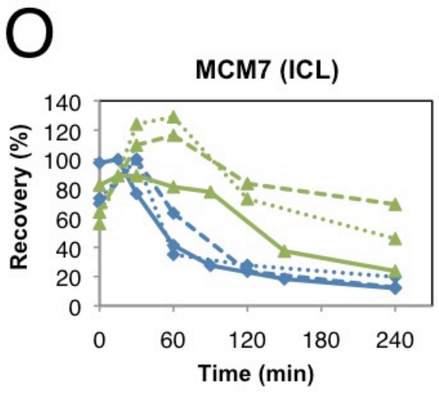
O
MCM7 (ICL)
Recovery (%)
Time (min)

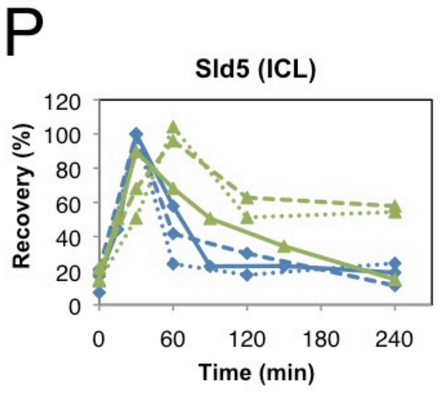
P
Sld5 (ICL)
Recovery (%)
Time (min)

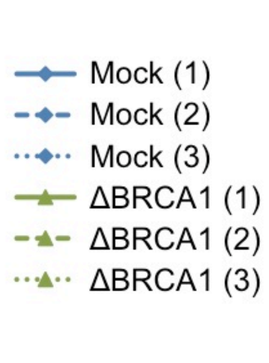
Mock (1)
Mock (2)
Mock (3)
ΔBRCA1 (1)
ΔBRCA1 (2)
ΔBRCA1 (3)

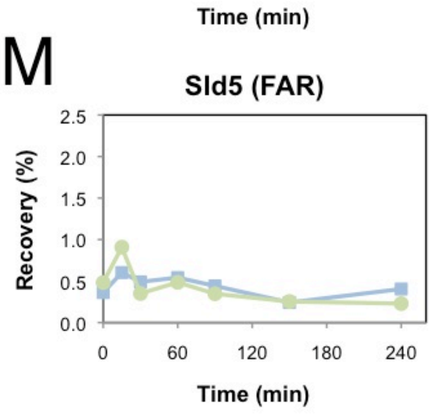
M
Sld5 (FAR)
Recovery (%)
Time (min)
Mock
ΔBRCA1

Figure S4

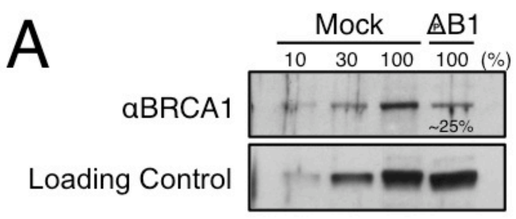
A
Mock
ΔB1
10 30 100 100 (%)
αBRCA1
~25%
Loading Control

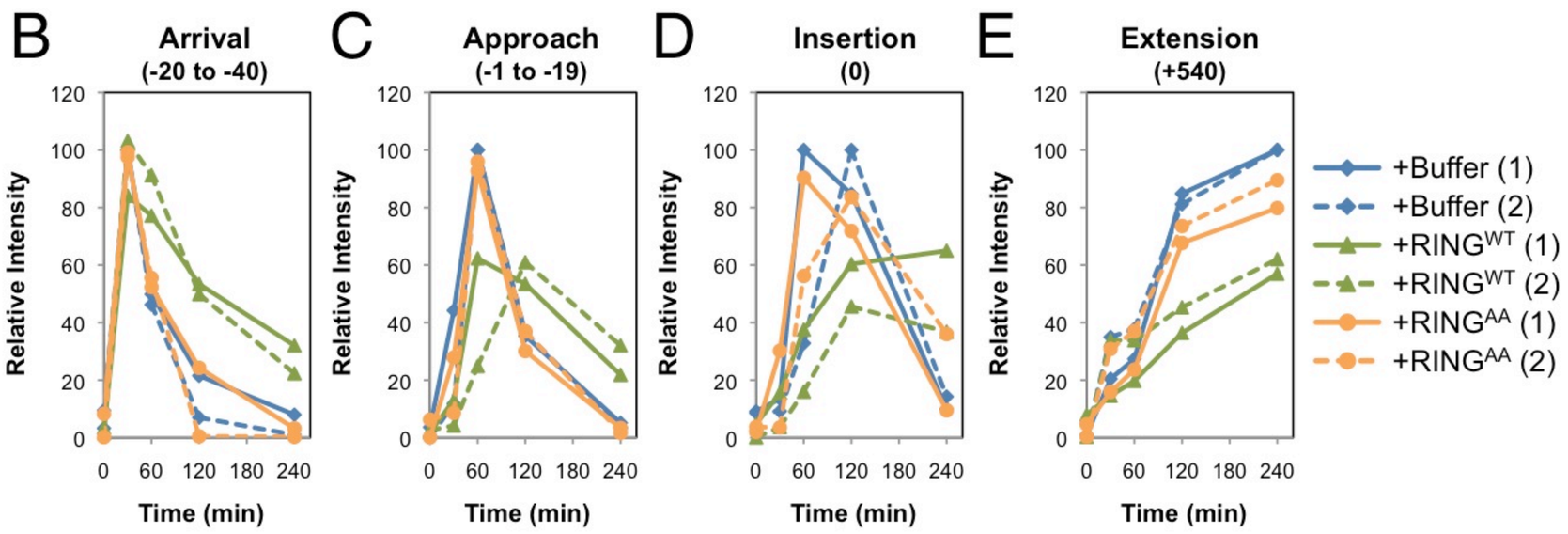
B
Arrival
(-20 to -40)
C
Approach
(-1 to -19)
D
Insertion
(0)
E
Extension
(+540)
Relative Intensity
Time (min)
+Buffer (1)
+Buffer (2)
+RINGWT (1)
+RINGWT (2)
+RINGAA (1)
+RINGAA (2)

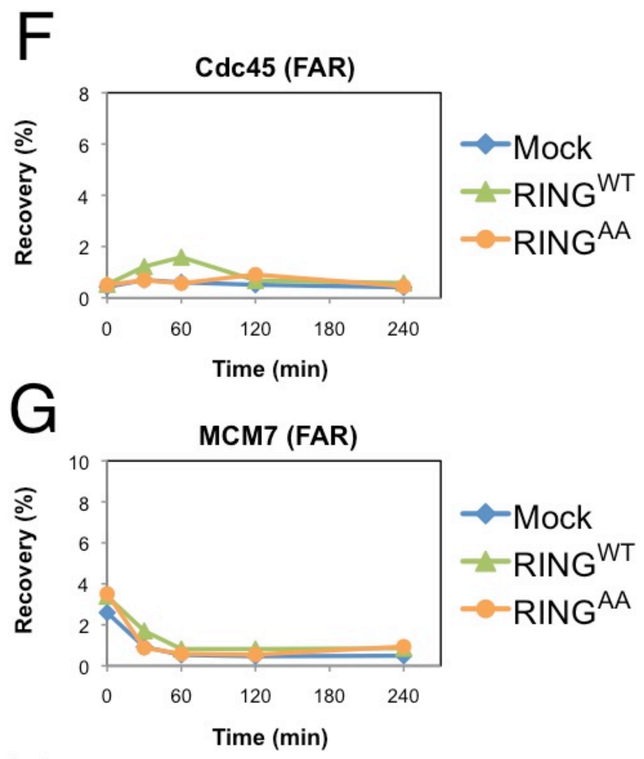
F
Cdc45 (FAR)
G
MCM7 (FAR)
H
Sld5 (FAR)
Recovery (%)
Time (min)
Mock
RINGWT
RINGAA

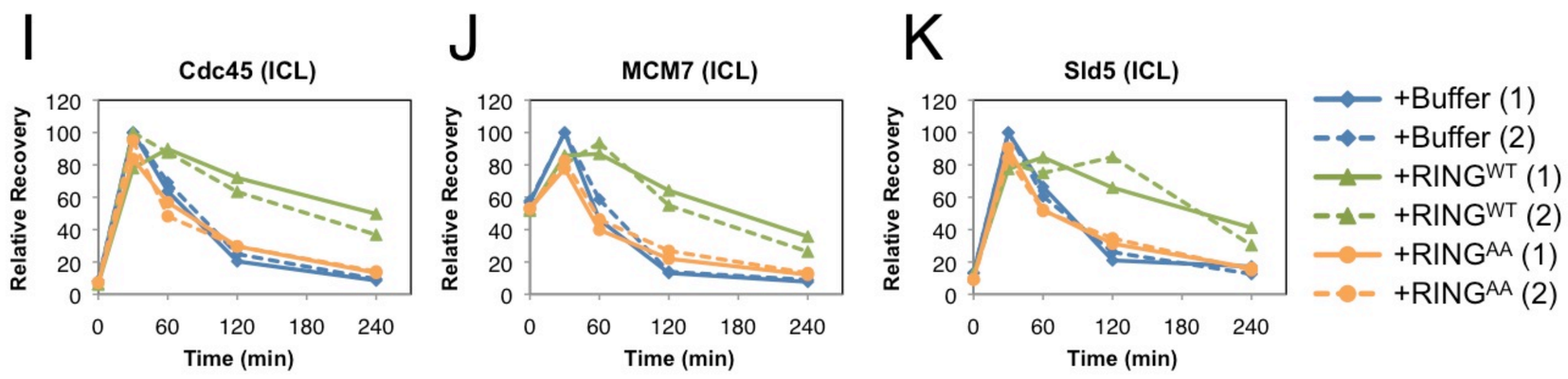
I
Cdc45 (ICL)
J
MCM7 (ICL)
K
Sld5 (ICL)
Relative Recovery
Time (min)
+Buffer (1)
+Buffer (2)
+RINGWT (1)
+RINGWT (2)
+RINGAA (1)
+RINGAA (2)

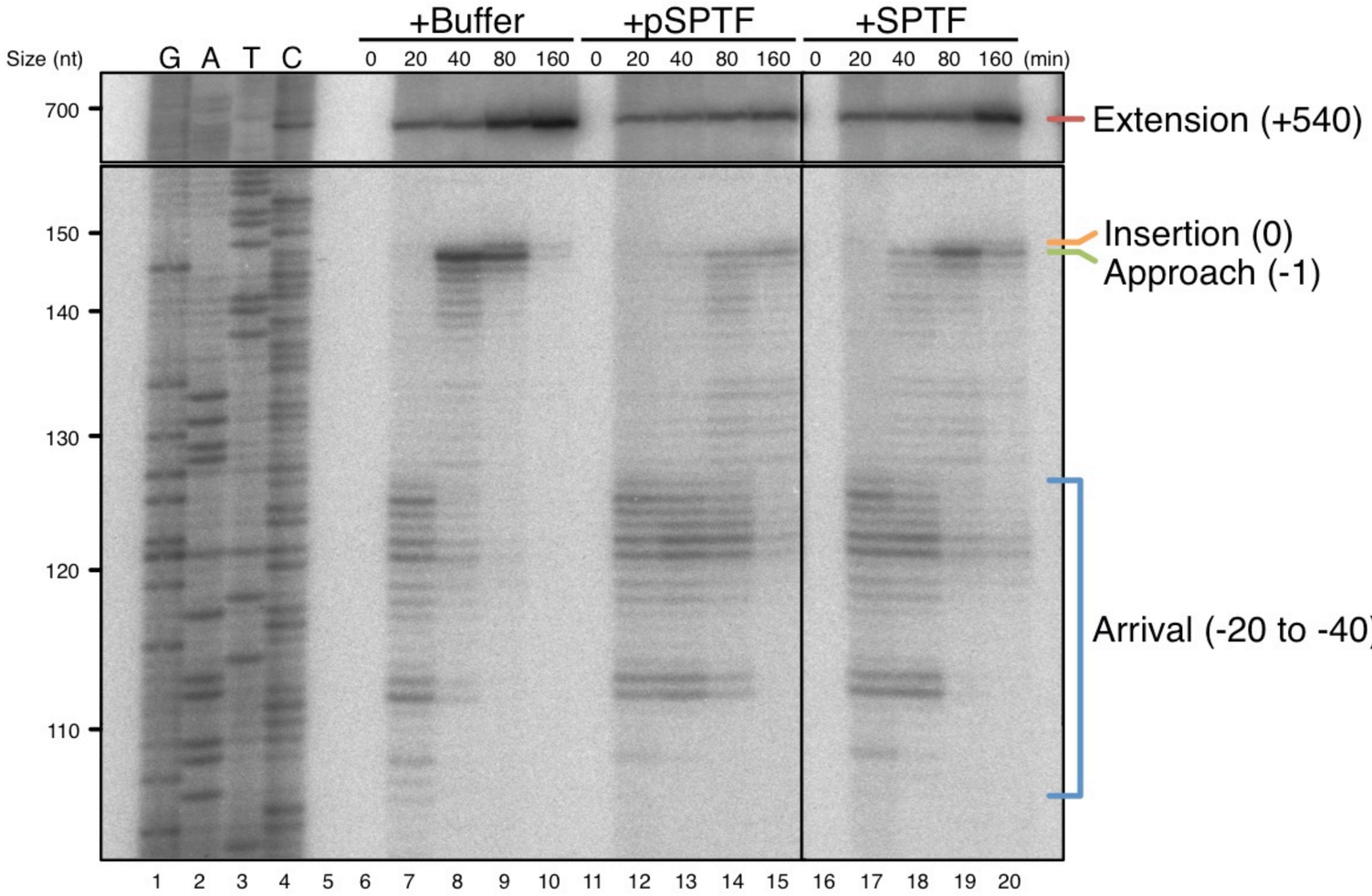
L
+Buffer
+pSPTF
+SPTF
Size (nt)
G A T C
0 20 40 80 160 0 20 40 80 160 0 20 40 80 160 (min)
700
150
140
130
120
110
Extension (+540)
Insertion (0)
Approach (-1)
Arrival (-20 to -40)
1 2 3 4 5 6 7 8 9 10 11 12 13 14 15 16 17 18 19 20

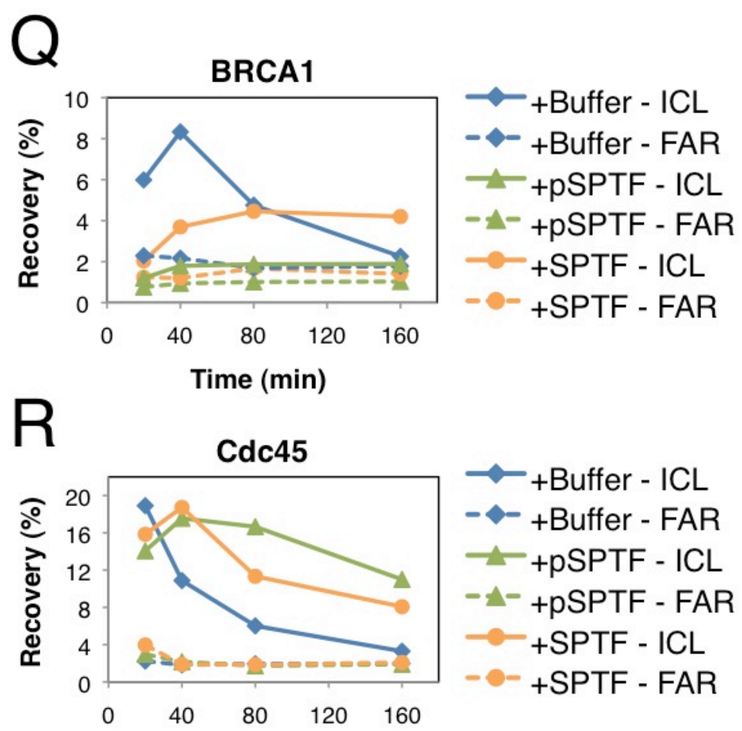
Q
BRCA1
R
Cdc45
S
MCM7
Recovery (%)
Time (min)
+Buffer - ICL
+Buffer - FAR
+pSPTF - ICL
+pSPTF - FAR
+SPTF - ICL
+SPTF - FAR

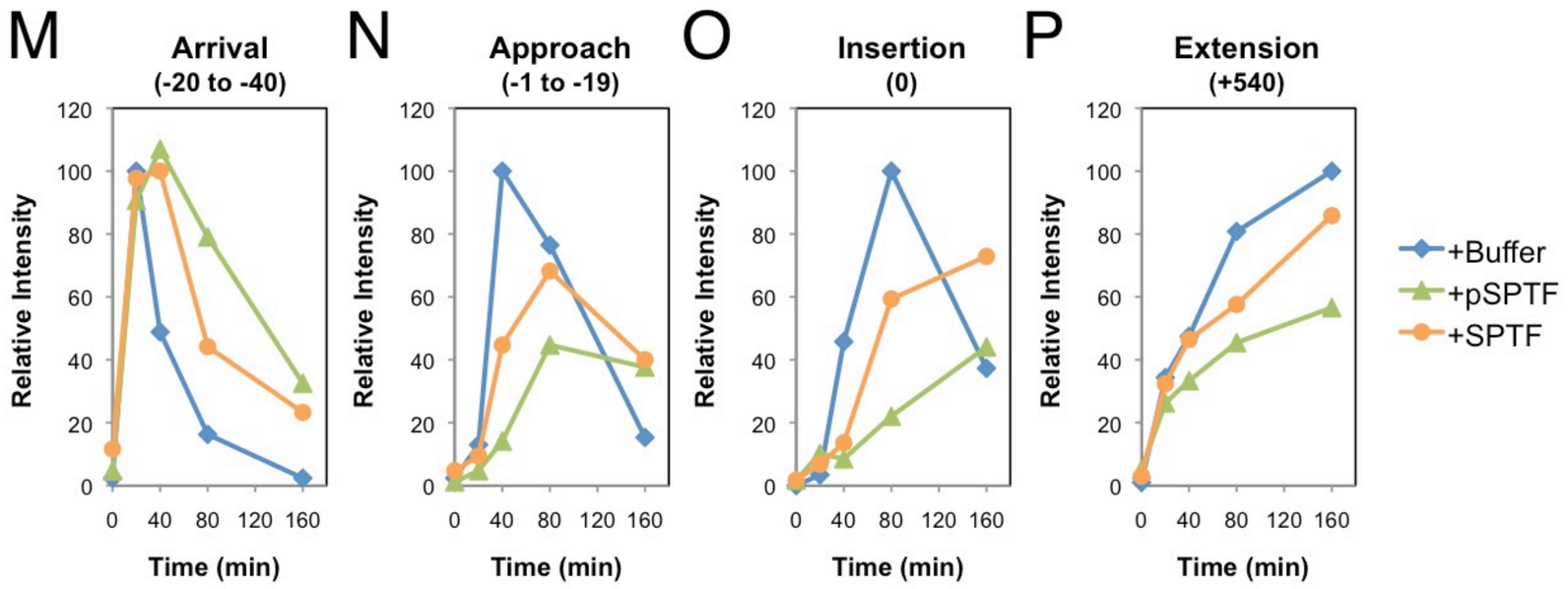
M
Arrival
(-20 to -40)
N
Approach
(-1 to -19)
O
Insertion
(0)
P
Extension
(+540)
Relative Intensity
Time (min)
+Buffer
+pSPTF
+SPTF

Figure S5

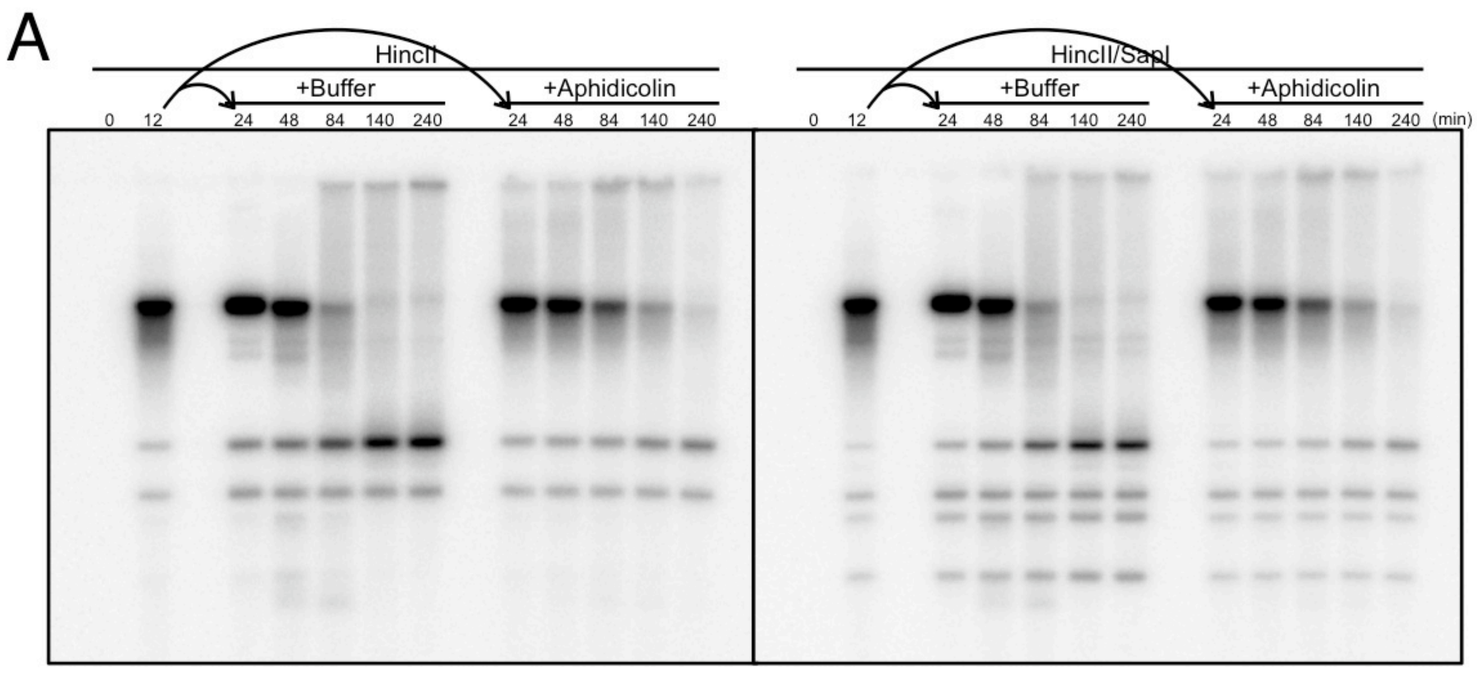
A
HincII
+Buffer
+Aphidicolin
0 12 24 48 84 140 240 24 48 84 140 240
HincII/SapI
+Buffer
+Aphidicolin
0 12 24 48 84 140 240 24 48 84 140 240 (min)

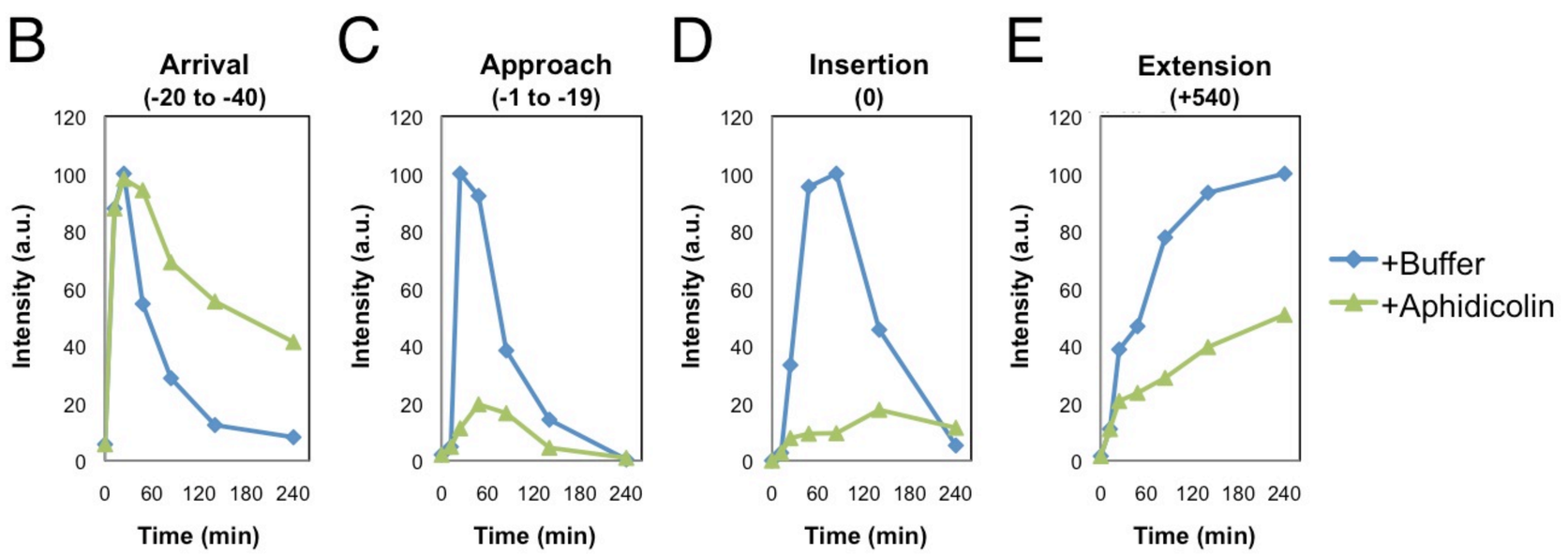
B
Arrival
(-20 to -40)
C
Approach
(-1 to -19)
D
Insertion
(0)
E
Extension
(+540)
Intensity (a.u.)
Time (min)
+Buffer
+Aphidicolin

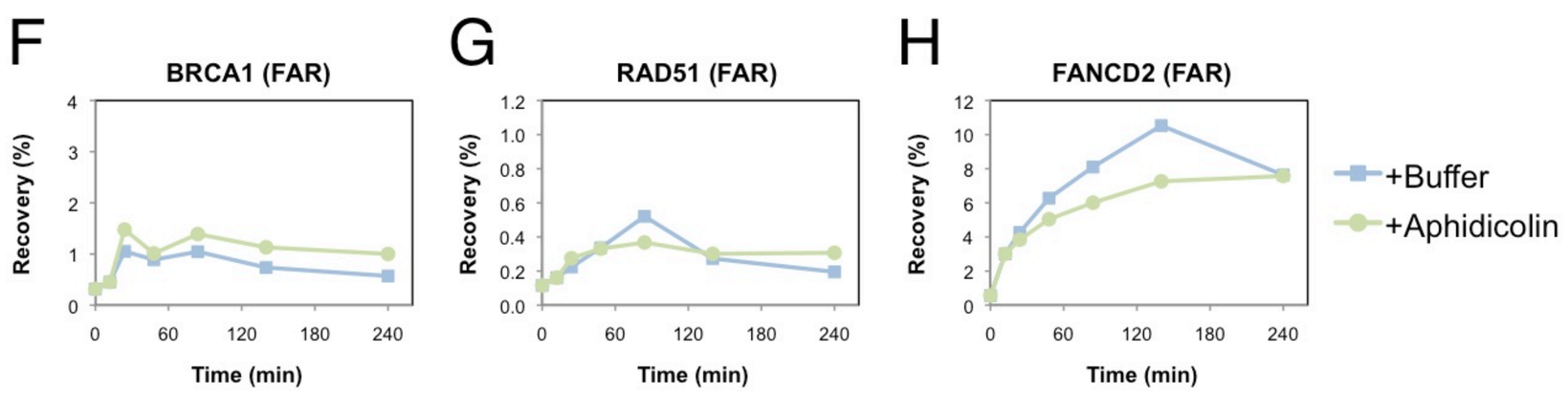
F
BRCA1 (FAR)
G
RAD51 (FAR)
H
FANCD2 (FAR)
Recovery (%)
Time (min)
+Buffer
+Aphidicolin

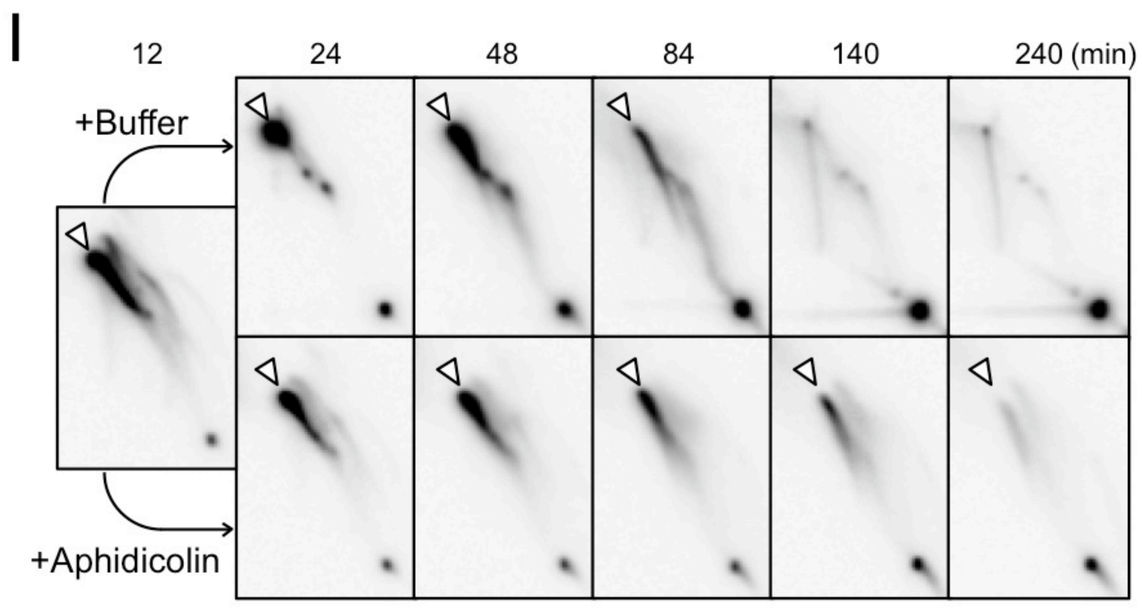
I
12 24 48 84 140 240 (min)
+Buffer
+Aphidicolin
Converged Forks

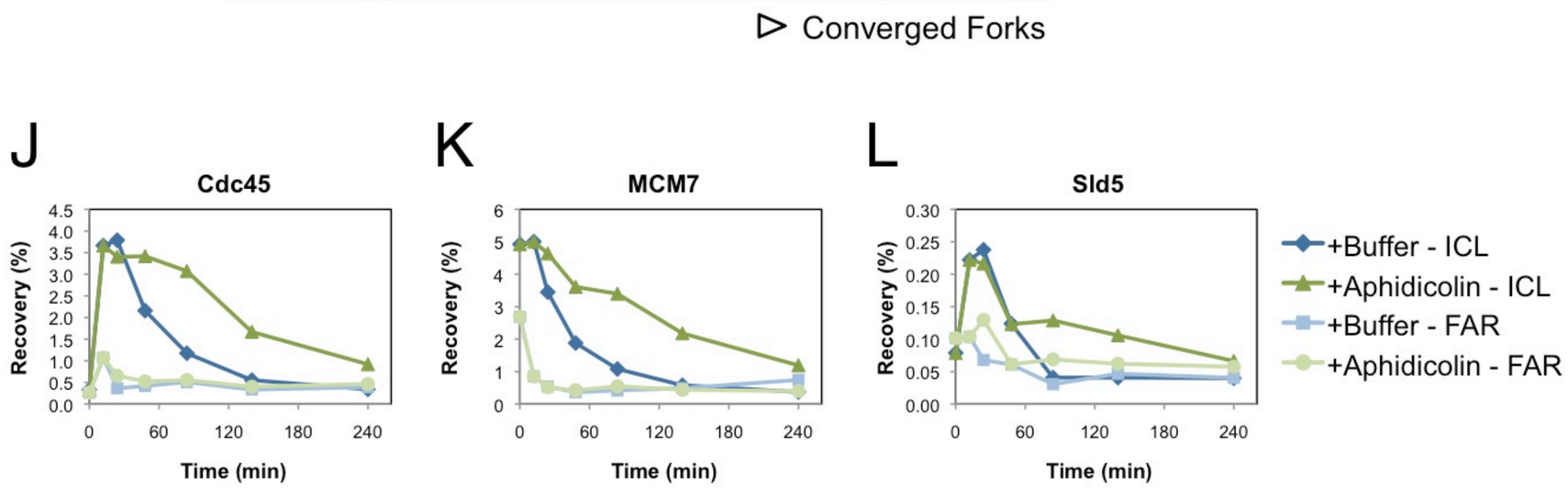
J
Cdc45
K
MCM7
L
Sld5
Recovery (%)
Time (min)
+Buffer - ICL
+Aphidicolin - ICL
+Buffer - FAR
+Aphidicolin - FAR

Figure S6

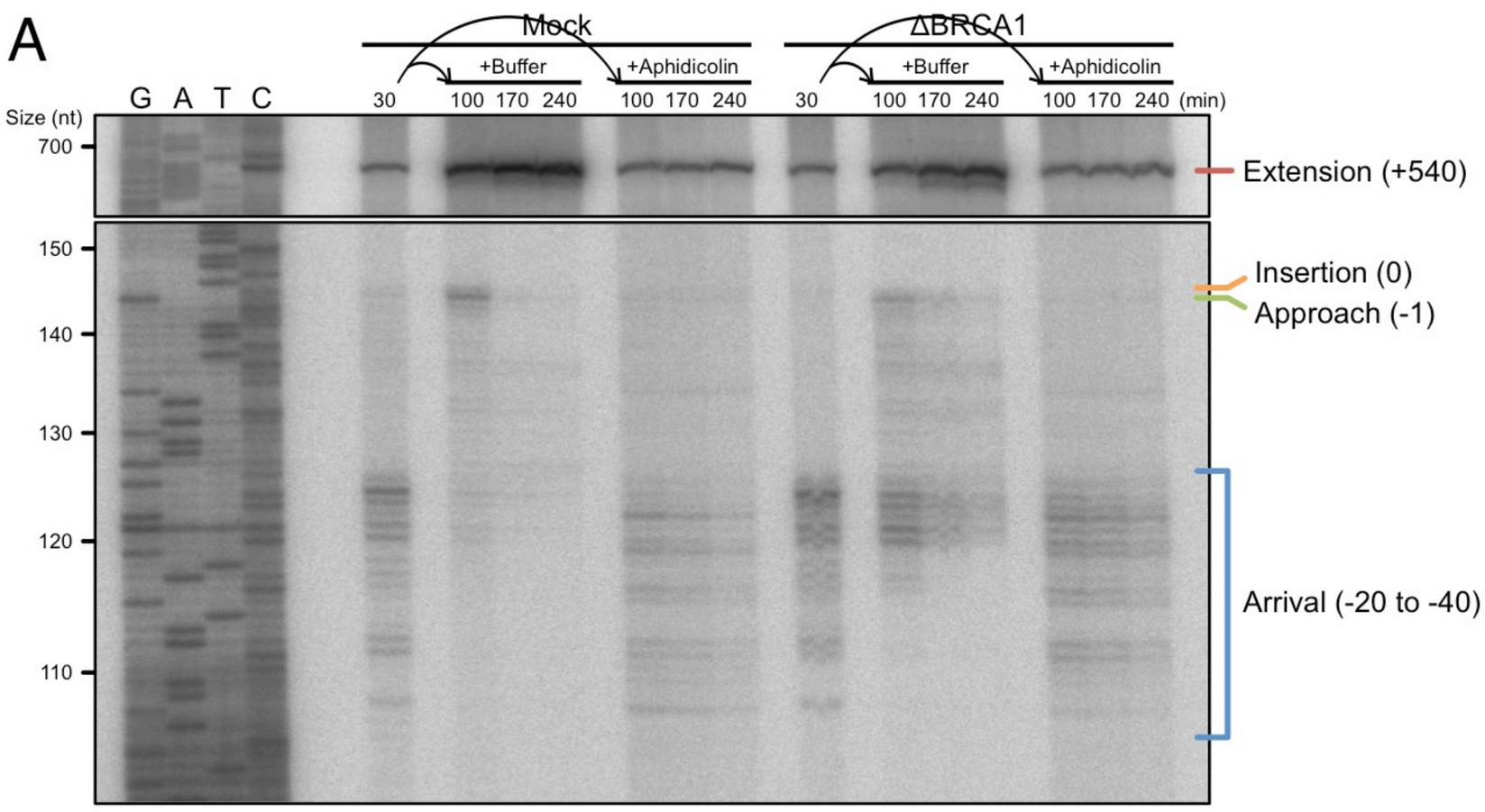
A
Mock
ΔBRCA1
+Buffer
+Aphidicolin
G A T C
30 100 170 240 100 170 240 (min)
Size (nt)
700
150
140
130
120
110
Extension (+540)
Insertion (0)
Approach (-1)
Arrival (-20 to -40)

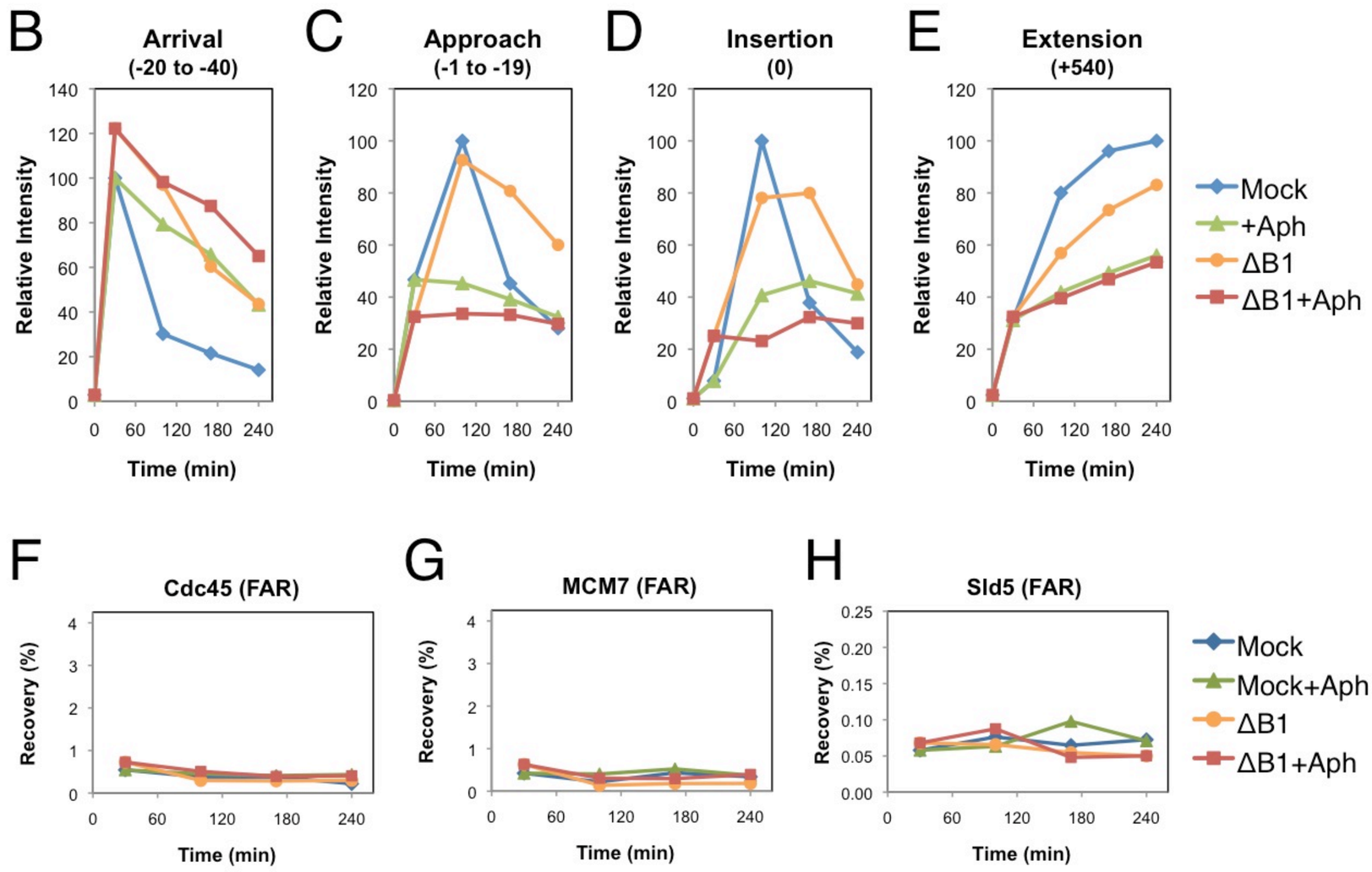
B
Arrival
(-20 to -40)
C
Approach
(-1 to -19)
D
Insertion
(0)
E
Extension
(+540)
Relative Intensity
Time (min)
Mock
+Aph
ΔB1
ΔB1+Aph
F
Cdc45 (FAR)
G
MCM7 (FAR)
H
Sld5 (FAR)
Recovery (%)
Mock
Mock+Aph
ΔB1
ΔB1+Aph

Figure S7

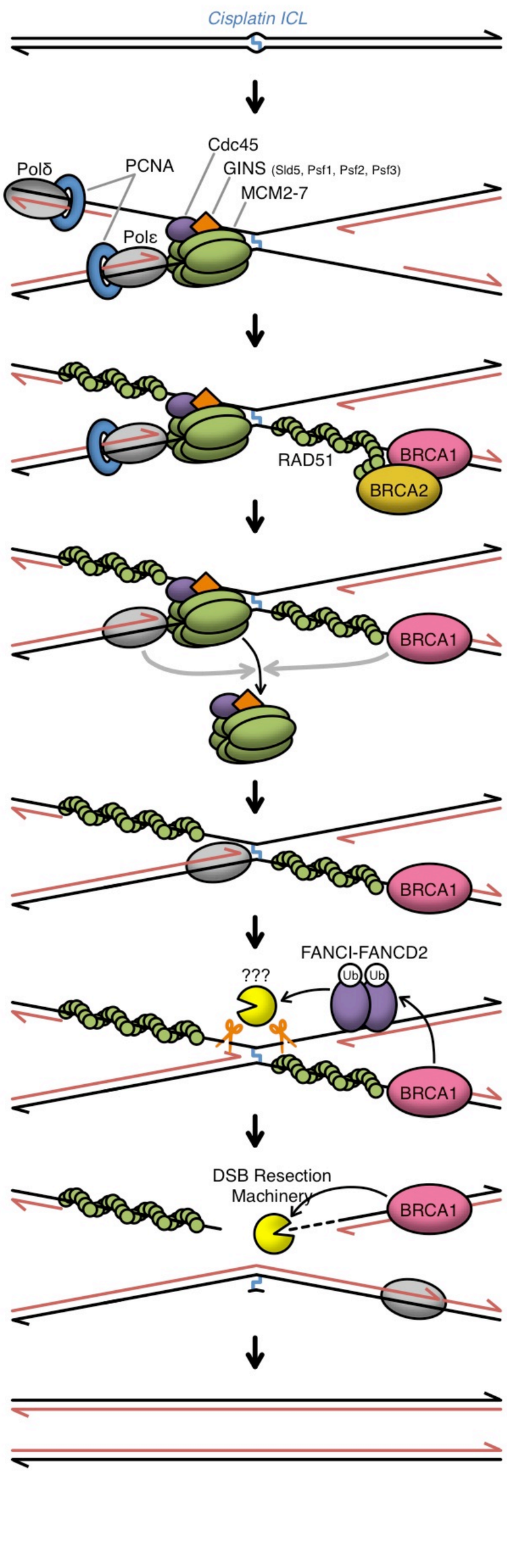

i. Fork Convergence

Replication forks converge on the ICL with leading strands stalling ~20 nucleotides from the crosslink due to the presence of the CMG replicative helicase complex.

ii. RAD51 Loading

Ubiquitin signaling promotes recruitment of BRCA1 and BRCA2 to ICL-stalled forks, followed by loading of RAD51 onto regions of ssDNA present at lagging strand gaps.

iii. Helicase Unloading

BRCA1 and the action of the polymerase cooperate to promote efficient unloading of the replicative helicase.

iv. Leading Strand Approach

Helicase eviction allows extension of leading strands to within 1 nucleotide of the ICL.

v. DNA Incisions

Leading strand extension creates a DNA structure that supports FANCI-FANCD2-dependent incisions by XPF-ERCC1 and other endonucleases.

vi. Lesion Bypass

Dual incisions unhook the ICL, creating a DSB in one sister chromatid and allowing lesion bypass to restore the other sister.

vii. HR and NER

Recombination repairs the DSB using the intact sister chromatid as a template for repair. The unhooked adduct is removed by excision repair.

Supplemental Figure Legends

Figure S1, related to Figure 2. (**A**) Samples from the reaction presented in Figure 2 were analyzed by Western blot with the indicated antibodies and quantified for (**B)** FANCD2 ubiquitylation and (**C**) Chk1 phosphorylation. (**D**) Primary data from which DNA Synthesis and ICL Repair was calculated for Figures 2A and B, respectively (described in *Methods*). pICL was replicated in extract supplemented with buffer (+Buffer), UbVS (+UbVS), or UbVS and ubiquitin (+UbVS+Ub) and DNA intermediates were digested with HincII or HincII and SapI. Samples were then separated by native agarose gel electrophoresis and visualized by phosphorimager. Intermediates used for quantification are indicated at right. (**E**-**J**) ChIP data from Figures 2C-E and 2H-J are shown with percent recovery values at the FAR locus. (**K**-**N**) Quantification of nascent strand products from Figure 2G (solid lines) is shown with two experimental replicates (dashed and dotted lines). Arrival (-20 to -40 position), Approach (-1 to -19), Insertion (0), Extension (+540). The abundance of each product is normalized to peak values in +Buffer samples. (**O**-**Q**) ChIP data from Figure 2H-J (solid lines) is shown with experimental replicates (dashed and dotted lines). Three replicates are shown for Cdc45 and two for MCM7 and Sld5.

Figure S2, related to Figure 3. (**A**) Western blot analysis of mock-depleted (Mock) and BRCA1-depleted (ΔB1) extracts. Relative protein levels in BRCA1-depleted extracts were determined by comparison with a dilution series of mock-depleted extract and indicated as a percentage in the figure. (**B**) Primary data from which Converged Forks accumulation was calculated for Figures 3A and B. pICL was replicated in extract supplemented with radioactive nucleotide to label nascent strands. Uncut DNA intermediates were separated by native agarose gel electrophoresis and visualized by phosphorimager. The radioactivity in the bands

encompassed by the bracket, which represent intact forks that have undergone varying degrees of resection, was quantified and graphed in Figures 3A and B. (**C**) Primary data from which DNA Synthesis and ICL Repair was calculated for Figures 3E and F, as in Figure S1. (**D** and **E**) ICL Repair data from two additional BRCA1 depletion experiments (#2 and #3, respectively). (**F**-**N**) ChIP data from Figure 3A-C are shown with percent recovery values for both ICL and FAR loci. (**O**-**R**) ChIP data from Figure 3G-J are shown with percent recovery values at the FAR locus.

Figure S3, related to Figure 5. (**A**) For the mock-depleted reaction from Figure 3, Arrival and Approach products (from *H* and *I*) were graphed relative to BRCA1 recruitment at the ICL as measured by ChIP (from Figure 3G). Mock- and BRCA1-depleted samples from Figure 3 were also used to analyze recruitment (by ChIP) of (**B**) Cdc45, (**C**) MCM7, and (**D**) Sld5 to an undamaged plasmid included in the replication reaction (pQuant, see *Methods*). (**E**) Pre-immune (Mock), BRCA1, or BARD1 antibodies were immobilized on protein A sepharose beads, then incubated with extract (input; IN). Beads were then pulled down and the supernatant (S) and pellet (P) fractions were blotted with the indicated antibodies. (**F**) Buffer, or the indicated BARD1 RING peptides were immobilized on glutathione sepharose beads, then incubated with extract, pulled down, and blotted as in *(E)*. Unlike the BRCA1 and BARD1 antibodies, which quantitatively precipitated both BRCA1 and BARD1, the $RING^{WT}$ peptide recovered only BRCA1, indicating that BARD1 was displaced from the complex. (**G**-**J**) Quantification of nascent strand products from Figure 5A (solid lines) is shown with two experimental replicates (dashed and dotted lines). The abundance of products at each time point is normalized to peak values in mock-depleted samples. (**K**-**M**) ChIP data from Figure 5B-D are shown with percent recovery values at the FAR locus. (**N**-**P**) ChIP data from Figure 5B-D (solid lines) are shown with two experimental replicates (dashed and dotted lines).

Figure S4, related to Figure 6. (**A**) Western blot analysis of mock-depleted (Mock) and partially BRCA1-depleted (ΔB1) extracts. The relative protein level was determined by comparison with a dilution series of mock-depleted extract. (**B**-**E**) Quantification of nascent strand products from Figure 6A (solid lines) is shown with two experimental replicates (dashed and dotted lines). The abundance of each product is normalized to peak values in +Buffer samples. (**F**-**H**) ChIP data from Figure 6B-D are shown with percent recovery values at the FAR locus. (**I**-**K**) ChIP data from Figure 6B-D (solid lines) are shown with an experimental replicate (dashed lines). pICL was replicated in egg extract for 18 minutes, then supplemented with buffer (+Buffer), phosphorylated SXXF peptide (+pSPTF), or non-phosphorylated SXXF peptide (+SPTF). At the indicated times, samples were then analyzed by denaturing polyacrylamide gel electrophoresis (**L; irrelevant lanes removed between lanes 15 and 16**) with strand products quantified in (**M**-**P**), and by ChIP with the indicated antibodies (**Q-S**).

Figure S5, related to Figure 7. (**A**) Primary data from which DNA replication (Figure 7B) and ICL repair (Figure 7G) were calculated. (**B**-**E**) Quantification of nascent strand products from Figure 7A. The abundance of products at each time point is normalized to peak values in +Buffer samples. (**F**-**H**) ChIP data from Figure 7C-E are shown with percent recovery values at the FAR locus. (**I**) Primary data from which Converged Forks accumulation (open arrowhead) was calculated (Figure 7F). (**J**-**L**) Samples from Figure 7A-G were analyzed by ChIP with the indicated antibodies at the ICL and FAR loci.

Figure S6, related to Figure 7. Primary data related to Figure 7H-J. (**A**) Nascent strand product formation in mock-depleted (Mock) and BRCA1-depleted (ΔBRCA1) extract supplemented with Buffer or Aphidicolin after 30 minutes. (**B**-**E**) Quantification of nascent strand products from *A*.

The abundance of products at each time point is normalized to peak values in the Mock+Buffer samples. (**F**-**H**) ChIP data showing Cdc45, MCM7, and Sld5 recovery at the FAR locus.

Figure S7, related to Figure 1. Schematic model of ICL repair in *Xenopus laevis* egg extracts. Parental DNA (black lines), nascent strands (red lines). HR (homologous recombination), DSB (double-strand break).

Article

Molecular Cell

Two-Stage Synapsis of DNA Ends during Non-homologous End Joining

Graphical Abstract

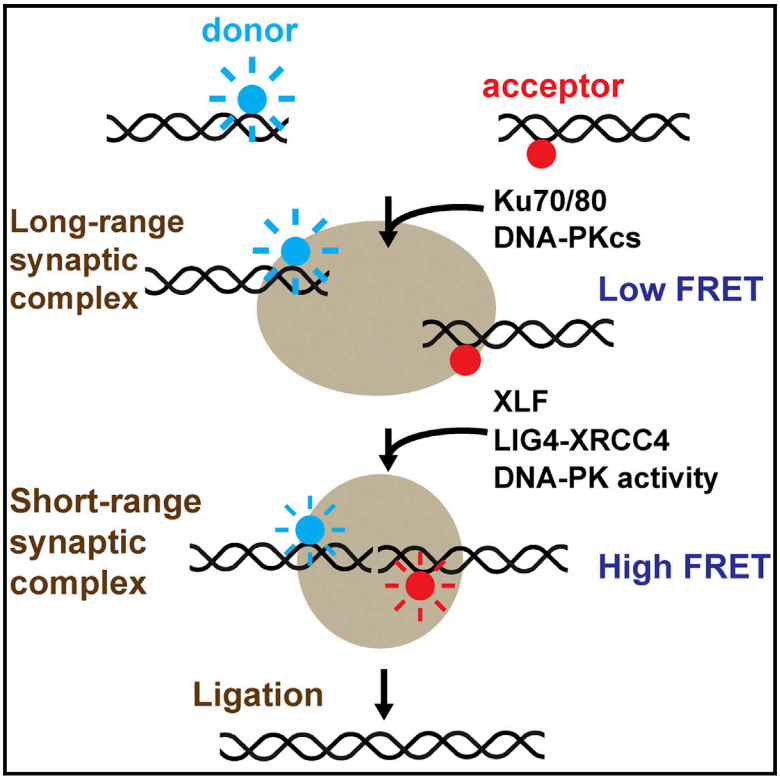

Highlights

- Non-homologous end joining (NHEJ) was monitored on single DNA molecules
- Synapsis of DNA ends during NHEJ proceeds through two distinct stages
- Different NHEJ factors are required at different stages of synapsis
- DNA-PK activity is required to transition between the two synaptic complexes

Authors

Thomas G.W. Graham, Johannes C. Walter, Joseph J. Loparo

Correspondence

johannes_walter@hms.harvard.edu (J.C.W.), joseph_loparo@hms.harvard.edu (J.J.L.)

In Brief

Graham et al. use single-molecule fluorescence imaging to monitor DNA repair by non-homologous end joining (NHEJ) in *Xenopus laevis* egg extract. Synapsis of DNA ends is found to proceed through two stages. Different NHEJ factors are required at each stage, and DNA-PK activity is required for the transition between stages.

Graham et al., 2016, Molecular Cell *61*, 850–858
March 17, 2016
http://dx.doi.org/10.1016/j.molcel.2016.02.010

CellPress

Molecular Cell
Article

Two-Stage Synapsis of DNA Ends during Non-homologous End Joining

Thomas G.W. Graham,[1,2] Johannes C. Walter,[2,3,*] and Joseph J. Loparo[2,*]
[1]Department of Systems Biology
[2]Department of Biological Chemistry and Molecular Pharmacology
[3]Howard Hughes Medical Institute
Harvard Medical School, Boston, MA 02115, USA
*Correspondence: johannes_walter@hms.harvard.edu (J.C.W.), joseph_loparo@hms.harvard.edu (J.J.L.)
http://dx.doi.org/10.1016/j.molcel.2016.02.010

SUMMARY

Repair of DNA double-strand breaks (DSBs) is essential for genomic stability. The most common DSB repair mechanism in human cells, non-homologous end joining (NHEJ), rejoins broken DNA ends by direct ligation. It remains unclear how components of the NHEJ machinery assemble a synaptic complex that bridges DNA ends. Here, we use single-molecule imaging in a vertebrate cell-free extract to show that synapsis of DNA ends occurs in at least two stages that are controlled by different NHEJ factors. DNA ends are initially tethered in a long-range complex whose formation requires the Ku70/80 heterodimer and the DNA-dependent protein kinase catalytic subunit. The ends are then closely aligned, which requires XLF, a non-catalytic function of XRCC4-LIG4, and DNA-PK activity. These results reveal a structural transition in the synaptic complex that governs alignment of DNA ends. Our approach provides a means of studying physiological DNA DSB repair at single-molecule resolution.

INTRODUCTION

Most DNA double-strand breaks (DSBs) in human cells are repaired by non-homologous end joining (NHEJ), a mechanism that directly ligates broken DNA ends (Chiruvella et al., 2013; Radhakrishnan et al., 2014). By using a range of DNA-processing enzymes, NHEJ can join a variety of damaged or mismatched substrates (Ma et al., 2005; Waters et al., 2014a). A drawback of this versatility is the potential to generate mutations, either by inserting or deleting nucleotides during processing or by joining the wrong pairs of ends. Understanding how cells minimize such errors, while ensuring timely repair of DSBs, requires a detailed picture of the protein complex that holds together DNA ends to be processed and ligated.

Broken DNA ends are first bound by the basket-shaped Ku70/80 heterodimer, which recruits the 469 kDa DNA-dependent protein kinase catalytic subunit (DNA-PKcs) to form the DNA-PK holoenzyme (Carter et al., 1990; Dvir et al., 1992, 1993; Gottlieb and Jackson, 1993; Lees-Miller et al., 1990). DNA-PKcs phosphorylates several NHEJ factors, including itself (Dobbs et al., 2010), and its kinase activity is essential for NHEJ (Dobbs et al., 2010; Jette and Lees-Miller, 2015; Jiang et al., 2015). During classical NHEJ (c-NHEJ), DNA ends are ligated by a complex of DNA ligase IV (LIG4) and XRCC4 (Critchlow et al., 1997; Grawunder et al., 1997). The XRCC4 paralog XLF (XRCC4-like factor) stimulates the activity of the XRCC4-LIG4 complex in vitro and is important for NHEJ in vivo (Ahnesorg et al., 2006; Buck et al., 2006; Gu et al., 2007; Lu et al., 2007; Tsai et al., 2007; Zha et al., 2007). Another recently discovered paralog of XRCC4 and XLF, PAXX, has been implicated in NHEJ, although its function is unclear (Craxton et al., 2015; Ochi et al., 2015; Xing et al., 2015).

Almost all of the factors described above have been proposed to play a role in bridging DNA ends. Early work reported DNA bridging by purified Ku70/80 protein (Ramsden and Gellert, 1998, but see Cottarel et al., 2013). In addition, DNA-PK holoenzyme complexes assembled with purified Ku70/80 and DNA-PKcs can dimerize to bridge DNA ends (Cary et al., 1997; DeFazio et al., 2002; Hammel et al., 2010; Spagnolo et al., 2006). Similar DNA pull-down experiments in a human cell-free extract support a role for Ku and DNA-PKcs in synapsis of DNA ends and additionally implicate LIG4, independent of its catalytic activity (Cottarel et al., 2013). Purified XLF and XRCC4 interact to form long, alternating oligomers capable of bridging DNA molecules in vitro (reviewed in Mahaney et al., 2013). However, a recent report that XRCC4-XLF interactions are dispensable for NHEJ in some cell types (Roy et al., 2015) suggests that XLF-XRCC4 filaments are not universally required for synapsis. Collectively, these observations have not coalesced into a coherent model of physiological synaptic complex assembly. Specifically, the steps in this process and the roles of individual NHEJ factors are unknown.

Here, we address these questions by visualizing joining of fluorescently labeled DNA ends in *Xenopus laevis* egg extracts, which support highly efficient NHEJ. We first demonstrate that ligation in this system requires Ku70/80, DNA-PKcs, DNA-PKcs kinase activity, XLF, and XRCC4-LIG4, indicating that it occurs by a physiological mechanism. Next, we present a single-molecule Förster resonance energy transfer (FRET) assay that reveals two conformational stages in end synapsis: (1) a long-range complex in which DNA ends are tethered but too far apart to detect FRET between end-proximal dyes and (2) a short-range complex

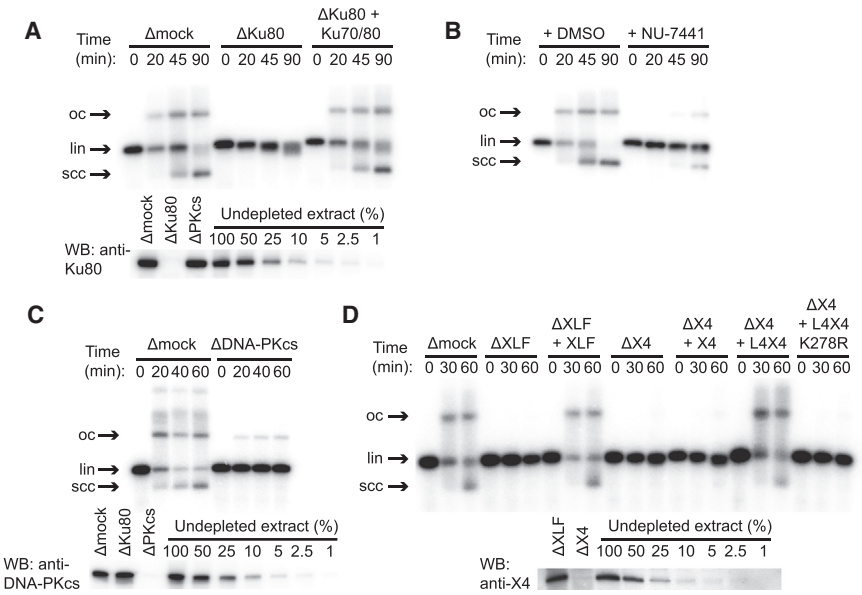

Figure 1. End Joining in *Xenopus* Egg Extract Depends on c-NHEJ Factors

(A) Inhibition of end joining by immunodepletion of Ku70/80 with αKu80 antibody and rescue with recombinant *X. laevis* Ku70/80. lin, linear DNA substrate; oc, open-circular products; scc, supercoiled closed-circular products. In other conditions, Ku immunodepletion selectively inhibited circularization, as previously reported (Figure S1C) (Labhart, 1999; Di Virgilio and Gautier, 2005).

(B) Inhibition of end joining by the DNA-PK inhibitor NU-7441.

(C) DNA-PKcs immunodepletion.

(D) Immunodepletion of XLF (ΔXLF) or XRCC4 (ΔX4) and rescue with recombinant *X. laevis* XLF, XRCC4 (X4), wild-type LIG4:XRCC4 (L4X4), or catalytically inactive LIG4^{K278R}:XRCC4 (L4X4 K278R).

Lower panels in (A), (B), and (D) are western blots of immunodepleted extract with indicated antibodies. Uncropped blots are shown in Figures S1F–S1H. XLF was not clearly visible in western blots of extract, but immunoprecipitated XLF was detected by western blotting and mass spectrometry (Figures S1J and S1K).

See also Figure S1.

in which DNA ends are closely apposed. Using small-molecule inhibitors, immunodepletion, and rescue with purified proteins, we define the roles of NHEJ factors at these two stages of synapsis. We find that long-range complex formation requires Ku70/80 and DNA-PKcs, but not DNA-PK catalytic activity. Subsequent transition to the short-range complex requires DNA-PK catalytic activity, XLF, and XRCC4-LIG4, but not LIG4 catalytic activity. These results define the molecular requirements for physiological NHEJ synaptic complex assembly and reveal that a programmed rearrangement of this complex is required for close alignment of DNA ends.

RESULTS

Validation of an In Vitro NHEJ System

To study NHEJ in vitro under physiological conditions, we used a cell-free extract of *X. laevis* eggs, which contains the entire soluble proteome and packages added DNA into nucleosomes (Laskey et al., 1977). Previous work showed that egg extract efficiently joins both compatible and incompatible DNA ends in a manner that depends on Ku70/80 and DNA-PK activity (Labhart, 1999; Postow et al., 2008; Thode et al., 1990; Di Virgilio and Gautier, 2005). Similarly, we observed that joining of blunt-ended linear DNAs was inhibited by immunodepletion of Ku (Figure 1A) and restored with recombinant *X. laevis* Ku70/80 (Figure 1A). End joining was also inhibited by small-molecule inhibitors or immunodepletion of DNA-PKcs, indicating that not only the presence but also the kinase activity of DNA-PKcs is required for end joining (Figures 1B, 1C, and S1A). Immunodepletion of XLF likewise abolished end joining, which was restored by recombinant *X. laevis* XLF protein (Figure 1D). Consistent with previous results suggesting a stable complex between XRCC4 and LIG4 (Bryans et al., 1999), anti-XRCC4 immunoprecipitates contained an adenylated protein of the molecular weight expected for *X. laevis* LIG4 (Figure S1B). Immunodepletion of extract with anti-XRCC4 antibody eliminated end joining, and end joining was restored by recombinant *X. laevis* LIG4:XRCC4 complex but not catalytically inactive LIG4^{K278R}:XRCC4 (Cottarel et al., 2013), XRCC4 alone, or XLF (Figures 1D and S1D). Taken together, these results demonstrate that *X. laevis* egg extract joins DNA ends efficiently in a manner that requires the c-NHEJ factors Ku70/80, DNA-PKcs, XLF, and LIG4:XRCC4, as well as DNA-PK catalytic activity.

Two-Stage Synapsis of DNA Ends during NHEJ

To address which NHEJ factors are required for synapsis of DNA ends in this system, we used a combination of single-molecule co-localization and FRET. A blunt-ended 100 bp DNA duplex labeled with Cy3 near one end and biotinylated at the other end (Cy3-DNA) was attached to a streptavidin-coated glass coverslip within a microfluidic channel (Figure 2A). Next, a blunt-ended 100 bp DNA duplex labeled near both ends with Cy5 (Cy5-DNA) was added to egg extract and drawn into the channel. In each case, Cy3 and Cy5 labels were placed seven nucleotides from the DNA end, which did not disrupt end joining (Figures S2A and S2B). Surface-tethered DNAs were imaged using total internal reflection illumination, alternating between excitation of Cy3 with a 532 nm laser and Cy5 with a 641 nm laser. Using a frame integration time of 1 s, only Cy5-DNAs tethered to Cy3-DNAs appeared as discrete spots (Figure S2C). FRET between Cy3 and Cy5 indicated close association between the two dyes.

Single-molecule intensity traces revealed a time delay between Cy5-DNA binding to Cy3-DNAs and the appearance of FRET (t_{lag} in Figures 2B and S2C). We refer to the Cy5-DNA-bound, low-FRET state as a long-range synaptic complex, because the dyes are outside of the ~100 Å maximum FRET radius, and the subsequent high-FRET state as a short-range synaptic complex. The lag time between long-range and short-range complex

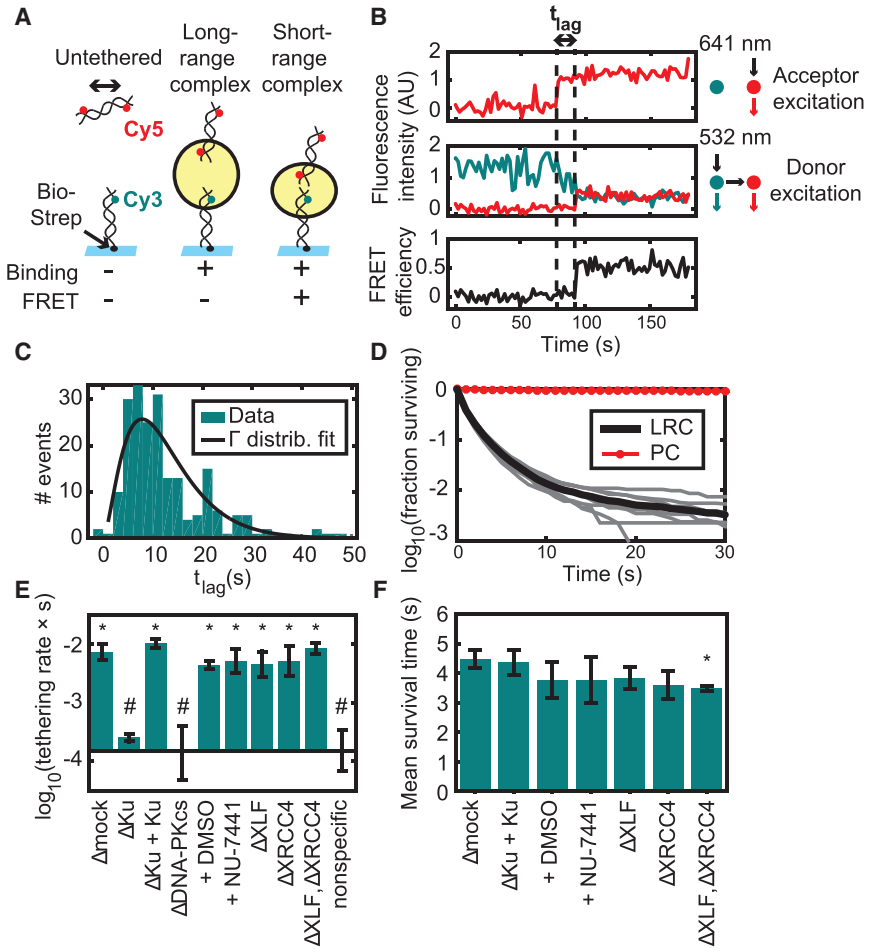

Figure 2. Two-Stage Synapsis of DNA Ends

(A) Schematic of the intermolecular tethering assay. A 100 bp DNA duplex biotinylated at one end (Bio) and labeled 7 bp from the other end with Cy3 was attached to a glass surface coated with streptavidin (Strep). A second 100 bp duplex labeled 7 bp from each end with Cy5 was added to egg extract and introduced into the flowcell. Cy5-DNA binding and FRET were monitored by alternating excitation of Cy3 and Cy5. The yellow circle represents the protein complex that bridges DNA ends.

(B) Example trajectory showing a lag time (t_{lag}) between Cy5-DNA binding and transition to a high-FRET state. Top: Cy5 signal with Cy5 (641 nm) excitation, which appears upon Cy5-DNA binding to the stationary Cy3-DNA. Middle: Cy3 (cyan) and Cy5 (red) signal with Cy3 (532 nm) excitation. Bottom: calculated FRET efficiency.

(C) Histogram of lag times between binding and transition to high FRET (n = 207 trajectories). A fit to a gamma distribution (k = 2.7, θ = 4.7 s) suggests that multiple steps are required for the long- to short-range transition, each with a time constant on the order of seconds.

(D) Survival curve of long-range complexes (LRCs) in mock-immunodepleted extract (n = 57921 events) and biotinylated Cy5-DNAs as a photostability control (PC; n = 3,907 molecules). The thick black line shows the mean of nine experimental replicates (thin gray lines).

(E) Long-range complex formation rate in extract immunodepleted of different factors or treated with DNA-PK inhibitor (NU-7441) or vehicle (DMSO). Elements of the two sets of conditions labeled * and # are significantly different from elements of the other set but not from elements of the same set ($p < 10^{-5}$, ANOVA with Tukey's post hoc test). Error bars indicate ±2 × SEM. See Table S1 for sample sizes.

(F) Mean survival time of tethered complexes was similar among different conditions, although slightly reduced by XLF/XRCC4 double depletion (p = 0.03 compared with Δmock, ANOVA with Tukey's post hoc test). Error bars indicate ±2 × SEM. XLF and XRCC4 depletion also appeared to reduce the fraction of long-range complexes that were extremely long lived (see Figure S2D).

See also Figure S2 and Table S1.

formation was not exponentially distributed, implying that this transition involves more than a single rate-limiting step (Figure 2C). Most long-range complexes were short lived, with 59% lasting only a single Cy5 excitation frame (~2 s; see Figure 2D). Among the 14% of long-range complexes that survived at least four Cy5 excitation frames (~8 s), about 1% progressed to a high-FRET state, while the rest dissociated (see Supplemental Experimental Procedures and Figure S4B). The low transition probability from the long-range to the short-range complex suggests that broken DNA ends typically interact many times before stably associating. Such repeated interactions would likely be facilitated by constrained diffusion of broken DNA ends within chromosomes (see also below) (Jakob et al., 2009; Kruhlak et al., 2006; Lucas et al., 2014; Soutoglou et al., 2007).

Molecular Requirements for Initial Tethering of DNA Ends

We next investigated the requirements for long-range synaptic complex formation. Immunodepletion of Ku70/80 or DNA-PKcs reduced the rate of long-range complex formation >30-fold, to a level that was indistinguishable from nonspecific Cy5-DNA binding to the surface in the absence of Cy3-DNAs (Figure 2E). The defect in Ku-depleted extract was reversed by addition of recombinant Ku70/80. In contrast, the rate of long-range complex formation was unaffected by kinase inhibitors of DNA-PK or immunodepletion of XRCC4-LIG4, XLF, or both (Figure 2E). The average survival time of long-range complexes was also similar among these conditions (Figure 2F). These results argue that the DNA-PK holoenzyme, independent of its catalytic activity, forms the initial long-range bridge between broken DNA ends.

Requirements for Short-Range Synapsis of DNA Ends

We next addressed which factors are required for the formation of the short-range synaptic complex. Because of the relatively low yield of high-FRET complexes in our intermolecular tethering assay, we designed an intramolecular NHEJ substrate to increase the frequency of collisions between DNA ends. A 2,000 bp PCR product with Cy3 and Cy5 labels incorporated

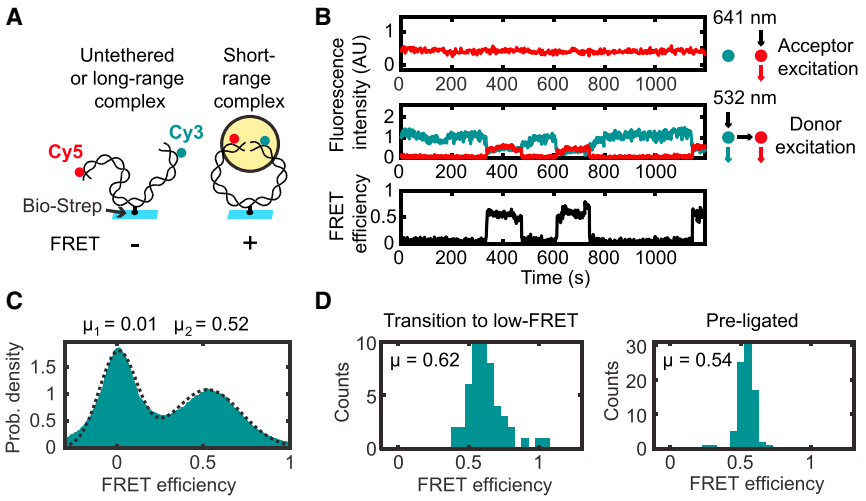

Figure 3. Single-Molecule Circularization Assay

(A) A 2 kb, blunt-ended DNA labeled 7 bp from one end with Cy3 and 7 bp from the other end with Cy5 was tethered by an internal biotin-streptavidin attachment to a glass coverslip, and FRET between Cy3 and Cy5 was measured after egg extract was added to the flowcell.

(B) Multiple transitions on a single substrate between low and high FRET. Top: Cy5 fluorescence intensity with direct (641 nm) excitation. Middle: Cy3 (cyan) and Cy5 (red) fluorescence with Cy3 (532 nm) excitation. Bottom: FRET efficiency.

(C) Histogram of FRET efficiencies in mock-immunodepleted extract, compiled over all substrates and all frames in three 30 min time course experiments (n = 434,397 substrates × frames).

(D) Histograms of average FRET efficiencies from high-FRET segments of long time course trajectories. Left: high-FRET complexes in extract that subsequently transitioned to a low-FRET state (indicating that they were unligated; n = 50 trajectory segments). Right: gel-purified circular standard generated by T4 DNA ligase (n = 83 trajectory segments).

See also Figure S3.

7 bp from either blunt end was bound to a coverslip by an internal biotin-streptavidin attachment (Figure 3A). Addition of egg extract led to the appearance of high-FRET complexes (Figures 3B and S3), some of which transitioned back to a low-FRET state (Figures 3B and S3H–S3O). Data compiled for many substrates showed a bimodal distribution of FRET efficiencies (Figure 3C). The center of the high-FRET peak in this distribution (E_{FRET} = 0.52) was similar to the FRET efficiency of DNA molecules that were pre-ligated with T4 DNA ligase before imaging in egg extract (E_{FRET} = 0.54), indicating close alignment of DNA ends within high-FRET complexes (Figures 3C and 3D). A similar mean FRET efficiency was seen for the subset of high-FRET molecules that subsequently reverted to a low-FRET state (E_{FRET} = 0.62). These results indicate that within the short-range complex, DNA ends are closely juxtaposed, even before ligation (Figure 3D).

To measure the kinetics of short-range synapsis while avoiding photobleaching, we sampled fresh fields of view every ~18 s after extract addition and obtained FRET efficiency histograms at each time point, which are displayed as kymographs in Figures 4A and 4B. In unperturbed extract, substrates transitioned from an initial zero-FRET state to a final state with FRET efficiency of ~0.5 (Figure 4A). The kinetics of this short-range synapsis were quantified by plotting the fraction of substrates with FRET efficiency > 0.25 as a function of time (e.g., the black curve in Figure 4E summarizes Figure 4A). As expected from a sequential mechanism of synaptic complex assembly, immunodepletion of Ku70/80 or DNA-PKcs, which disrupts formation of the long-range synaptic complex (Figure 2E), also prevented formation of the short-range synaptic complex (Figures 4C and 4D). In contrast to the long-range synaptic complex, the short-range synaptic complex was abolished by small-molecule inhibitors of DNA-PK or immunodepletion of XLF or XRCC4-LIG4 (Figures 4E, 4F and 5A). Purified XLF protein rescued short-range synapsis in XLF-depleted extract (Figure 4F). Analogous results were seen for short-range complex formation in the intermolecular synapsis assay, although not all comparisons were statistically significant (Figure S4). Collectively, these results show that in addition to the factors required to form the long-range complex (Ku70/80 and DNA-PKcs), formation of the short-range complex requires DNA-PK catalytic activity, XLF, and XRCC4-LIG4.

A Non-catalytic Role for LIG4 in Short-Range Synapsis

Interestingly, short-range synapsis in XRCC4-depleted extract was rescued by LIG4:XRCC4 but not by XRCC4 alone (Figures 5A and S1I), indicating that LIG4 is required for short-range synapsis of DNA ends. Catalytically inactive $LIG4^{K278R}$:XRCC4 also rescued short-range complex formation, although high-FRET complexes accumulated to a lower level (Figure 5A), were shorter lived than high-FRET complexes formed in undepleted extract (Figure 5B), and were dissociated by 1% SDS (Figure 5C), consistent with synapsis without ligation. Short-range complexes formed in the presence of catalytically inactive LIG4:XRCC4 were nonetheless much longer lived than the long-range synaptic complex (compare Figures 2D and 5B). These results reveal that the presence of LIG4, independent of its catalytic activity, is required for a conformational transition in the synaptic complex that aligns DNA ends and stabilizes their association.

DISCUSSION

Here, we report that in addition to Ku70/80 and DNA-PK (Labhart, 1999; Postow et al., 2008; Di Virgilio and Gautier, 2005), end joining in *X. laevis* egg extract requires the NHEJ factors XLF and XRCC4-LIG4. These results further validate egg extracts as a physiologically realistic in vitro system for studying NHEJ. Using single-molecule fluorescence imaging in extract,

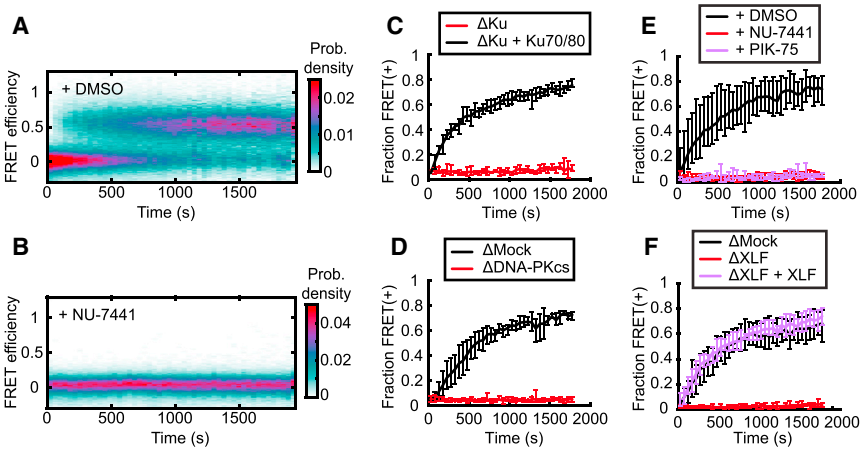

Figure 4. Requirements for Short-Range Synapsis of DNA Ends

(A and B) Time-resolved FRET efficiency histograms for a population of substrates in extract treated with NU-7441 (B) or DMSO solvent control (A).

(C–F) Fraction of circularization substrates with a FRET efficiency greater than 0.25 as a function of time after extract addition. Mean (thick line) and range (error bars) of all replicates. See Table S2 for sample sizes. (C) Ku-immunodepleted extract or Ku-immunodepleted extract supplemented with purified Ku70/80 ($p = 0.003$, t test of overall fraction FRET positive by replicate). (D) DNA-PKcs-immunodepleted extract and mock depletion with pre-immune IgG ($p = 0.008$, t test of overall fraction FRET positive by replicate). (E) Treatment with NU-7441, another DNA-PK inhibitor (PIK-75), or DMSO solvent ($p = 0.002$ for DMSO versus NU-7441, $p = 0.014$ for DMSO versus PIK-75, NU-7441 versus PIK-75 comparison not significant; t test with Bonferroni correction of overall fraction FRET positive by replicate). Black and red curves are derived from the histograms in (A) and (B), respectively. (F) Immunodepletion of XLF and rescue with recombinant XLF protein ($p = 0.0007$ for ΔMock versus ΔXLF, $p = 0.0014$ for ΔXLF versus ΔXLF + XLF, ΔMock versus ΔXLF + XLF comparison not significant, t test with Bonferroni correction of overall fraction FRET positive by replicate).

See also Figure S4 and Table S2.

we have monitored a complete DSB repair reaction at nanometer resolution in real time.

Our results identify two stages of DNA end synapsis during NHEJ (Figure 6). Ku70/80 and DNA-PKcs form an initial long-range complex in which DNA ends are held sufficiently far apart that no FRET is detected between the Cy3 and Cy5 labels. The absence of FRET in this initial complex is not surprising given the large dimensions of DNA-PKcs (~160 × 120 × 100 Å for a monomer) (Sibanda et al., 2010). Conversion of the long-range synaptic complex to the short-range complex, in which the DNA ends are closely aligned, requires DNA-PK catalytic activity, XLF, and LIG4:XRCC4, but not LIG4 catalytic activity.

Given that our extract system contains the complete soluble proteome, and that end joining depends on key NHEJ factors, it is reasonable to expect that the stepwise process of synapsis that we observe in vitro also occurs in intact cells. However, it is likely that the kinetics of the process are different between extract and intact cell nuclei, given differences in the overall concentration of DNA and repair factors. We also cannot exclude the possibility that alternative mechanisms of synapsis might occur in intact cells. For instance, DNA bridging interactions within chromatin domains larger than our in vitro substrates (Bassing and Alt, 2004) might increase the effective local concentration of DNA ends, facilitating subsequent long- and short-range complex formation.

Recently, Reid et al. (2015) proposed a model in which XLF, XRCC4, and LIG4 filaments initially bridge DNA ends in a side-by-side orientation. The ends subsequently slide past one another, aligning them for ligation. This model is based primarily on their observation that in reactions containing Cy3- and Cy5-labeled DNA duplexes and purified Ku70/80, XLF, XRCC4, and LIG4, FRET efficiency fluctuated in individual traces, resulting in a broad distribution of values. However, it is unclear whether DNA bridging complexes formed under these conditions were physiological, given that DNA-PKcs was not present in the mixture and that ligation was not shown to depend on Ku70/80 or XLF. In contrast, our extract system ligates DNA ends in a manner that requires key NHEJ factors, including DNA-PKcs. A central role for DNA-PK in synaptic complex formation is consistent with its importance for NHEJ in vivo (Dobbs et al., 2010; Jette and Lees-Miller, 2015; Jiang et al., 2015; Lees-Miller et al., 1995; Peterson et al., 1995). Notably, the model of Reid et al. (2015) would predict that in our experiments, formation of the short-range complex is preceded by a transient high-FRET intermediate as donor and acceptor dyes slide past each other, yet this is not observed (Figures 3B and S3H–S3O). Instead, our FRET efficiency measurements exhibit a bimodal distribution indicating that alignment of DNA ends involves a transition between discrete structural intermediates. Reid et al. (2015) also based their model on super-resolution images of fixed cells in which a fraction of immunostained XRCC4, XLF, and LIG4 foci co-localized with Ku or TUNEL staining and appeared filamentous. However, these experiments lack the resolution to determine the location of DNA ends relative to each other and therefore cannot distinguish between different models of synaptic complex assembly. Thus, we believe that our cell extract-based approach currently provides the highest resolution view of physiological end joining.

Our result that LIG4 is required for synapsis independent of its catalytic activity is in line with previous results from pull-down experiments in human cell extracts (Cottarel et al., 2013). Although Cottarel et al. (2013) observed an overall decrease in DNA bridging in the absence of LIG4, we find that LIG4 is required for short-range but not long-range synapsis. Our observations and those of Cottarel et al. (2013) are reconciled by the fact that the short-range complex is much longer lived than the long-range complex (Figures 2D and 5B). Although an ensemble pull-down assay could potentially detect both complexes, our results suggest it would preferentially detect the short-range complex, which would dissociate more slowly than the long-range complex during wash steps. This interpretation also explains why depletion of Ku70/80 or DNA-PKcs, which disrupt

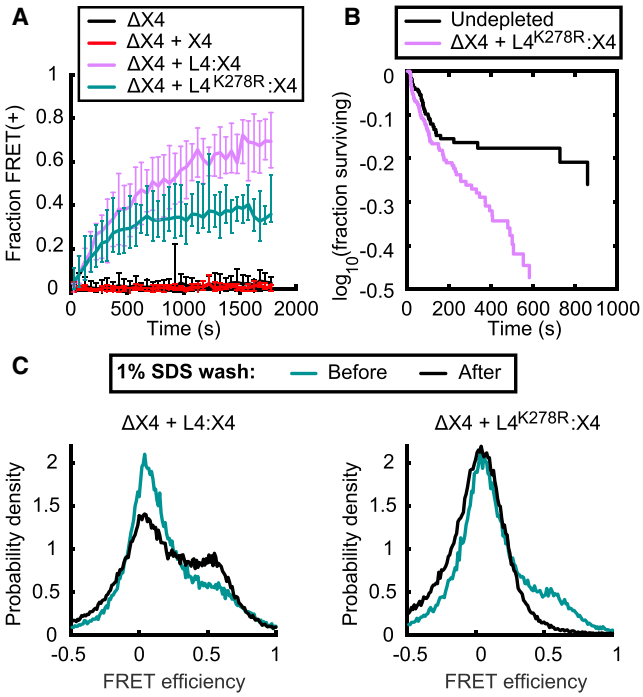

Figure 5. A Non-catalytic Role of LIG4 in Short-Range Synapsis

(A) Kinetics of circularization, as in Figure 4, for extract immunodepleted of XRCC4 (ΔX4). Mean (thick line) and range (error bars) of all replicates. Successful rescue with recombinant wild-type or catalytically inactive (K278R) LIG4:XRCC4 complex (L4:X4) but not XRCC4 alone (X4). p = 0.0004 for ΔX4 versus ΔX4 + L4:X4, p = 0.0009 for ΔX4 versus ΔX4 + $L4^{K278R}$:X4, ΔX4 versus ΔX4 + X4 comparison not significant, t test with Bonferroni correction of overall fraction FRET positive by replicate.

(B) Kaplan-Meier survival curves of high-FRET complexes formed in undepleted extract (n = 124) or XRCC4-depleted extract supplemented with $LIG4^{K278R}$:XRCC4 (n = 180). The two curves differ significantly (p = 0.01, two-tailed log-rank test).

(C) FRET efficiency histograms before and after a 1% SDS wash of substrates incubated for 30 min in XRCC4-depleted extract supplemented with either wild-type or catalytically inactive (K278R) LIG4:XRCC4. Left: the apparent increase in the high-FRET population after SDS wash is likely due to the fact that the pre-wash histogram is compiled from a time-lapse movie in extract, during which the high-FRET population was increasing.

See also Figures S4 and S5 and Table S2.

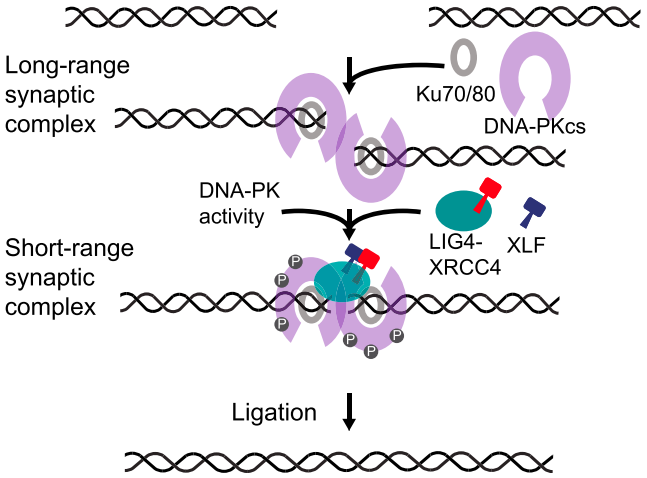

Figure 6. Two-Stage Model of NHEJ Synaptic Complex Assembly

DNA ends are initially tethered in a long-range complex and then brought together after several seconds into a short-range complex. Formation of the initial long-range complex requires Ku70/80 and DNA-PKcs, whereas formation of the short-range complex requires DNA-PK catalytic activity, XLF, and LIG4:XRCC4, but not LIG4 catalytic activity. Close alignment of the ends in the short-range complex positions them to be ligated.

both long- and short-range complex formation in our assay, caused a more complete DNA bridging defect than LIG4 depletion in ensemble experiments (Cottarel et al., 2013).

An important question is how end processing is coordinated with the two stages of end synapsis. Previous work suggested that autophosphorylation induces a conformational change in DNA-PKcs that makes bound DNA ends accessible to processing enzymes (Calsou et al., 1999; Ding et al., 2003; Dobbs et al., 2010; Hammel et al., 2010; Weterings et al., 2003). The DNA-PK-dependent conformational transition that we observe in the synaptic complex may therefore regulate not only ligation but also processing of DNA ends. Consistent with this idea, XRCC4-LIG4 and XLF, which we have shown are also required for this conformational transition, are necessary for DNA-PKcs autophosphorylation and for some types of end processing (Akopiants et al., 2009; Cottarel et al., 2013; Lee et al., 2003). Coupling LIG4 recruitment with the switch to a processing-competent state would position LIG4 to ligate broken ends as soon as they are compatible (Waters et al., 2014b), helping minimize genetic alterations during NHEJ.

EXPERIMENTAL PROCEDURES

Egg Extract Preparation

High-speed supernatant (HSS) of egg cytosol was prepared as described previously (Lebofsky et al., 2009). All experiments with animals were approved by the Harvard Medical Area Institutional Animal Care and Use Committee.

Cloning and Protein Purification

See Supplemental Experimental Procedures.

Bulk End Joining Assays

Extract was supplemented with nocodazole to a final concentration of 7.5 ng/μl if nocodazole had not already been added prior to immunodepletion. For the experiments shown in Figure 1, 10 μl extract was mixed with 0.5 μl of ~20 ng/μl radiolabeled linear substrate DNA (see Supplemental Experimental Procedures for description of substrate preparation), 1 μl of 1 μg/μl closed-circular pBluescript II DNA, and 0.3 μl of an ATP regeneration mixture containing 65 mM ATP, 650 mM phosphocreatine, and 160 ng/μl creatine phosphokinase (Sigma, Catalog No. C-3755; Type I from rabbit muscle). The addition of closed-circular "carrier" DNA to the reaction was necessary for efficient end joining of dilute linear substrate, similar to the dependence on total DNA concentration seen for DNA replication in extract (Lebofsky et al., 2011). An initial 2 μl sample (0 min) was withdrawn while the reactions were on ice and mixed with 5 μl stop solution and loading dye (80 mM Tris [pH 8], 8 mM EDTA, 0.13% phosphoric acid, 10% Ficoll, 5% SDS, 0.2% bromophenol blue). Reactions were transferred to room temperature, and additional 2 μl samples were withdrawn at the indicated times and mixed with 5 μl stop solution and loading dye. Samples were digested at room temperature for at least 1 hr with 1 μg proteinase K per sample, and products were separated by electrophoresis on a 1× Tris-borate-EDTA, 0.8% agarose gel. Gels were sandwiched between filter paper and a

HyBond-XL nylon membrane (GE Healthcare), dried on a gel dryer, and exposed to a storage phosphorscreen, which was imaged using a Personal Molecular Imager (BioRad) or Typhoon FLA 7000 imager (GE Healthcare Life Sciences).

Antibody Generation

Antibodies were raised in rabbits by New England Peptide against synthetic peptides corresponding to C-terminal sequences from *X. laevis* XLF (Ac-CGASKPKKKAKGLFM-OH), XRCC4 (Ac-CKNTPDPDDLFSDI-OH), and Ku80 (Ac-CMEDEGDVDDLLDMM-OH). Antibodies were affinity-purified by the supplier using resin coupled to the corresponding peptide through its N-terminal cysteine. Anti-DNA-PKcs antibody was raised by Pocono Rabbit Farm and Laboratory against an insoluble fragment of *X. laevis* DNA-PKcs spanning the PIKK and FATC domains (see Supplemental Experimental Procedures). For affinity purification of antibody, antigen dissolved in 1× PBS with 6 M urea and 5 mM β-mercaptoethanol was coupled to AminoLink Coupling Resin (Thermo Fisher Scientific), following the manufacturer's instructions. Rabbit serum was passed over antibody-coupled resin by gravity flow, and the resin was washed with 1× PBS. Bound antibody was eluted with 200 mM glycine (pH 2.6), and elution fractions were rapidly neutralized with 0.14 volumes of 1 M Tris-HCl (pH 8.8). Mock IgG for the experiment in Figure 1B was purified by protein A Sepharose affinity chromatography from pre-immune serum of the rabbit used to produce anti-DNA-PKcs antibody. Antibody was eluted from the resin as described above. Details about immunodepletion and rescue experiments can be found in Supplemental Experimental Procedures.

Western Blotting

Extract samples for western blotting were diluted with four volumes of SDS-PAGE sample buffer, and additional serial dilutions were made of undepleted extract in SDS-PAGE sample buffer. Samples were separated by SDS-PAGE, transferred to polyvinylidene fluoride membranes, and probed with the indicated antibodies. Details can be found in Supplemental Experimental Procedures.

Single-Molecule Tethering Assay

Biotin-100 bp-Cy3 duplexes (see Supplemental Experimental Procedures) were tethered at a 1:1,000 dilution on a streptavidin-coated coverslip in degassed egg lysis buffer (ELB; 10 mM HEPES [pH 7.7], 50 mM KCl, 2.5 mM $MgCl_2$) for 3–5 min, after which the flowcell was washed with 200 μl ELB (see Supplemental Experimental Procedures for details about microscope and flowcell construction). HSS (25 μl) was mixed with 2.5 μl of 1 mg/ml closed-circular pBluescript II DNA, 0.8 μl of ATP regeneration mix (see Bulk End Joining Assays), 0.6 μl of 250 mM protocatechuic acid (PCA) in ELB (adjusted to pH 7.7), 0.6 μl of 5 μM protocatechuate 3,4-dioxygenase (PCD; storage buffer 10 mM HEPES [pH 7.5], 50 mM KCl, 1.25 mM $MgCl_2$, 50% glycerol), 0.6 μl of 50 mM Trolox (6-hydroxy-2,5,7,8-tetramethylchroman-2-carboxylic acid) in DMSO, and 1 μl of 100 nM Cy5-labeled 100 bp duplex, in that order. PCA and PCD form an oxygen-scavenging system, while Trolox serves as a triplet-state quencher. The extract was drawn into the channel, and images were acquired continuously at a rate of 1 s/frame with alternating 532 and 641 nm laser excitation. The surface power density was 4 W/cm^2 for the 532 nm laser and 0.9 W/cm^2 for the 641 nm laser. To determine the nonspecific background rate of tethering (Figure 2E), Biotin-100 bp-Cy3 duplexes were omitted, and the correct plane of focus was maintained by imaging 605 nm quantum dots (Life Technologies) nonspecifically adsorbed to the surface. For Cy5 photostability measurements (Figure 2D), a biotinylated, Cy5-labeled PCR product was imaged in egg extract under the same imaging conditions. Data were analyzed using custom MATLAB (The MathWorks) scripts (see Supplemental Experimental Procedures).

Single-Molecule Circularization Assay

The intramolecular end joining substrate shown in Figure 3A (see Supplemental Experimental Procedures) was tethered to a streptavidin-coated coverslip within a flowcell channel. An extract mixture was prepared as described above for single-molecule tethering experiments and drawn into the flowcell. For the experiments shown in Figures 3C, 4, and 5A, 100 ms exposures were taken stroboscopically every 1 s, alternating between two frames of 532 nm excitation (surface power density 16 W/cm^2) and one frame of 641 nm excitation (surface power density 7 W/cm^2). A different field of view was typically imaged every 18 frames. To obtain the kymographs shown in Figures 4A and 4B and the kinetic traces shown in Figures 4C–4F and 5A, FRET efficiency data from all replicates were pooled and binned in 36 s windows. For long-time-course imaging (Figures 3B, 3D, 5B, and S3), images were taken continuously at a rate of 1 frame/s, alternating between 2 frames of 532 nm excitation (surface power density 4 W/cm^2) and 1 frame of 641 nm excitation (surface power density 0.9 W/cm^2). Data analysis is described in Supplemental Experimental Procedures.

SUPPLEMENTAL INFORMATION

Supplemental Information includes Supplemental Experimental Procedures, five figures, and two tables and can be found with this article online at http://dx.doi.org/10.1016/j.molcel.2016.02.010.

AUTHOR CONTRIBUTIONS

All authors designed experiments and wrote the manuscript. T.G.W.G. performed experiments and data analysis.

ACKNOWLEDGMENTS

We thank members of the Walter and Loparo laboratories for helpful discussions, James Kath for homemade Pfu polymerase, Hyeongjun Kim and Jacob Sargent for help with microscope construction and advice on FRET experiments, Dan Floyd for calibration grid fabrication, Ravi Amunugama for advice on protein expression in Sf9 cells, Hironori Funabiki for plasmids and a sample of his lab's anti-Ku80 antibody, Martin Wühr for help searching *X. laevis* sequence databases, Ross Tamaino at the Taplin Mass Spectrometry Facility for assistance with mass spectrometry, and Katheryn Meek for anti-DNA-PKcs mouse monoclonal antibody used for western blotting. We would also like to thank Jennifer Waters and Talley Lambert at the Harvard Medical School Nikon Imaging Facility for assistance with preliminary time course FRET experiments. This work was funded by a National Science Foundation Graduate Research Fellowship (to T.G.W.G.), National Institutes of Health grant R01GM115487 (to J.J.L), the Stewart Trust Fellows Award (to J.J.L.), and a Department of Defense grant (BC120436) and the Howard Hughes Medical Institute (J.C.W.).

Received: November 18, 2015
Revised: December 21, 2015
Accepted: February 7, 2016
Published: March 17, 2016

REFERENCES

Ahnesorg, P., Smith, P., and Jackson, S.P. (2006). XLF interacts with the XRCC4-DNA ligase IV complex to promote DNA nonhomologous end-joining. Cell *124*, 301–313.

Akopiants, K., Zhou, R.-Z., Mohapatra, S., Valerie, K., Lees-Miller, S.P., Lee, K.-J., Chen, D.J., Revy, P., de Villartay, J.-P., and Povirk, L.F. (2009). Requirement for XLF/Cernunnos in alignment-based gap filling by DNA polymerases lambda and mu for nonhomologous end joining in human whole-cell extracts. Nucleic Acids Res. *37*, 4055–4062.

Bassing, C.H., and Alt, F.W. (2004). H2AX may function as an anchor to hold broken chromosomal DNA ends in close proximity. Cell Cycle *3*, 149–153.

Bryans, M., Valenzano, M.C., and Stamato, T.D. (1999). Absence of DNA ligase IV protein in XR-1 cells: evidence for stabilization by XRCC4. Mutat. Res. *433*, 53–58.

Buck, D., Malivert, L., de Chasseval, R., Barraud, A., Fondanèche, M.-C., Sanal, O., Plebani, A., Stéphan, J.-L., Hufnagel, M., le Deist, F., et al. (2006). Cernunnos, a novel nonhomologous end-joining factor, is mutated in human immunodeficiency with microcephaly. Cell *124*, 287–299.

Calsou, P., Frit, P., Humbert, O., Muller, C., Chen, D.J., and Salles, B. (1999). The DNA-dependent protein kinase catalytic activity regulates DNA end processing by means of Ku entry into DNA. J. Biol. Chem. *274*, 7848–7856.

Carter, T., Vancurová, I., Sun, I., Lou, W., and DeLeon, S. (1990). A DNA-activated protein kinase from HeLa cell nuclei. Mol. Cell. Biol. *10*, 6460–6471.

Cary, R.B., Peterson, S.R., Wang, J., Bear, D.G., Bradbury, E.M., and Chen, D.J. (1997). DNA looping by Ku and the DNA-dependent protein kinase. Proc. Natl. Acad. Sci. U S A *94*, 4267–4272.

Chiruvella, K.K., Liang, Z., and Wilson, T.E. (2013). Repair of double-strand breaks by end joining. Cold Spring Harb. Perspect. Biol. *5*, a012757.

Cottarel, J., Frit, P., Bombarde, O., Salles, B., Négrel, A., Bernard, S., Jeggo, P.A., Lieber, M.R., Modesti, M., and Calsou, P. (2013). A noncatalytic function of the ligation complex during nonhomologous end joining. J. Cell Biol. *200*, 173–186.

Craxton, A., Somers, J., Munnur, D., Jukes-Jones, R., Cain, K., and Malewicz, M. (2015). XLS (c9orf142) is a new component of mammalian DNA double-stranded break repair. Cell Death Differ. *22*, 890–897.

Critchlow, S.E., Bowater, R.P., and Jackson, S.P. (1997). Mammalian DNA double-strand break repair protein XRCC4 interacts with DNA ligase IV. Curr. Biol. *7*, 588–598.

DeFazio, L.G., Stansel, R.M., Griffith, J.D., and Chu, G. (2002). Synapsis of DNA ends by DNA-dependent protein kinase. EMBO J. *21*, 3192–3200.

Di Virgilio, M., and Gautier, J. (2005). Repair of double-strand breaks by nonhomologous end joining in the absence of Mre11. J. Cell Biol. *171*, 765–771.

Ding, Q., Reddy, Y.V.R., Wang, W., Woods, T., Douglas, P., Ramsden, D.A., Lees-Miller, S.P., and Meek, K. (2003). Autophosphorylation of the catalytic subunit of the DNA-dependent protein kinase is required for efficient end processing during DNA double-strand break repair. Mol. Cell. Biol. *23*, 5836–5848.

Dobbs, T.A., Tainer, J.A., and Lees-Miller, S.P. (2010). A structural model for regulation of NHEJ by DNA-PKcs autophosphorylation. DNA Repair (Amst.) *9*, 1307–1314.

Dvir, A., Peterson, S.R., Knuth, M.W., Lu, H., and Dynan, W.S. (1992). Ku autoantigen is the regulatory component of a template-associated protein kinase that phosphorylates RNA polymerase II. Proc. Natl. Acad. Sci. U S A *89*, 11920–11924.

Dvir, A., Stein, L.Y., Calore, B.L., and Dynan, W.S. (1993). Purification and characterization of a template-associated protein kinase that phosphorylates RNA polymerase II. J. Biol. Chem. *268*, 10440–10447.

Gottlieb, T.M., and Jackson, S.P. (1993). The DNA-dependent protein kinase: requirement for DNA ends and association with Ku antigen. Cell *72*, 131–142.

Grawunder, U., Wilm, M., Wu, X., Kulesza, P., Wilson, T.E., Mann, M., and Lieber, M.R. (1997). Activity of DNA ligase IV stimulated by complex formation with XRCC4 protein in mammalian cells. Nature *388*, 492–495.

Gu, J., Lu, H., Tsai, A.G., Schwarz, K., and Lieber, M.R. (2007). Single-stranded DNA ligation and XLF-stimulated incompatible DNA end ligation by the XRCC4-DNA ligase IV complex: influence of terminal DNA sequence. Nucleic Acids Res. *35*, 5755–5762.

Hammel, M., Yu, Y., Mahaney, B.L., Cai, B., Ye, R., Phipps, B.M., Rambo, R.P., Hura, G.L., Pelikan, M., So, S., et al. (2010). Ku and DNA-dependent protein kinase dynamic conformations and assembly regulate DNA binding and the initial non-homologous end joining complex. J. Biol. Chem. *285*, 1414–1423.

Jakob, B., Splinter, J., Durante, M., and Taucher-Scholz, G. (2009). Live cell microscopy analysis of radiation-induced DNA double-strand break motion. Proc. Natl. Acad. Sci. U S A *106*, 3172–3177.

Jette, N., and Lees-Miller, S.P. (2015). The DNA-dependent protein kinase: A multifunctional protein kinase with roles in DNA double strand break repair and mitosis. Prog. Biophys. Mol. Biol. *117*, 194–205.

Jiang, W., Crowe, J.L., Liu, X., Nakajima, S., Wang, Y., Li, C., Lee, B.J., Dubois, R.L., Liu, C., Yu, X., et al. (2015). Differential phosphorylation of DNA-PKcs regulates the interplay between end-processing and end-ligation during nonhomologous end-joining. Mol. Cell *58*, 172–185.

Kruhlak, M.J., Celeste, A., Dellaire, G., Fernandez-Capetillo, O., Müller, W.G., McNally, J.G., Bazett-Jones, D.P., and Nussenzweig, A. (2006). Changes in chromatin structure and mobility in living cells at sites of DNA double-strand breaks. J. Cell Biol. *172*, 823–834.

Labhart, P. (1999). Ku-dependent nonhomologous DNA end joining in Xenopus egg extracts. Mol. Cell. Biol. *19*, 2585–2593.

Laskey, R.A., Mills, A.D., and Morris, N.R. (1977). Assembly of SV40 chromatin in a cell-free system from Xenopus eggs. Cell *10*, 237–243.

Lebofsky, R., Takahashi, T., and Walter, J.C. (2009). DNA replication in nucleus-free Xenopus egg extracts. Methods Mol. Biol. *521*, 229–252.

Lebofsky, R., van Oijen, A.M., and Walter, J.C. (2011). DNA is a co-factor for its own replication in Xenopus egg extracts. Nucleic Acids Res. *39*, 545–555.

Lee, J.W., Yannone, S.M., Chen, D.J., and Povirk, L.F. (2003). Requirement for XRCC4 and DNA ligase IV in alignment-based gap filling for nonhomologous DNA end joining in vitro. Cancer Res. *63*, 22–24.

Lees-Miller, S.P., Chen, Y.R., and Anderson, C.W. (1990). Human cells contain a DNA-activated protein kinase that phosphorylates simian virus 40 T antigen, mouse p53, and the human Ku autoantigen. Mol. Cell. Biol. *10*, 6472–6481.

Lees-Miller, S.P., Godbout, R., Chan, D.W., Weinfeld, M., Day, R.S., 3rd, Barron, G.M., and Allalunis-Turner, J. (1995). Absence of p350 subunit of DNA-activated protein kinase from a radiosensitive human cell line. Science *267*, 1183–1185.

Lu, H., Pannicke, U., Schwarz, K., and Lieber, M.R. (2007). Length-dependent binding of human XLF to DNA and stimulation of XRCC4.DNA ligase IV activity. J. Biol. Chem. *282*, 11155–11162.

Lucas, J.S., Zhang, Y., Dudko, O.K., and Murre, C. (2014). 3D trajectories adopted by coding and regulatory DNA elements: first-passage times for genomic interactions. Cell *158*, 339–352.

Ma, Y., Lu, H., Schwarz, K., and Lieber, M.R. (2005). Repair of double-strand DNA breaks by the human nonhomologous DNA end joining pathway: the iterative processing model. Cell Cycle *4*, 1193–1200.

Mahaney, B.L., Hammel, M., Meek, K., Tainer, J.A., and Lees-Miller, S.P. (2013). XRCC4 and XLF form long helical protein filaments suitable for DNA end protection and alignment to facilitate DNA double strand break repair. Biochem. Cell Biol. *91*, 31–41.

Ochi, T., Blackford, A.N., Coates, J., Jhujh, S., Mehmood, S., Tamura, N., Travers, J., Wu, Q., Draviam, V.M., Robinson, C.V., et al. (2015). DNA repair. PAXX, a paralog of XRCC4 and XLF, interacts with Ku to promote DNA double-strand break repair. Science *347*, 185–188.

Peterson, S.R., Kurimasa, A., Oshimura, M., Dynan, W.S., Bradbury, E.M., and Chen, D.J. (1995). Loss of the catalytic subunit of the DNA-dependent protein kinase in DNA double-strand-break-repair mutant mammalian cells. Proc. Natl. Acad. Sci. U S A *92*, 3171–3174.

Postow, L., Ghenoiu, C., Woo, E.M., Krutchinsky, A.N., Chait, B.T., and Funabiki, H. (2008). Ku80 removal from DNA through double strand break-induced ubiquitylation. J. Cell Biol. *182*, 467–479.

Radhakrishnan, S.K., Jette, N., and Lees-Miller, S.P. (2014). Non-homologous end joining: emerging themes and unanswered questions. DNA Repair (Amst.) *17*, 2–8.

Ramsden, D.A., and Gellert, M. (1998). Ku protein stimulates DNA end joining by mammalian DNA ligases: a direct role for Ku in repair of DNA double-strand breaks. EMBO J. *17*, 609–614.

Reid, D.A., Keegan, S., Leo-Macias, A., Watanabe, G., Strande, N.T., Chang, H.H., Oksuz, B.A., Fenyo, D., Lieber, M.R., Ramsden, D.A., and Rothenberg, E. (2015). Organization and dynamics of the nonhomologous end-joining machinery during DNA double-strand break repair. Proc. Natl. Acad. Sci. U S A *112*, E2575–E2584.

Roy, S., de Melo, A.J., Xu, Y., Tadi, S.K., Négrel, A., Hendrickson, E., Modesti, M., and Meek, K. (2015). XRCC4/XLF interaction is variably required for DNA repair, and is not required for Ligase IV stimulation. Mol. Cell. Biol. *35*, 3017–3028.

Sibanda, B.L., Chirgadze, D.Y., and Blundell, T.L. (2010). Crystal structure of DNA-PKcs reveals a large open-ring cradle comprised of HEAT repeats. Nature *463*, 118–121.

Soutoglou, E., Dorn, J.F., Sengupta, K., Jasin, M., Nussenzweig, A., Ried, T., Danuser, G., and Misteli, T. (2007). Positional stability of single double-strand breaks in mammalian cells. Nat. Cell Biol. *9*, 675–682.

Spagnolo, L., Rivera-Calzada, A., Pearl, L.H., and Llorca, O. (2006). Three-dimensional structure of the human DNA-PKcs/Ku70/Ku80 complex assembled on DNA and its implications for DNA DSB repair. Mol. Cell *22*, 511–519.

Thode, S., Schäfer, A., Pfeiffer, P., and Vielmetter, W. (1990). A novel pathway of DNA end-to-end joining. Cell *60*, 921–928.

Tsai, C.J., Kim, S.A., and Chu, G. (2007). Cernunnos/XLF promotes the ligation of mismatched and noncohesive DNA ends. Proc. Natl. Acad. Sci. U S A *104*, 7851–7856.

Waters, C.A., Strande, N.T., Wyatt, D.W., Pryor, J.M., and Ramsden, D.A. (2014a). Nonhomologous end joining: a good solution for bad ends. DNA Repair (Amst.) *17*, 39–51.

Waters, C.A., Strande, N.T., Pryor, J.M., Strom, C.N., Mieczkowski, P., Burkhalter, M.D., Oh, S., Qaqish, B.F., Moore, D.T., Hendrickson, E.A., and Ramsden, D.A. (2014b). The fidelity of the ligation step determines how ends are resolved during nonhomologous end joining. Nat. Commun. *5*, 4286.

Weterings, E., Verkaik, N.S., Brüggenwirth, H.T., Hoeijmakers, J.H.J., and van Gent, D.C. (2003). The role of DNA dependent protein kinase in synapsis of DNA ends. Nucleic Acids Res. *31*, 7238–7246.

Xing, M., Yang, M., Huo, W., Feng, F., Wei, L., Jiang, W., Ning, S., Yan, Z., Li, W., Wang, Q., et al. (2015). Interactome analysis identifies a new paralogue of XRCC4 in non-homologous end joining DNA repair pathway. Nat. Commun. *6*, 6233.

Zha, S., Alt, F.W., Cheng, H.-L., Brush, J.W., and Li, G. (2007). Defective DNA repair and increased genomic instability in Cernunnos-XLF-deficient murine ES cells. Proc. Natl. Acad. Sci. U S A *104*, 4518–4523.